LOW DIFFERENTIAL PRESSURE AND MULTIPHASE FLOW MEASUREMENTS BY MEANS OF DIFFERENTIAL PRESSURE DEVICES

A Dissertation

by

JUSTO HERNANDEZ RUIZ

Submitted to the Office of Graduate Studies of
Texas A&M University
in partial fulfillment of the requirements for the degree of

DOCTOR OF PHILOSOPHY

August 2004

Major Subject: Interdisciplinary Engineering

LOW DIFFERENTIAL PRESSURE AND MULTIPHASE FLOW

MEASUREMENTS BY MEANS OF DIFFERENTIAL PRESSURE

DEVICES

A Dissertation

by

JUSTO HERNANDEZ RUIZ

Submitted to Texas A&M University
in partial fulfillment of the requirements
for the degree of

DOCTOR OF PHILOSOPHY

Approved as to style and content by:

<table>
<tr><td>Gerald L. Morrison
(Chair of Committee)</td><td>Kenneth R. Hall
(Member)</td></tr>
<tr><td>Stuart L. Scott
(Member)</td><td>Dennis O' Neal
(Member)</td></tr>
<tr><td>Karen Butler-Purry
(Head of Department)</td><td></td></tr>
</table>

August 2004

Major Subject: Interdisciplinary Engineering

ABSTRACT

Low Differential Pressure and Multiphase Flow Measurements by Means of Differential
Pressure Devices. (August 2004)

Justo Hernandez Ruiz, B.S., National Polytechnic Institute, Mexico;

M.S., National Polytechnic Institute, Mexico

Chair of Advisory Committee: Dr. Gerald L. Morrison

The response of slotted plate, Venturi meter and standard orifice to the presence of two phase, three phase and low differential flows was investigated. Two mixtures (air-water and air-oil) were used in the two-phase analysis while a mixture of air, water and oil was employed in the three-phase case. Due to the high gas void fraction ($\alpha > 0.9$), the mixture was considered wet gas. A slotted plate was utilized in the low differential pressure analysis and the discharge coefficient behavior was analyzed. Assuming homogeneous flow, an equation with two unknowns was obtained for the multi-phase flow analysis. An empirical relation and the differential response of the meters were used to estimate the variables involved in the equation.

Good performance in the gas mass flow rate estimation was exhibited by the slotted and standard plates for the air-water flow, while poor results were obtained for the air-oil and air-water oil flows. The performance of all the flow meter tested in the analysis improved for differential pressures greater than 24.9 kPa (100 in_H_2O). Due to the tendency to a zero value for the liquid flow, the error of the estimation reached values of more than 500% at high qualities and low differential pressures. Air-oil and air-water-oil flows show that liquid viscosity influences the response of the differential pressure meters. The best results for high liquid viscosity were obtained in the Venturi meter using the recovery pressure for the gas flow estimation at differential pressures greater than 24.9 kPa (100 in_H_2O).

A constant coefficient C_d was used for the low differential pressure analysis and results did show that for differential pressure less than 1.24 kPa (5 inH_2O) density changes are less than 1% making possible the incompressible flow assumption. The average of the computed coefficients is the value of C_d.

This work is dedicated to my wife Yesica and my sons Mauricio and Donaji.

ACKNOWLEDGEMENTS

I want to thank Dr. Gerald L. Morrison for his time and assistance in the development of this dissertation.

I appreciate the help provided by the Turbomachinary Laboratory staff and the financial support received from ANUIES, the National Polytechnic Institute of Mexico and from the State of Texas.

I also want to thank Vasanth Muralidharan and Park Sang Hyun for their technical support and help received in the experimental work.

TABLE OF CONTENTS

Page

CHAPTER I

INTRODUCTION

Flow measurement is a means to obtain primary information necessary to generate an invoice for billing purposes and/or to control, alarm or indicate a process condition in the industry related to fluids. The competitive environment of this industry dictates flow has to be measured accurately, making the flow measurement technology flourish and new flow meters be developed.

A flow meter is a device that measures the rate at which fluid flows in a duct using a physical principle. Physical phenomena discovered centuries ago have been the starting point for many viable flow meters designs. Technical development, namely in fluid mechanics, optics, acoustics, electromagnetism and electronics, have resulted not only in improved sensor and electronic designs but also in new flow meters concepts.

Different physical principles are used to measure fluid flow which result in different flow meter types: differential pressure, positive displacement, turbine, ultrasonic, and oscillatory meters to name a few. From these meter types, differential-pressure devices represent an important part of all the flow meters due to its economy and simplicity.

Differential pressure devices

Differential pressure devices have been the most widely applied instruments for flow rate measurements in pipes that require accurate measurements at reasonable cost. This type of flow meter has a flow restriction in the line that causes a differential pressure between two measurements locations as a result of the velocity change in the flowing fluid. Velocity is computed using the measured differential pressure. The volumetric or mass flow rate can then be calculated.

_____

This dissertation follows the style and format of the Journal of Flow Measurement and Instrumentation.

The most commonly used differential pressure flow meters types are:

- Orifice plates
- Venturi
- Nozzle
- Pitot static tube

Others special designs of differential pressure devices include:

- V-cone flow meter
- Wedge
- Spring-loaded variable temperature
- Laminar flow element
- Dall tube
- Dall orifice
- Elbow
- Slotted plate

The last of the listed devices, the slotted plate, was developed in recent years at Texas A&M University by Drs. Gerald L. Morrison of the Mechanical Engineering Department and Ken R. Hall and J. C. Holste of the Chemical Engineering Department [1]. The main advantages of the differential pressure devices are listed below:

- Simple construction
- Relatively inexpensive
- No moving parts
- External transmitting instruments
- Low maintenance
- Wide application of flowing fluid
- Ease of instrumentation and range selection

- Extensive product experience and performance data base

- An abundance of application and selection guides

- Readily available standards and codes of practice

The main disadvantages of the differential meters are the following:

- Flow rate is not a linear function of the differential pressure

- Low flow rate rangeability with normal instrumentation

- Effects of multiphase flow not fully understood

- Fouling and erosion effects on the obstruction

All differential pressure meters use the same equation to estimate the mass flow rate. It can be derived from the Bernoulli and continuity equations. Applying Bernoulli's equation to the system shown in figure 1, considering single phase flow and neglecting gravity effects:

$$\frac{P_1}{\rho_1} + \frac{U_1^2}{2} = \frac{P_2}{\rho_2} + \frac{U_2^2}{2} \qquad (1)$$

From continuity equation

$$\rho_1 \cdot U_1 \cdot A = \rho_2 \cdot U_2 \cdot A_d$$

(2)

Assuming:

$$\rho_1 = \rho_2$$

And defining

$$\beta = \sqrt{\frac{A_d}{A}}$$

Then

$$\dot{m} = \frac{A \cdot \beta^2 \cdot C_d}{\sqrt{1-\beta^4}} \cdot \sqrt{2 \cdot \rho \cdot \Delta P} \qquad (3)$$

Coefficient C_d is added to equation 3 to take into account pressure losses and expansion through the differential pressure device. C_d is typically dependent upon β and Reynolds number (Re). However, Morrison [2] has shown that the Euler number (Eu) can be used in place of the Reynolds number. This effectively eliminates one measured property (viscosity) required to operate the meter. Different modifications of equation 3 are also utilized in multiphase flow measurements.

Multiphase flow measurements

Multiphase flow is the simultaneous flow of different components through a pipe system (for example gas and oil). In this work, the components can be in the same state but differ in their physical properties such as density and viscosity. Measurement of the mass flow rate components of the multiphase flow as they pass through a system is the goal of this work.

Multiphase flow measurement has been increasing its importance in order to improve the efficiency of the process where multiphase flow is present, for example the oil and gas industry. These measurements have been commonly made by means of a test separator. This device separates the phases (for example air, water and gas) and carries out flow measurement of the resulting single-phase flow [3].

This type of multiphase flow measurement is expensive and requires considerable space for the facilities but has the advantage that the single-phase measurements performed after the separation can be very accurate if separation is complete. Frequently, there is some carry over, gas in the liquid and liquid in the gas, resulting in errors ranging from 1

to 10% of the indicated value. Focusing on the oil industry, phase separation has the following limitations [4]:

1. Costly to install due to its weight and the necessity to provide test lines, manifolds, etc.
2. Costly and difficult to engineer and install on a sub sea application
3. The time taken to test a well is considerable

On the other hand, in-line multiphase meters are characterized in that the complete measurement of phase fractions and phase flow rates are performed directly, in the multiphase flow line, without separation of the flow. For the case of the oil industry, multiphase flow meters have the following advantages:

1. They can be designed to be installed sub sea
2. They provide instantaneous measurement of oil, gas and water produced by the well
3. The meters can work at any pressure and temperature
4. Relatively light and substantially more compact than a separator system

To justify the previous claims, it is desirable that the meter fit the following basic parameters of design, accuracy and reliability:

1. The meter must be capable of working with 0-100% of oil, water and gas or any mixture of the three phases within acceptable accuracy.
2. Accuracy of 5% or better over a turndown ratio of 20 to 1 with long term stability.
3. The expectancy of life must be 10 to 20 years with the period between maintenance of 3 to 10 years.

Currently, there is not a multiphase meter capable of working with 0-100% of oil, water and gas or any mixture of the three phases within the desired acceptable accuracy. Studies performed to date concentrate on specific multiphase flows; gas rich and liquid rich streams for example. [5]

The biggest obstacle to the successful implementation of multiphase metering is the general lack of understanding of the different flow regimes and when they are present in the pipe. Flow regime maps have been determined by subjective observation in laboratory test loops, almost always for two-phase mixtures: oil/gas or water/gas. These maps vary for temperature, pressure, density, surface tension, viscosity or pipe orientation.

Only a few complex flow regime maps exist for three-phase flow [5]. At the present time it is not practical to predict the performance of multiphase meters from first principles. Thus empirical work is required to evaluate the performance of specific flow meters subjected to specific flow conditions.

Authors differ in the classification of multiphase meters. Jamieson [5] identified four general approaches to multiphase metering:

1. Compact separator systems
2. Phase fraction and velocity measurement
3. Tracers
4. Pattern recognition

The first approach is applied worldwide but does not have the full benefits of multiphase metering. The others are being implemented due to the advantages of the online multiphase measurement.

Mehdizadeh [6] classifies multiphase measurements systems as type I, II and III. In type I systems, one or more phases are completely separated then measured. In type II systems, the main flow stream is divided into gas rich and liquid rich streams; each stream is subjected to multiphase measurements then recombined to form the original stream. In type III systems, all three phases go through a single conduit and are measured at the same time.

Most of the current multiphase meters use a combination of component fraction and component velocity measurement techniques to achieve multiphase measurements. The techniques and strategies used in each meter dictate its strength and its limitations for certain applications. There is currently no widely accepted standard by which these meters can be graded.

Wet gas

Wet natural gas metering is becoming an increasingly important technology to the operators of natural gas producing fields. This is a commonly used term in the industry but there is not a general definition for it. Some researchers adopt the definition of the wet gas range, which is a flow with gas volume fraction greater than 95% [7]. Other authors said the gas volume fraction in wet gas is greater than 90%.

Wet gas can then be defined as gas containing liquid. The amount of liquid can vary from a small amount of water or liquid hydrocarbon to a substantial amount of water and liquid hydrocarbon. The amount and nature of the liquid, as well as the temperature and pressure of the flow stream can impact the selection and accuracy of the measurement system [6].

Mehdizadeh [6] characterizes wet gas as type I, II and III. Wet gas type I is defined as the region with Lockhart-Martinelli number equal or less than 0.02; this corresponds to a range of high gas volume fraction at 99% and above. Type II wet gas is defined as the region between Lockhart-Martinelli number greater than 0.02 and equal or less than 0.30.

Type III wet gas corresponds to the regions outside of the Lockhart-Martinelli parameter (LM) that defines types I and II. This region of wet gas is encountered during the measurements of streams with proportionate gas and liquid content, which may also contain high fraction of water.

CHAPTER II
LITERATURE REVIEW

There are many types of flow meters available for measuring the flow rate of single-phase fluids. Several can be used in two phase and multiphase flow as well. This literature review will emphasize the standard orifice, slotted plate and Venturi meter. Attention will be drawn to their application to low differential pressure measurements and multiphase measurements.

Standard orifice plates

Due to their simplicity and economic characteristics, orifice flow meters have been used for a long time and represent an important percentage of the current flow meters used in the industry. Studies have been completed by many investigators with an ultimate goal to improve the performance of orifice plates. However, there are still a considerable number of unanswered questions pertaining to these devices. Teyssandier [8] addressed the needs of the oil and gas industry; he classifies measurements into three categories:

- Allocation
- Custody Transfer
- Process Control

The orifice flow meter research needs of the industry are delegated mainly within the categories listed above. Plate bending effects, installation effects, orifice coefficients and low pressure differential are some of the topics currently under investigation.

Orifice plates usually produce greater overall pressure loss than the other differential pressure devices. However, in order to obtain a good accuracy, it is a practice to keep the differential pressure as high as possible within the limitations of the strength of the orifice, the range of the differential pressure measuring device, and the limitations of the expansion factor [9].

At low differential pressure, error in flow rate estimation is increased, so orifice plates have a very narrow turndown (about 3:1) and in practice do not measure low flow rates well. If acceptable measurements can be made at low pressure-drop, turndown ratios would increase and there would be a reduction in equipment and manpower costs.

Orifice plates are also employed to estimate the flow rate in multiphase flows. However an improvement in its performance is required to improve the multiphase flow measurement. More details about multiphase measurements and low differential pressures are given below.

Slotted orifice plate

The slotted plate is an array of radial slots as opposed to a single bore in an orifice plate. Figure 9 shows an example of slotted plates and figure 10 presents slot details. Results from the study of the slotted orifice plate [1,10] show that

- Compared to an orifice flow meter, this device is relatively immune to ill-conditioned flows leading to a reduction of the meter run length required for the flow meter.
- The ideal slot width to plate thickness ratio is approximately 0.25.
- There is no apparent change in measured differential pressure when the slotted orifice plate is rotated within its flanges.
- Increasing of plate thickness increases immunity of the meter to ill-conditioned flow, however, permanent head loss is also increased.
- Pressure recovery usually occurs within one pipe diameter.

Morrison et al. [1] compared the performance of a standard and a slotted plate. They reported that the slotted plate has characteristics superior to those of the standard plate. They found that the slotted plate is less sensitive to upstream flow conditioning compared to a standard plate with the same β ratio. The discharge coefficient variation with changing the inlet velocity profile for the standard plate was -1% to 6% while in the slotted plate varied only $\pm 0.25\%$. This study was for a swirl free flow.

When swirl was presented the variation for the standard plate was up to 5% while those of the slotted plate were below 2%. Because of the slot distribution on the pipe cross section, the slotted plate stops the damming effect of contaminants; this affects the performance of the standard plate.

Because of their similar form, substitution of normal plates for slotted plates is easy. The only modification required is either the recalibration of the flow computer or the use of post-processing software to correct for the larger discharge coefficient value of the slotted plate and a different expansion factor. More information needs to be generated for these devices. For example, the effect of some factors such as wear and dirt upon their performance is needed.

Venturi

A Venturi flow meter is a restriction with a relatively long passage with smooth entry and exit. It produces less permanent pressure loss than a similar sized orifice but is more expensive. It is often used in dirty flow streams since the smooth entry allows foreign material to be swept through instead of building up as it would in front of an orifice plate.

The Venturi meter is installed between two flanges intended for this purpose. Pressure is sensed between a location upstream of the throat and a location at the throat. In this way, the same equation for the orifice flow meter is applied to this device. The Venturi meter performs better than an orifice plate and does not have as much operational factors that affect the meter accuracy as in the orifice plate case.

Low differential pressure measurements

Low differential pressure measurement has an important effect especially in orifice plates. Few attempts have been made to measure flow rates at low differential pressures and few data exists to determine orifice meter accuracy at these conditions. The following paragraphs describe some of the studies carried out in low-pressure differential flow measurements.

D. C. G. Lewis developed a low loss pressure difference flow meter, the flow tube [11]. It consist basically of a Venturi shaped insert mounted centrally in a short length of flanged pipe to measure clean water and gases. The value of the discharge coefficient of the flow tube remains constant for a much greater flow range than other differential pressure devices. The analysis of the performance of this flow meter showed that temperature has considerable effects on the computed flow.

D. L. George and T. B. Morrow [9] performed a series of measurements using natural gas on a 0.12 m (4 inch) diameter orifice run with three different β ratios, 0.5, 0.67 and 0.75, over a range of differential pressures from 0.247 kPa to 49.3 kPa (1 to 200 in_H_2O) using 0-49.3 kPa (0-200 in_H_2O) Rosemount pressure transducers. Results were compared with the Reader-Harris/Gallagher (RG) equation [12, 13].

RG equation was developed using orifice Reynolds numbers from 1700 to 70,000,000 for a variety of β ratios, pipe sizes and fluids. The differential pressures taken into account in the development of the equation were above 0.6 kPa.

Results for $\beta=0.5$ indicated that for differential pressures from 4.7 kPa to 53 kPa (19 to 215 in_H_2O) the experimental discharge coefficient lie within the 95% confidence interval of the RG equation and within ±0.25% of their averages. At ΔP= 2.4 kPa (9.72 in_H_2O) the coefficient of variance ($2\sigma_{Cd}$) is above 0.5% becoming smaller at ΔP=1.53 kPa (6.2 in_H_2O).

At ΔP=0.86 kPa, 0.38 kPa and 0.096 kPa (3.5, 1.55 and 0.39 in_H_2O) the scatter of the data becomes large. Although the fluctuations at low ΔP are smaller compared to that for greater pressure differentials, the ratio of the fluctuation to the ΔP value increases as pressure differential decreases. As a result, for pressure differential less than 2.5 kPa (10 in_H_2O) the error increased.

Results for $\beta=0.67$ showed that for ΔP=1.6kPa to 46.4kPa (6.41 to 188 in_H_2O) the experimental discharge coefficients exhibit of variance within ±0.5%. The scatter increases with decreasing differential pressure, moving well beyond the RG confidence interval to the order of a few percent at 0.22 kPa (0.9 in_H_2O). The average discharge coefficients begin to extend beyond the RG confidence intervals at ΔP=4.2 (17 in_H_2O).

The scatter in the measured discharge coefficients for $\beta=0.75$ was less than for the other beta ratios. For ΔP=0.68 kPa to 26.14 (2.74 to 106 in_H_2O) the measured discharge coefficients show variance values less than 0.5% and all values lie within the RG confidence interval. At ΔP=0.22 kPa, 0.12 kPa and 0.05kPa (0.889, 0.488 and 0.201 in_H_2O) the scatter of the data exceed 1%. The confidence intervals of the averages of the measured Cd values extended beyond the RG confidence interval for ΔP below 5.15 kPa (21.9 in_H_2O).

George and Morrow concluded that pressure differential less than 1.5 kPa (6 in_H_2O) should be avoided for all β ratios. Most of the experimental coefficient values below this differential pressure are either scattered over a broad range or have high measurement uncertainties. For the different β ratios analyzed, different lower limits of pressure differential were expected based on different causes of uncertainty.

They also concluded that for β=0.75, ΔP values as low as 0.68 kPa (2.74 in_H_2O) produce discharge coefficients that agreed with Reader-Harris/Gallagher equation and demonstrated little fluctuation about their mean. However, based on observed instability in the measurements, error analysis suggest that data from ΔP values below approximately 5.43 kPa (22 in_H_2O) have a strong uncertainty associated with the transmitter accuracy and calibration, and this values were suggested as a lower limit. For β=0.67 the recommended lower limit is 4.2 kPa (17 in_H_2O). For β=0.5 the suggested lower ΔP limit is 4.7 kPa (19 in_H_2O).

In the study performed by George and Morrow, the fluctuations in the differential pressure measurements were lowest at the low flow rate, however, although the pressure instabilities were smallest at the low flow rates, the drop with decreasing pressure difference is not linear. The standard deviation expressed as a percent of the differential pressure became largest at the lowest differential pressure making flow rate measurements more sensitive to dynamics in this region.

Hussein and Teyssandier [14] investigated the effects of orifice-generated flow disturbances and the frequency response of pressure transducers on the differential pressure measurement. The objective of their work was to isolate and determine the influence of the orifice generated disturbance on the differential pressure, and identify effects of the response frequency on the measurement of the time average value of the differential pressure. The following conclusions were obtained:

1. For a given orifice plate, the amplitude of the orifice induced pressure fluctuations at the downstream pressure tap increases with the increasing flow rates.

2. For the same line size, the magnitude of flow-induced disturbances at the downstream pressure tap increases with increasing orifice plate bore sizes.

3. In a steady flow line where noticeable periodicities are present the measured mean differential pressure is unaffected by the frequency response of the pressure transducers even when the response frequency is orders of magnitude lower than the periodic disturbances present in the actual pressure signal.

George, Morrow and Nored [15] mention the use of stacked pressure differential transmitters. In a stacked configuration, multiple pressure transmitters are cascaded, or connected in parallel across the pressure taps. The operating ranges of the differential pressure transmitters dictate which unit is used to collect data for a particular flow rate. Then, only one transmitter at a time is used to measure the differential pressure across the orifice plate.

Considering an orifice plate where the expected range of differential pressures is 6.2 to 49.3 kPa (25 to 200 in_H_2O), the commercial pressure transmitter chosen has a 0-61.7 kPa (0-250 in_H_2O) range and a stated 0.1% uncertainty of full scale. Then, the percent uncertainty equals an absolute uncertainty of 0.062 kPa (0.25 in_H_2O). If the required percent error in all measurements must be ≤0.25% of reading, this transmitter could only be used at or above 24.7 kPa (100 in_H_2O). Below 24.7 kPa (100 in_H_2O), appropriate transmitters should be selected so that the ΔP be measured within the 0.25% accuracy required.

With the use of the stacked differential transmitter, the turndown ratio can be maximized, uncertainty in the flow measurements is reduced and low-pressure drops can be used to estimate the mass flow rate. However, it increases the cost of the flow meter system.

Two-phase flow measurements

Orifice plates, wedges, Venturi and nozzles have been used as two-phase flow meters. Different correlations have been obtained to compute the mass phase fractions of the components. However, uncertainties in the flow measurements are considerable compared to that of the single phase.

Martinelli et al. [16] completed a study of the two-phase where the differential pressure in horizontal pipes was studied for different mixtures of gases and liquids. He developed an equation to predict pressure drop per unit length of pipe for two-phase flow when the liquid and gas phases flow with turbulent motion and another when the liquid is flowing viscously and the gas turbulently. In both cases, the equations predicted the experimental pressure drop with a maximum error of about ±30%.

Lockhart and Martinelli [17] correlated the pressure drop resulting from turbulent-turbulent, viscous-turbulent, turbulent-viscous and viscous-viscous two-phase flows in pipes. They use a parameter equal to the square root of the ratio of the pressure drop in the pipe if the liquid flowed alone to the pressure drop if the gas flowed alone. This work resulted in a generalized procedure to correlate the data obtained in other works. This parameter became the Lockhart-Martinelli parameter (LM).

$$LM = \frac{1 - Qual}{Qual} \cdot \sqrt{\frac{\rho_g}{\rho_l}} \tag{4}$$

Zivi [18] carried out an analysis of steam void fraction considering a steady state two-phase flow and using the principle of minimum entropy generation. He took into account the effects of liquid entrainment and wall friction. It was found that the slip ratio (gas velocity to liquid velocity) equals the cubic root of the ratio of the liquid density to the gas density for the idealized steady state annular flow. The void fraction estimation was better as pressure was increased.

Murdock [19] considered the orifice plate as being a very rough pipe of short length. In this way, the basic correlation parameters for pipes are identical to orifice plates. Murdock developed a dimensionless equation and compared it to experimental data and found that the gas flow coefficient is the same as the two-phase gas flow coefficient. He also found that the relation of liquid flow coefficient to the two-phase liquid flow coefficient was 1.26.

Murdock computed the total mass flow rate using the experimentally obtained constant M=1.26 and assuming that the quality of the mixture is known. He stated that the two-phase flow might be computed with a tolerance of 1.5 percent. The limits that he established were: β ratio between 0.25 and 0.5, standard tap locations, minimum liquid Reynolds number of 50, minimum gas Reynolds number of 10,000, maximum liquid weight fraction of 0.9, minimum volume ratio gas to liquid of 100:1 and minimum gas expansion coefficient of 0.98.

Chisholm [20] developed some equations to predict pressure drop over sharp-edged orifices during the flow of incompressible two-phase flow. He reported that, when the Lockhart-Martinelli parameter LM is greater than 1, the slip ratio is equal to the square root of the ratio of the liquid density to the homogeneous mixture density. When LM is less than 1, the slip ratio is equal to the fourth root of the ratio of the liquid density to the gas density.

Fincke et al [21] used Murdock's analysis and the experimentally obtained constant M, to compute the gas mass flow rate in a two-phase flow in a Venturi meter at different qualities. The results obtained were not satisfactory. Then, they adjust the constant M to fit the data and found that the constant M is not universal.

Fincke et al explored the performance of an extended throat Venturi meter with multiple differential pressure measurements under high void fraction conditions (≥0.95) to estimate liquid and gas flow rate without previous knowledge of liquid mass fraction. They assumed that, because the multiphase pressure response differs from that of the single phase, the pressure differentials could be a unique function of the mass flow rate of each phase.

Considering that only the liquid phase is in contact with the wall to take into account the friction effect, they applied the Bernoulli equation to each phase. A pressure drop term experienced by the gas phase, due to irreversible work done by the gas phase in accelerating the liquid, appeared in the Bernoulli equation for the gas phase. This same term and a friction factor appeared in the Bernoulli equation for the liquid phase.

It was found that the irreversible pressure drop term was proportional to the pressure drop in the extended throat, then considering that the gas void fraction very close to 1, the gas mass flow rate was computed. Fincke estimate the liquid velocity and computed the total flow rate. The uncertainty in % of total mass flow reported was ± 4% for the gas phase, ±4% for total mass flow and ±5% for liquid phase.

The Solartron ISA Company [22] developed a method to determine the mass flow rate in two-phase flow. They wanted to replace the conventional way to measured two-phase flow (phase separator) with a simple low cost two-phase flow meter based around pressure differential devices.

A Venturi meter with two pressure differential devices upstream and downstream the Venturi was used. Tests were conducted with nitrogen/kerosene mixtures at pressure of 4000 and 6000 kPa. Under the assumption of dry gas, measurements exhibited over-readings with liquid present. These over-readings were correlated to the quality, if the quality can be measured, then the over-readings, gas and liquid flow rate can be determined. In this way the previous liquid/gas ratio is not required.

Two methods were employed to determine the quality. The first was based on Murdock's analysis for two flow meters placed in series. The second one was an empirical equation based on five pressure differential measurements. The two flow meters placed in series required having significantly different Murdock correlations.

The results reported show that the maximum relative error reached at 4000 kPa was 7% for gas using a straight line fit at a low gas void fraction range from 90 to 96% and 30% for liquid using a quadratic fit from 90 to 99% of gas void fraction. At 6000 kPa the maximum relative error was 5% for gas and 21% for liquid.

Steven [7] compared the performance of 5 two-phase correlations used in orifice plates and two wet gas Venturi correlations in a horizontally mounted Venturi meter at different pressures. The orifice plate correlations analyzed were the homogeneous-flow model, the Murdock correlation, the Chisholm correlation, the Lin equation and the Smith & Leang correlation. The Venturi correlations analyzed were the modified Murdock correlation and the de Leeuw correlation

The de Leeuw correlation had the best performance at all the tested pressures, limited to a maximum gas flow rate of 1000m^3/h. The homogeneous model had a good performance, improving with increasing pressure. The Venturi Murdock correlation did not perform better than it was expected. Steven observed that the pressure influences the magnitude of the Venturi meter wet gas error.

Using a surface fit software package; Steven found a correlation for two-phase flow in the Venturi as a function of a modified Lockhard-Martinelli parameter and Froude number. The performance of the correlation developed by Steven was better than that of all the previously mentioned, limited to a maximum gas flow rate of 1000m^3/h. It must be noted that all the above correlations, including Steven correlation, require the liquid flow rate as an initial input.

In actual two-phase metering field applications, the liquid flow rate is not known [7]. A meter which can measure the flow rate of the two phase flow components in a simple and economical way, without the requirement of the initial liquid flow rate knowledge is the goal of the oil and gas industry in the future.

Three-phase flow measurements

Literature on three-phase flow meters is almost entirely focused on the description of the types (construction) of multiphase meters. Most of the literature does not reveal the theory followed to determine the output of the multiphase flow meter such as the gas, liquid or oil flow rate, quality, gas volume fraction, velocity, etc. Some of the work performed on three-phase flow measurements is described.

Johansen and Jackson [23] used a dual mode densitometry method to measure the gas volume fraction in gas/oil/water pipe flows independent of the salinity of the water component. They applied this method to homogeneous and annular flows making use of the different responses in photoelectric attenuation and Compton scattering to changes in salinity.

The dual mode densitometry method used by Johansen and Jackson detects changes in salinity using one gamma-ray energy and two detectors. A traditional detector located outside the pipe is used to find the total attenuation coefficient. A second detector positioned between the source and transmission detector is used to measure the scatter response.

Results of the work showed that it is possible to measure the gas void fraction in homogeneously mixed multiphase flows using the dual modality densitometry principle independent of the salinity of the water. For the annular flow, the gas void fraction measurement was dependent on the salinity of the water due to the densitometer being less sensitivity to changes farther away from the source side of the pipe.

Fischer [24] proved experimentally that it is potentially feasible to measure oil/salt water/gas mixtures in pipelines using a combination of instruments consisting of a Venturi meter, a capacitance meter and a single beam gamma densitometer. The application of this method was for projects such as the exploitation of marginal offshore fields, oilfields and the piping of such mixed fluids to central production platforms onshore.

Pipe orientations studied were both horizontal and vertical. The test indicated that the instrument combination functions optimally with simple signal interpretation only if there is a truly homogeneous flow in pipeline. This means that the phase components should be distributed uniformly over the pipe cross section and flow approximately at the same velocities.

The measuring principle examined was subject to limitations in respect to installation position, pressure range and mixture composition. Fischer recommended a vertical installation for the instrument combination with the flow directed upwards. The smaller gravitational influence on the vertical arrangement made this one preferable to a horizontal arrangement. Actually, horizontal gravity causes stratification, which is bad for this system. Vertically upward flow causes churning and mixing across the pipe making the flow more homogeneous.

Fischer also mentions that symmetrical flow patterns are encountered in the pipeline or in the inlet section of the Venturi meter when the instrument combination is installed vertically. This helps assure the homogenization of the gaseous air phase and the liquid oil and water phases in the throat section. He also recommended the installation of a mixing device directly in front of the Venturi to achieve even better homogenization of components in separated flows.

Oddie et al. [25] conducted experiments on steady state and transient water-gas, oil-water and oil-water-gas multiphase flows in a transparent 11 m long, 0.15 m diameter, inclinable pipe using kerosene, tap water and nitrogen. The pipe inclination was varied from 0° (vertical) to 92° and the flow rate were 2, 10, 40, 100 and 130 m^3/hr for water, 5, 20, 50 and 100 m^3/hr for gas and 2, 10 and 40 m^3/hr for oil phase. The experiments were carried out at gage pressures below 6 bar.

Bubble, churn, elongated-bubble, slug and stratified/stratified-wavy flows were observed for the water-gas, and oil-water-gas flows, while dispersed/homogeneous, mixed/semi-mixed and segregated/semi-segregated flows were observed for the oil-water flows. The effects of the flow rates upon the different phases and pipe orientation on holdup were evaluated. Three major techniques were employed to measure steady state holdup: shut-in, electrical probe and nuclear gamma densitometer.

The employed electrical probe consists of ten electrical probes, regularly spaced along the pipe to measure the water depth. Each probe comprises of two parallel brass rods which are fixed along the pipe diameter. The measurement of the resistance between the wires allows for the determination of the water level around the probe.

Detailed flow pattern maps were generated over the entire range of flow rates and pipe inclinations for all of the fluid systems. The maps for the water-gas and oil-water-gas systems were found to be qualitatively similar. The observed flow patterns were compared with those predicted by a mechanistic model developed by Petalas and Aziz [26]. This mechanistic model was able to predict the experimentally observed flow pattern and holdup with high accuracy.

Hall, Reader-Harris and Millington [27] investigate the performance of different Venturi meters in multiphase flows. The meters were tested using a mixture of stabilized crude oil, magnesium sulfate solution and nitrogen gas with the gas void fraction ranging from 10 to 97.5% and 5 to 100% water cut. The β ratios tested were 0.4, 0.6 and 0.75.

The Venturi meters were installed in a horizontal orientation and consisted of an adaptor from class 150 to class 600 flanges, a machined spool piece, the Venturi meter, pressure recovery spool piece and an adaptor from class 150 to class 600 flanges. The whole assembly was installed in a 4 in horizontal line.

The discharge coefficient was evaluated for each test condition based on the mass flow rate from the reference metering system. Measurements of differential pressure between the Venturi throat and the upstream tapping and of the density from a gamma ray densitometer were made to complete the calculation.

The calculated discharge coefficient showed a significant variation with reference gas volume fraction and a smaller effect with reference water cut. A 0.6 β ratio and 21° cone angle Venturi was selected for the final evaluation. The results of the evaluation were empirically modeled. This model produces uncertainties of ±5% of liquid flow rate and ±10% of gas flow rate relative to the reference measurements.

CHAPTER III
OBJECTIVES

This work focuses in three objectives related to gas flow and multiphase flow measurements (wet gas) using differential pressure devices:

- To obtain high accuracy gas mass flow rate measurements using differential pressure meters at low differential pressure.

- To obtain the mass flow rate of the gas and liquid components in two-phase flows (wet gas) using differential pressure devices.

- To obtain the mass flow rate of the gas, liquid and oil components in three phase flows (wet gas) using differential pressure devices.

To reach these objectives, experimental work is done at the Turbomachinary Laboratory at Texas A&M University to generate the data. Three different pressure differential devices are used: slotted plate, standard orifice plate and a Venturi meter.

To meet the first objective, a slotted orifice plate is inserted in a 0.051 m (2 in) pipe to create a differential pressure in an air stream at different line pressures. A sonic nozzle bank is used to compute the mass flow rate through the system. The coefficient C_d is calculated and its behavior analyzed.

For the second objective, a wet gas is generated and the response of the differential pressure devices as a liquid flow rate is added to a gas stream is observed. To create the wet gas flow, water or oil is injected into the air stream in order to have a homogeneous two phase flow in which 90% or more of the volume flow rate be in the gas phase (gas void fraction). The quality of the homogeneous flow is varied at different line pressures and the theory developed by Fincke is applied.

To meet the third objective, a three component multiphase flow consisting of oil, water and air with gas void fraction equal or greater than 90% is used to observe the response of the differential pressure devices. Water and oil are mixed in a tank and then pumped into the air stream. It is suppose that the well-mixed liquids will act as a single liquid and then the same theory used in the two-phase flow is applied.

CHAPTER IV
EXPERIMENTAL FACILITIES

This chapter describes all physical aspects required to generate the data for low-differential pressure drop, two and three phase flow measurements. A description of the differential pressure devices used in the experimentation, included the instrumentation utilized to measure pressure, temperature and mass flow rate, is given. The data acquisition and data reduction procedures are also included.

General facilities

Figure 2 illustrates the general facilities employed in the experimental work. A Sullair compressor model 25-150 (17 m^3/hr at 860 kPa, 600 SCFM at 125 psig) and/or oil free Ingersoll-Rand compressor model SSR-1200H (34 m^3/hr at 860 kPa, 1200 SCFM at 125 psig) supplies air to the 2 in pipe system. After the air is dried and filtered, the air flow rate is measured using either a Quantum Dynamics turbine meter, model QLG 32 VWR1SC (0.142-7.08 m^3/min 5-250 ACFM range), a Daniel turbine meter model 3000 (0-2.83 m^3/min 0-100 ACFM range) or a sonic nozzle bank shown in figure 7.

A Rosemount 3050c model gage pressure transmitter measures air pressure and a T type thermocouple is used to measure temperature upstream of the turbine meter locations. An electro-pneumatic Masoneillan valve model 35-35212 (valve 2) is located after the turbine meters to control the mass flow-rate to the system.

The liquid is stored in a 0.81 m^3 stainless steel tank. A gear or a plunger pump is used to pump liquid. Either an Elite large Coriollis model CMF 025M319NU or small Coriollis model CMF 010 M323NU flow meter (for liquid mass flow rate less than 0.03 kg/s, 4 lb/min the small Coriollis flow meter is used) measures the liquid mass flow rate and density.

After the large Coriollis flow meter, a Massolinean valve (valve 3) controls the liquid flow rate. For the small Coriollis flow meter, the flow is split in two lines where two needle control valves regulate the flow rate. Liquid temperature is measured by a T-type thermocouple.

Water and/or oil are injected into the air stream and the two or three phases are mixed before the test zone. Gage pressure and temperature are measured after mixing by means of a Rosemount 3050c-model gage pressure transmitter (0-758 kPa, 0-110 psi range) and a T-type thermocouple respectively. A Massolinean valve (valve 1) is used to control the pressure in the meter run.

The flow meters, gage and differential pressure transducers and thermocouples are connected to a data acquisition system. The control valves are connected to control boxes to manually regulate the mass flow rate and the pressure in the system. A labView program controls the data acquisition system acquiring the raw data. A data file is generated which is then analyzed.

Test zone for two-phase measurements

For the two-phase flow measurements, a mixture of air-water or air-oil is used to produce a wet gas flow. Stacked Rosemount 3050c-model pressure-differential transmitters are used to measure pressure-differential. A stacked array of pressure-differential device with varying measurement ranges is shown in figure 3. Temperature between the individual components of the flow meters and at the end of meter run is measured using T-type thermocouples.

A single differential pressure device used for multiphase measurements would be the ideal case. However, not enough information is usually obtained from a single meter to estimate the gas and liquid flow rates. A combination of differential pressure devices has been used in many studies [21,22] in order to complement the information to compute the mixture component flow rates.

Three differential pressure devices are used in this work: slotted plate, Venturi meter and standard orifice plate. Because the slotted plate has shown good performance to ill-conditioned flows and less pipe length to recovery pressure [1], this device is located upstream.

Figure 4 presents arrangement of the meter components investigated in the two-phase air-water study. A combination of two slotted plates (β=0.43 and β=0.467 respectively) is tested in the first round. Then, a Venturi meter (β= 0.5271) is installed downstream of the β=0.467 plate for the second round. Finally, a standard orifice plate (β=0.508) replaces the Venturi meter for the third round. Additionally, a combination of slotted and standard plate (β=0.43 and β=0.508 respectively) is tested.

Oil (0.88 specific gravity and 0.1002 kg/m·s dynamic viscosity) and water are used as the working liquids for the two-phase work. The gear pump supplies the water while a plunger pump is used for the oil. The qualities of the mixture flow are obtained in two ways: in the first case, a volumetric air flow rate is set and the liquid flow rate is varied to change the mixture quality. This process is repeated for different upstream line pressures.

In the second case, the liquid flow rate is maintained constant at a specified upstream line pressure and the gas flow rate is varied to change the mixture quality. The liquid flow rate is then changed to obtain another set of data at the same upstream line pressure. The process is repeated for different upstream line pressure. Valves 1 and 2 are utilized to set the gas volumetric flow rate in both cases.

The differential pressure transducers illustrated in figure 3 are identified as 1A, 2A, 3A, 1B, 2B, 3B, 1C, 2C and 3C. These transducers are used for the air-water flow case. The A transducers are calibrated in a 0-241 kPa (0-35 psi) range; the B transducers are calibrated in a 0-69 kPa (0-10 psi) range and the C transducers in a 0-14 kPa (0-2 psi) range. A combination of three different differential pressure flow meters can be used in this test section.

In the air-oil flow study, the 0.43 slotted plate-0.467 slotted plate-Venturi meter arrangement is utilized as shown in figure 5. SMG 170-A1A and SMG 170-E1A model multivariable Honeywell digital transducers are used to monitor the upstream pressure, differential pressure, and temperature in the β 0.43 and 0.467 slotted plates respectively.

To measure the temperature, a T-type thermocouple is connected to the multivariable transducers. A Honeywell STD120-E1A differential transducer (0-103 kPa, 0-15 psi range) monitors the Venturi pressure drop. The Honeywell transmitters are connected to the data acquisition computer by way of a digital interface.

Test zone for three-phase measurements

The facility for three phase flow measurements is basically the same as for two-phase measurements. The supply tank is filled with an oil/water mixture and the facility is operated the same way as the two-phase facility. It is intended that the oil-water flow acts as it were a single liquid. The oil used emulsified very well with the water. A 25% oil and 75% water liquid combination showed negligible separation after three weeks setting in a jar.

To assure a uniform mixture, the oil and water are mixed in the tank by means of a mixer as shown in figure 6 and then pumped to the system by a triplex plunger pump. Depending of the mass flow rate, the small or large Coriollis meter is used to measure the mass flow rate as well as the density of the liquid mixture.

A Massoneilan valve controls the liquid mixture flow rate when the flow passes through the large Coriollis meter or by two needle valves when the flow passes through the small Coriollis meter. The β=0.43 and β=0.467 slotted plates followed by the Venturi meter arrangement is tested for the three-phase flow.

SMG 170-A1A and SMG 170-E1A model multivariable Honeywell digital transducers are used to monitor the upstream pressure, differential pressure and temperature in the β 0.43 and 0.467 slotted plates respectively. A Honeywell STD120-E1A differential transducer (0-103 kPa, 0-15 psi range) monitors the Venturi differential pressure. The recovery pressure is measured in the Venturi meter to investigate a possible technique to measure the mass flow rate of the multiphase flow components. A Rosemount gage pressure transmitter is used to obtain this differential pressure.

Two liquid mixture specific gravities are set for the three-phase flow: 0.91 and 0.94. A third specific gravity of 0.97 was tried; however, the pump system was not able to supply this liquid mixture to the meter run. It is supposed that the air bubbles trapped inside the liquid cause the pump to fail.

The specific gravities are obtained by adding water to the oil in the mixing tank and measuring the resulting mixture density with the Coriollis flow meter. To assure through liquid mixing, the mixture is allowed to flow through the pipe system and recirculates for a certain time.

To set different qualities in the mixture flow, the liquid flow rate is maintained constant at a specified upstream line pressure and the gas flow rate is varied to change the mixture quality. The liquid flow rate is then changed to obtain another set of data at the same upstream line pressure. The process is repeated for different upstream line pressure. Valves 1 and 2 are utilized to set the gas volumetric flow rate in both cases.

Test zone for low differential pressure measurements

A β=0.467 slotted plate was tested to determine its response at low differential pressures in single-phase flow measurements. As shown in figure 7, air is supplied to the 0.051 m pipe (2 in) system by the oil free Ingersoll-Rand compressor. A Rosemount pressure transducer (model 3050c with a 0-758 kPa, 0-110 psi range) and a T-type thermocouple are used to measure pressure and temperature respectively before the Massoneillan control valve (valve 2).

Two sonic nozzles (critical flow Venturi) are used to measure the air mass flow rate. Sonic nozzle 1 has a 0.322 cm (0.127 in) throat and 0.785 cm (0.309 in) exit diameter respectively; sonic nozzle 2 has a 0.457 cm (0.18 in) throat and 1.077 cm (0.424 in) exit diameter respectively. A Honeywell pressure transducer model STG17L-E1G (with a 0-1034 kPa, 0-150 psi range) is used to measure the upstream pressure in nozzle 1 while a Rosemount gage pressure transducer model 3500c (with a 0-758 kPa, 0-110 psi range) measures the upstream pressure in nozzle 2

It is assumed that the temperature difference in the inlet of the two sonic nozzles is negligible, hence, only one T-type thermocouple is used to measure the temperature in both sonic nozzles as indicated in figure 7. An Omega pressure transducer with a 0-689.5 kPa (0-100 psi) range is located near the thermocouple to monitor the upstream nozzle pressure. Two ball valves (Vb1 and Vb2) block the air flow-rate when either nozzle 1 or nozzle 2 is not used.

Two Honeywell multivariable transducers, model SMA110-A1A (0-68.9 kPa, 0-10 psi range) and SMG170-E1G 0-13.79 kPa (0-2 psi) range, are utilized to measure the upstream pressure, temperature and differential pressure for the slotted plate as shown in figure 8. The multivariable transducer measures simultaneously the pressure drop, gage pressure, and temperature. A T-type thermocouple is connected to the 0-68.9 kPa (0-10 psi) range multivariable transducer.

Valve 2 controls the air mass flow rate in the system. A Masoneillan control valve (valve 4) is placed at the end of the system to control the upstream slotted plate pressure. When the sonic nozzles are choked, the mass flow rate is attained from the measured sonic nozzles upstream conditions.

As long as the pressure drop across the sonic nozzle is sufficient to choke the flow, various lower downstream pressures are possible. Thus, it is possible to operate the slotted plates at different line pressures for a given mass flow rate, which results in varying pressure differential.

Differential pressure devices

Figure 9 illustrates the β=0.43 and β=0.467 slotted plates utilized in the experimental work. Figure 10 shows the slot details of the plates. Each plate has two arrays of slots. The peripheral array in the β=0.43 plate has 32 slots while the central array has 8 slots. According to the geometrical dimension shown in figure 10, the β=0.43 slot has an area of 0.1212 cm^2 (0.0188 in^2), then the total area is 3.88 cm^2 (0.6016 in^2). The square root of the ratio of the total slot area to the pipe cross section is the beta ratio.

The peripheral array of the β=0.467 plate has 18 slots and the central array has 8 slots. The slot area for this plate is 0.17 cm^2 (0.0264 in^2); then, the total area is 4.4284 cm^2 (0.6864 in^2). Figures 11 and 12 show the sharp edge orifice plate and the Venturi meter respectively used in the experimental work. The Venturi meter was machined at the Turbomachinary Laboratory shop. It is basically an aluminum piece inserted in two stainless steel spools.

Data acquisition

This section presents the data acquisition system utilized in the experimental work. A description of the hardware and software components is given. The first part of the description focuses on the analog instruments employed in the experimentation. The system was modified during the study to include the digital multivariable transducers.

Hardware

A MicroAge computer powered by a Pentium II processor is the central component of the data acquisition system hardware. The computer housed two data acquisition boards (DAQ) manufactured by Measurement Computing Inc: CIO-DAS802/16 and CIO-EXP32. These boards are used for converting analog signals into a digital form.

The CIO-DAS802/16 board has 8 analog inputs with 16-bit resolution. Only 4 of these inputs are used. Three of them are designated as 0, 1 and 7 respectively and are connected to the CIO-EXP32 expansion board. The CIO-EXP32 board has 32 channels, 16 of these channels (0-15) are multiplexed on to channel 0 of the CIO-DAS802/16 board, and the other 16 are multiplexed to channel 1. Channel 7 is a cold junction reference for thermocouple inputs.

Six out of the 16 channels contained in 0 are used for temperature measurement. These channels correspond to the thermocouple located near the Daniel and Quantum turbine meter, the thermocouple located in the liquid section and four thermocouples located in the test zone to monitor the upstream and downstream temperatures of the differential pressure devices under test.

Of the 16 channels contained in 1, 2 channels are used for recording gage pressure in the turbine meter and the upstream test section respectively. Nine channels are used for the differential pressure reading, 2 for the liquid density from the Coriollis meters and 3 for the flow rates from the Coriollis and turbine meters. Cold junction compensation temperature of the screw terminal on the computer board is recorded by Channel 7 of the CIO-DAS802/16 board. The fourth channel from the CIO-DAS802/16 board is used in measuring pressure.

A connection was established from the expansion board to the CIO-DAS802/16 board in the computer through a 37-pin connector. The CIO-DAS802/16 board only can detect a voltage signal while the output signals from all the instruments is in a 4-20 mA range form. These signals must be passed through a resistor to create a voltage drop, which is supplied as an input to the CIO-DAS802/16 board.

Software

A LabVIEW graphical program is used for monitoring and recording pressure, density, temperature, and flow rate. The program utilizes the calibration curve of every instrument to compute the variable value from the signals received from the experimental system. The calibration performed on each instrument is a linear function of the voltage.

The calibration is represented by a straight-line equation given by:

$$y = m{\cdot}x + c. \tag{5}$$

The quantity to be measured is represented by y, x is the voltage signal produced by the measuring instrument, m the slope of the linear curve fit and c the interception of the linear curve for the instrument calibration.

The LabView program has a module where the calibration equations are input. There are nine inputs for the differential pressure transducers, two for the absolute pressure transducers, two for the water flow rates, two for the water densities, and one for the air flow rate. The input values can be changed depending on the instrument in use. A channel number is assigned to each variable, corresponding to a certain channel on the expansion board.

The number of data points to be recorded is set to 100 at a sampling rate of 500 milliseconds between each data point. This process is performed twice. Mean and standard deviation of the results for each of these 100 data points are calculated and averaged. The percentage error is calculated by subtracting the mean of the first 100 samples from the mean of the second 100 samples and dividing this difference by the mean of the first 100 samples.

The percentage difference is compared to a maximum allowable percentage difference specified in the program. If the percentage difference is within the limit, the data is saved. If the percentage difference is found to be very high, an error message is displayed and data must be retaken. Plots of the real time data are supplied in a separate window to visualize the behavior of the parameters.

Hardware and software modification for digital instruments

Digital multivariable transducers were obtained as a donation from Honeywell part way through the project. Therefore they are used in the experimental work to analyze their effect in the measuring process. These instruments measure the upstream gage pressure, differential pressure and upstream temperature in the differential pressure flow meters under investigation. The hardware and software described above used with the analog instruments are also used with the digital instruments

A four-channel RGC circuit board is utilized to acquire the multivariable transducer outputs in digital form. The board is connected to a Dell700 laptop computer where the RGC/2000 controller software is used to establish digital communication between the laptop computer and the transducers.

To input the multivariable transducer readings into the LabView program, there must be a connection between the Dell7000 computer and the data acquisition system (DAC) in the MicroAge computer. To establish the connection, the Dell7000 system is placed on a local network with the MicroAge computer. The LabView program can access a data file name livedata.txt.

The livedata.txt file is continuously updated with the most recent readings from the Honeywell transmitters. The LabView program utilizes these readings in the same manner as the analog readings.

Instrument calibration

The following procedures were used to calibrate the pressure transducers, the Coriollis flow meters and the turbine meters. Calibrations were performed using the computer system, so transducer, A/D board, etc. were calibrated as one unit. LabView was also used for the calibration process.

Pressure transducer calibration

Nine Rosemount differential pressure transducers and two absolute pressure transducers were used for differential pressure and gage pressure measurements respectively. The differential transducers were calibrated en masse. The absolute pressure transducers were calibrated separately. The calibration of these instruments was done without removing them from their fixed positions.

An Ametek Model RK-300 pneumatic dead weight pressure tester was used to calibrate the Rosemount pressure transducers. The dead weight pressure tester was attached to a common line for the differential pressure meters. It was done in such a way that an equal pressure be applied on all the high-pressure port legs, one for each meter.

The high-pressure ports of all the transducers were pressurized in this way. The common line allowed the high-pressure port to be pressurized without letting any gas into the slotted plate section. The low-pressure port leg connected to the low-pressure ports of all the nine transducers was opened to the atmosphere.

Each differential pressure meter had three pressure transducers (figure 3) and they were calibrated for three different ranges. These transducers were arranged from top to bottom in the range of high, medium and low pressures, respectively. The zero and span of each row of transducers is set.

Zero corresponded to the minimum differential pressure measured by the transducer. Applying the maximum desired differential pressure and then pushing the span button set the span of the transducer.

A LabView program was made for the pressure transducers calibrating process. This program recorded the value of the average voltage signal over 200 data points corresponding to the pressure applied by the dead weight tester. Calibration was done comparing the pressure from the dead weight tester to the voltage output from the pressure transducer.

The pressure applied for each row of transducers was plotted against the voltage. Linear curve fits were made to express the differential pressures as a function of the voltage output for each transducer as shown in equation 5. These linear curve fits were then entered into the data acquisition

Calibration of the absolute pressure transducers was made individually using the dead weight pressure tester. Pressure was applied in an increasing order then plotted against voltage for each transducer. Linear curve fits were obtained representing the pressure as a function of the voltage as defined in equation 5.

Coriollis flow meter calibration

The weighing method is used to calibrate the small and large Coriollis flow meters. A bucket weighed before the calibration was used for collecting water, which flowed out of the meter. A LabView program was used for data acquisition. The liquid flow rate was set using the needle valves for the small Coriollis meter and the Massoneillan valve (valve 3) for the large Coriollis meter. Water was allowed to flow into the bucket once the program was started. At the end of data acquisition the bucket was removed. The time taken for the data to be recorded was simultaneously measured using a stopwatch.

The bucket was again weighed this time with water in it. The weight of the water was calculated from this. The voltage corresponding to this flow rate was measured simultaneously. From the weight of the water collected in the bucket and the time taken for filling the bucket, the flow rate of water was calculated. This procedure was repeated for different flow rates. The flow rates thus obtained were plotted against voltages and a linear curve fit (equation 5) was obtained from this plot. This equation was then used in the data acquisition program.

Turbine meter calibration

The Daniel and Quantum turbine meters were calibrated against a sonic nozzle bank, which consists of 4 nozzles inserted in parallel 0.051 (2 in) pipes. The throat diameter for each nozzle is 0.35 cm (0.138 in), 0.493 cm (0.194 in), 0.699 cm (0.275 in) and 0.988 cm (0.389 in) respectively. The nozzles were combined to obtain different mass flow rates.

Because the turbine meter gives the volumetric flow rate as a frequency of the pulses generated by the rotor, a frequency/ pulse signal conditioner model DRN-FP was used to convert the frequency to DC output (0-10 Volt range, 10 mA maximum current). In this way, the turbine meter has a voltage output range similar to that of the other transducers.

An omega pressure transducer with a 0-689.5 kPa (0-100 psi) range and a T-type thermocouple measure the upstream pressure and temperature of the nozzle bank. Volumetric flow rate in the turbine meter was obtained from the sonic nozzle combinations and was plotted against the voltage to obtain an expression in the form of equation 5.

Data reduction

The procedure employed to calculate the parameters such as density, quality, discharge coefficient, velocity, etc. is given in this section. Two-phase data reduction is shown first followed by the three-phase case. Finally the low pressure differential analysis is presented. The data recorded from the various instruments and stored in the data files are used to calculate the results.

<u>Two-phase flow data reduction</u>

The raw data were analyzed using MathCad V2000. It was assumed that a homogeneous air-water and air-oil mixture flowed through the meters. The first parameter computed from the measured quantities, assuming an ideal gas, is the gas density as shown in equation 6. The liquid density was assumed to be a known value. The flow's quality is computed using the measured gas and liquid flow rates as shown in equation 7.

$$\rho = \frac{P}{R \cdot T} \qquad\qquad (6)$$

$$Qual = \frac{\dot{m}_g}{\dot{m}_g + \dot{m}_l} \tag{7}$$

Where $\dot{m}_l$ is given directly for the Coriollis meters and $\dot{m}_g$ is calculated by multiplying the volumetric flow rate by the gas density for the turbine flow meters.

Knowing the quality, the gas and liquid density, the mass based mixture density is calculated by means of equation 8. By using this equation, no phase change of the water is assumed. Another parameter to be used in the analysis is the ratio of the pressure drop to the upstream absolute pressure presented in equation 9.

$$\rho_{mix} = \frac{\rho_g \cdot \rho_l}{Qual \cdot \rho_l + (1 - Qual) \cdot \rho_g} \tag{8}$$

$$dP/P = \frac{\Delta P}{Pabs} \tag{9}$$

In order to know the upstream velocity of each phase, the volumetric flow rate and the gas void fraction of the mixture must be known. The first parameter is computed applying equation 10 to the gas, liquid and mixture flow. Then, the gas void fraction, equation 11, is computed and, from the continuity equation, the gas, liquid and mixture velocities are obtained using equations 12, 13 and 14.

The downstream velocities are obtained with the same procedure, equations 15, 16 and 17. These vary from the upstream velocities due to the gas density change with pressure difference across each meter and the smaller cross-sectional flow area in the meter.

$$q = \frac{\dot{m}}{\rho} \tag{10}$$

$$\alpha = \frac{q_g}{q_g + q_l} \tag{11}$$

$$U_{gu} = \frac{\dot{m}_g}{\alpha_u \cdot \rho_u \cdot A} \tag{12}$$

$$U_{lu} = \frac{\dot{m}_l}{(1-\alpha_u) \cdot \rho_l \cdot A} \tag{13}$$

$$U_{mu} = \frac{\dot{m}_g + \dot{m}_l}{\rho_{mixu} \cdot A} \tag{14}$$

$$U_{gd} = \frac{\dot{m}_g}{\alpha_d \cdot \rho_{gd} \cdot A_o} \tag{15}$$

$$A_o = \beta^2 \cdot A$$

$$U_{ld} = \frac{\dot{m}_l}{(1-\alpha_d) \cdot \rho_l \cdot A_o} \tag{16}$$

$$U_{md} = \frac{\dot{m}_g + \dot{m}_l}{\rho_{mixd} \cdot A_o} \tag{17}$$

From the homogeneous flow assumption, gas, liquid and mixture velocities must be the same. Figure 13 shows a comparison of the upstream and downstream velocities for the $\beta=0.43$ plate taken at different upstream line pressures. The same behavior is observed in all the differential pressure devices analyzed. It is seen that all three of the computed velocities are essentially the same.

Three-phase flow data reduction

If two different liquids (water and oil) are present in the wet gas flow and the assumption that they act as a single liquid is made then, the resulting three-phase flow (air, oil and water) could be considered as two-phase flow and the two-phase procedure applied.

If the last assumption is correct, parameters such as Ug and ρ_{mix} can be estimated in the same way as in the two-phase flow. What would remain is to estimate the oil and water flow. This estimation requires either the liquid density or the water cut. However these parameters are unknown in the three-phase flow since they depend on the amounts of water and oil. The water cut is defined by equation 18.

$$WC = \frac{q_w}{q_w + q_o} \qquad (18)$$

Low pressure drop analysis data reduction

For the low-pressure drop analysis, the first parameter to be computed is the mass flow rate from the sonic nozzles. It is supposed that the pressure gage and temperature measured at the nozzle inlet are similar to the stagnation conditions. Assuming an ideal gas, when the nozzle is choked, the throat conditions are computed as follows:

$$T_t = 0.8333 \cdot T_o \qquad (19)$$

$$P_t = 0.5283 \cdot P_o \qquad (20)$$

The t and o subscripts in equations 19 and 20 indicates throat and stagnation conditions respectively. Pressure and temperature are in absolute values. The density at the throat can then be computed using equation 6 and, assuming a Mach number of 1, the velocity at the throat can be calculated by means of equation 21. Finally, the mass flow rate can be obtained from equation 22.

$$U_t = \sqrt{k \cdot R \cdot T_t} \tag{21}$$

$$\dot{m} = C_d \cdot A_t \cdot \rho_t \cdot U_t \tag{22}$$

The values of Cd for the sonic nozzles were supplied by CEESI (Colorado Engineering Experimental Station Inc) who performed a NIST (National Institute of Standards and Technology) traceable calibration of the nozzle.

Knowing the mass flow rate through the slotted plate, the discharge coefficient C_d is estimated by means of equation 23. The parameters in equation 23 correspond to the upstream slotted plate position; the density is computed using equation 6. To compute dP/P and velocity, equations 9 and 12 are respectively used.

$$C_d = \frac{\dot{m} \cdot \sqrt{1 - \beta^4}}{A \cdot \beta^2 \cdot \sqrt{2 \cdot \rho \cdot \Delta P}} \tag{23}$$

CHAPTER V
RESULTS AND DISCUSSION

The response of differential pressure flow meters to the presence of air and water in the fluid stream was investigated to look for a correlation that describes the meter response. This was done for a standard orifice plate, two slotted plates and a Venturi flow meter. The effects of meter interaction and fluid stream content were investigated. A correlation that involves only one pressure drop meter is evaluated first, then the responses of the differential pressure devices are combined.

Following the work presented by Fincke [21], the Bernoulli equation is applied to each phase. In addition, it is also applied to the mixture flow, from upstream of the obstruction to the flow at the smallest area of the meter. The upstream half of the Bernoulli equation for the gas, liquid and mixture flow appears in equation 24, 25 and 26 defined as the head symbolized by H_{gu}, H_{lu} and H_{mu} respectively. The downstream half of Bernoulli equation appears in equations 27, 28 and 29 represented by H_{gd}, H_{ld} and H_{md} for the gas, liquid and mixture flow respectively. For ideal flow conditions, $H_{gu}=H_{gd}$, $H_{lu}=H_{ld}$ and $H_{mu}=H_{md}$.

$$H_{gu} = P_u + \frac{1}{2} \cdot \rho_{gu} \cdot U_{gu}^2 \tag{24}$$

$$H_{lu} = P_u + \frac{1}{2} \cdot \rho_{water} \cdot U_{lu}^2 \tag{25}$$

$$H_{mu} = P_u + \frac{1}{2} \cdot \rho_{mixu} \cdot U_{mu}^2 \tag{26}$$

$$H_{gd} = P_d + \frac{1}{2} \cdot \rho_{gd} \cdot U_{gd}^2 \tag{27}$$

$$H_{ld} = P_d + \frac{1}{2} \cdot \rho_{water} \cdot U_{ld}^2 \tag{28}$$

$$H_{md} = P_d + \frac{1}{2} \cdot \rho_{mixd} \cdot U_{md}^2 \tag{29}$$

Because of the irreversible losses through the meter, the upstream and downstream heads of the Bernoulli equation are not equal. To take into account these losses, three terms are defined for the gas, liquid and mixture flow: equations 30, 31 and 32. These terms are the difference between the upstream and downstream part of the Bernoulli equation.

$$\Delta H_g = H_{gu} - H_{gd} \tag{30}$$

$$\Delta H_l = H_{lu} - H_{ld} \tag{31}$$

$$\Delta H_m = H_{mu} - H_{md} \tag{32}$$

Combining the Bernoulli and continuity equations and assuming no density change through the meter, a standard obstruction flow meter discharge coefficient is defined by equations 33, 34 and 35 for the gas, mixture and liquid flow respectively. Figures 14, 15 and 16 present the C_g, C_l and C_m coefficients for the slotted plates (β=0.43 and β=0.467) Venturi meter and standard plate respectively.

Figure 14 shows the dependence on dP/P of the C_g coefficient for the Slotted plates (β=43 and β=467), the Venturi and standard plate. It is observed a similar slope for all the meters, which means a similar expansion factor.

The interception point for the standard plate is less than that of the other meters while that of the slotted plates and the Venturi is similar, showing the Venturi meter a light deviation from the slotted plate lines as dP/P increases. It is interesting to observe that moving the Reynolds number dependence to ΔH and letting the expansion factor separate, all the three types of differential pressure meters have the same slope over such a wide range of dP/P.

Figure 15 presents the C_l dependence on dP/P for the Slotted plates (β=43 and β=467), the Venturi and standard plate. The slope of the curves is similar as in the C_g case but the difference in the interception between the standard plate and the other meters tends to reduce. C_m dependence on dP/P is shown in figure 16; its behavior is basically the same as the C_g coefficient. The plots were done in a Reynolds number range of 112000-440000 and quality range of 0.37-0.99.

$$C_g = \frac{\dot{m}_g \cdot \sqrt{1-\beta^4}}{\alpha_u \cdot A \cdot \beta^2 \cdot \sqrt{2 \cdot \rho_{gu} \cdot (\Delta P - \Delta H_g)}} \qquad (33)$$

$$C_m = \frac{(\dot{m}_g + \dot{m}_l) \cdot \sqrt{1-\beta^4}}{A \cdot \beta^2 \cdot \sqrt{2 \cdot \rho_{mixu} \cdot (\Delta P - \Delta H_m)}} \qquad (34)$$

$$C_l = \frac{\dot{m}_l \cdot \sqrt{1-\beta^4}}{(1-\alpha_u) \cdot A \cdot \beta^2 \cdot \sqrt{2 \cdot \rho_{water} \cdot (\Delta P - \Delta H_l)}} \qquad (35)$$

Figure 17 to 28 show the curve fitting for C_g, C_l and C_m as a function of dP/P for each differential pressure meter with an equation in the form $y = a \cdot x + b$. It can be seen that the value of the slope for the coefficient C_g is similar in all but the Venturi meter. This is probably due to wall friction effects.

A value greater than 1 is observed in the interception point (the incompressible factor) for the slotted plates and the Venturi meter. The greatest error in the curved fitting process is exhibited by the $\beta=0.467$ slotted plate with a standard deviation of 0.000904.

The coefficient C_l shows a similar slope for the two slotted plates as seen in figure 21 and 22. This slope differs from that of the Venturi meter and the standard orifice. It is seen that the interception point for the C_l coefficient is similar for the slotted plates and the Venturi meter while that of the standard orifice has a less value. The greatest error in the C_l curve fitting is shown by the standard orifice with a standard deviation of 0.00081. The behavior of the coefficient C_m is similar to that of C_g.

The cross sectional flow area for the gas flow in equation 33 is defined by $\alpha_u \cdot A$ while $(1-\alpha_u) \cdot A$ represents the liquid cross section area (equation 35). The highly repeatable and accurate values of discharge coefficients as a function of dP/P are very desirable. Thus, to calculate the mass flow rate of the individual components of the mixture, the void fraction, gas, liquid or mixture density and head loss terms must be determined first.

Two methods were tried to compute the terms defined by equations 30, 31 and 32. The first one is based in an empirical correlation that involves Euler number. The second one uses the pressure drop response of the differential pressure device to estimate the parameters.

Proposed velocity estimation based on Euler number

From the Bernoulli and continuity equation applied to the gas flow, the gas mass flow rate is expresses by equation 36.

$$\dot{m}_g = \frac{\alpha \cdot A \cdot \beta^2 \cdot C_g}{\sqrt{1-\beta^4}} \cdot \sqrt{2 \cdot \rho_g \cdot (\Delta P - \Delta H_g)} \qquad (36)$$

Since $m_g = \alpha \cdot A \cdot \rho_g \cdot U_g$, then the void fraction can be eliminated from the equation by solving for the gas velocity (volumetric flow rate)

$$\rho_g \cdot U_g = \frac{\beta^2 \cdot C_g}{\sqrt{1-\beta^4}} \cdot \sqrt{2 \cdot \rho_g \cdot (\Delta P - \Delta H_g)} \tag{37}$$

There are two unknowns in this equation: the upstream gas velocity U_g and the head loss in the gas phase ΔH_g; C_g can be obtained from calibration as a function of dP/P and it is assumed the gas density is known as in a single phase meter. Since no other equation can be obtained from theory, an empirical relation where ΔH_g and U_g are related is necessary.

An empirical relationship (equation 38) which expresses ΔH_g as a function of ρ_{gd}/ρ_{gu} and the gas Euler number was obtained using TableCurve 3D v4. Figure 29, 36 and 39 show the correlations for the slotted plate, the Venturi meter and the standard plate. DenR, Eu_{dPs} and $Eu_{\Delta Hg}$ are defined by equations 39, 40 and 41 respectively. The density presented in these equations corresponds to the gas phase.

$$\Delta H_g = (\frac{\rho_{gd}}{\rho_{gu}}, Eu_g) \tag{38}$$

$$DenR = \frac{\rho_{gd}}{\rho_{gu}} \tag{39}$$

$$Eu_{\Delta Ps} = \frac{\sqrt{\frac{dP}{\rho_g}}}{U_g} \tag{40}$$

$$Eu_{\Delta Hg} = \frac{\Delta H_g}{\rho_g \cdot U_g^2} \tag{41}$$

Equation 37 is solved for the ΔH_g term, which is combined with the empirical correlation. The Euler number ($\Delta P/\rho U^2$) has been shown by Morrison et al to be an important parameter for two-phase flows [2]. This procedure was applied to the slotted plate, the standard plate and the Venturi.

Proposed ΔH_g estimation based on pressure drop

The second method used to estimate the parameter defined by equations 30 31 and 32 uses the pressure drop from the differential pressure devices. ΔH_g, ΔH_l and ΔH_m describe the loss experienced by the gas, liquid and mixture flow respectively. Since these losses are expressed as a function of the pressure drop, velocity and density, and the last two parameters depend on pressure drop, a correlation indicated by equations 42, 43 and 44 was tried to get ΔH_g, ΔH_l and ΔH_m.

The assumption described previously was applied to the slotted plates, the Venturi meter and the standard orifice plate. For the Venturi meter case the recovery pressure was also utilized. The combination of the pressure differentials from the different devices used in the tested arrangements was also used to estimate ΔH_g, ΔH_l and ΔH_m.

$$\Delta H_g = f(\Delta P, \rho_g) \tag{42}$$

$$\Delta H_l = f(\Delta P, \rho_l) \tag{43}$$

$$\Delta H_m = f(\Delta P, \rho_m) \tag{44}$$

Air-water test results

Experiments with air-water flows with qualities higher than 0.3, gas void fractions higher than 0.98 (wet gas) and line pressure from 207 to 620.5 kPa (30 to 90 psi) were carried out. Results presented in the following paragraphs correspond to the velocity estimation based on Euler number applied to the slotted plate, Venturi and standard plate and to the ΔH_g estimation based on the pressure drop response.

Results using the velocity estimation based on Euler number (air-water flow)

It was found that by selecting a certain form of the empirical correlation for ΔH_g, which include polynomial terms of ρ_{gd}/ρ_{gu} and added terms of Eu_{dPs} and $Eu_{\Delta Hg}$, and then combined with equation 37, a simple quadratic equation for U_{gu} in terms of known quantities can be obtained. This procedure was applied to the slotted plate, standard plate and Venturi meter. Results are shown in the following paragraphs.

Slotted plate (air-water flow)

Figure 30 shows the two roots for the quadratic equation corresponding to the $\beta=0.43$ slotted plate. For all the analyzed set of data the approximately correct solution is the root:

$$U_{root} = \frac{-B_c - \sqrt{B_c^2 - 4 \cdot A_c \cdot C_c}}{2 \cdot A_c} \tag{45}$$

Where

$$A_c = f(\Delta P, P_u, \rho_{gu}, \rho_{gd}) \tag{46}$$

$$B_c = f(\Delta P, \rho_{gu}) \tag{47}$$

$$C_c = f(\Delta P) \tag{48}$$

It can be seen that the estimation of the flow velocity is a function of the relatively easy measured or calculated parameters: ΔP, P_u, ρ_{gu} and $\rho_{gd.}$

Mixture density estimation using the calculated velocity (air-water flow)

At this point, the gas flow rate can be estimated by assuming $\alpha \approx 1$. Figure 31 shows that this is a reasonable assumption. To know the liquid and the total mass flow rate, either the gas void fraction, the quality or the mixture density must be known.

It was found that the gas void fraction can be empirically obtained using the estimated gas velocity, U_{root}, the differential and upstream pressure, and the upstream gas density (figure 32).

$$\varepsilon = f(U_{root}, \Delta P, \rho_g, P_u) \tag{49}$$

$$\varepsilon = 1/\alpha \tag{50}$$

Under the assumption of homogeneous flow, the mixture density can be estimated from equation 51.

$$\rho_{mix}=\alpha \cdot \rho_g + (1-\alpha) \cdot \rho_l \tag{51}$$

Once the mixture density is known, the flow's quality may be calculated. All of this analysis was performed with an air/water mixture. It may change when other fluid combinations are considered.

Figure 33 shows the error of the estimated mass flow for the gas, liquid and total flow. It is seen that for the gas flow rate, the maximum error is approximately 4%; the maximum error for the total mass flow rate is approximately 5%. For the water flow rate, error increases abruptly when quality is greater than 0.95 reaching 250%.

Standard deviations for the estimated gas, liquid and total flow rates which is computed using equation 52, are 0.015, 0.21 and 0.014 respectively. For quality values greater than 0.95, liquid flow rate tends to zero, so liquid error computation is divided by a number that tends to zero making a large number as result.

$$\sigma = \sqrt{\sum_{i=0}^{N} \frac{1}{N} \left(\frac{X_{fit}}{X_{meas}} - 1 \right)^2} \tag{52}$$

Error for the estimated quality and gas void fraction is presented in figure 34. It is seen that the maximum error for the quality is 4% approximately. The estimated gas void fraction maximum error is -2% approximately validating the use of the assumed value of one. The last three parameters show certain relationship with the differential pressure. The error in the estimated flow velocity is similar to that of the gas mass flow rate.

Venturi meter (air-water flow)

Figure 35 shows the dP/P dependence of the Venturi coefficients defined by equations 32, 33 and 34 for the gas, liquid and air-water mixture flow rate. A quadratic empirical equation, which express ΔH_g as a function of the gas velocity, is presented in figure 36. This equation is combined with equation 37 in order to obtain a quadratic equation for the gas velocity.

The Fstat parameter in the plot shown in figure 36 is considerable less than that of the $\beta=43$ slotted plate case. Fstat is the ratio of the mean square regression to the mean square error and is defined in equation 53; together with the coefficient of determination (r^2) and the standard deviation (FitStdErr) indicates the goodness of the correlation. The greater the Fstat value the better.

The coefficient of determination (r^2) and the standard deviation do not exhibit a considerable difference from that of the slotted plate case. The results for the gas flow computation for the Venturi meter, using the before mentioned procedure are presented in figure 37. A much larger error than in the slotted plate meter is seen in figure 37, it is probably due to the wall friction effects on the converging section of the Venturi. The standard deviation for this estimation is 0.066

$$\text{Fstat} = \frac{n - m}{m - 1} \cdot \sum_{i=1}^{n} \frac{(z_i - \bar{z})^2 - (\hat{z}_i - z_i)^2}{(\hat{z}_i - z_i)^2} \tag{53}$$

Standard plate (air-water flow)

The air-water results for the standard orifice plate are presented in figures 38, 39 and 40. The arrangement used in these experiments is the β43-β467-β508. Figure 38 shows the dP/P dependence of the orifice plate discharge coefficients defined by equations 33, 34 and 35 for the gas, liquid and air-water mixture flow rate respectively. The correlation for the ΔH_g term as a function of the gas velocity is shown in figure 39.

The Fstat parameter in the plot shown in figure 39 is considerable less than that of the β=43 slotted plate case. The coefficient of determination and the standard deviation dot not exhibit a considerable difference from that of the slotted plate case. Figure 40 presents the results for the gas flow computation with the standard orifice plate. The standard deviation for this estimation is 0.0071.

The performance of the standard plate is better than that of the Venturi meter and could be an indication that the wall friction influences the Venturi meter response. Probably the homogenization due to the β43 and β467 slotted plates increases the accuracy of the standard plate. The pressure difference range for the plot shown in figure 40 is 12.4-97 kPa (50-389 in_H20).

No a relation similar to that exhibited by the slotted plate was found for the standard orifice and the Venturi meter to estimate the mixture density. Then, only the gas flow rate was estimated with the empirical relation technique.

Results using the ΔHg estimation based on pressure drop response (air-water flow)

The response of the differential pressure device combination was tested for the air-water flow. It was found that the ΔH_g term could be estimated as a function of the standard plate pressure drop and also as a function of the Venturi pressure drop and the Venturi recovery pressure.

No relationship was found between the pressure and ΔH_g for the slotted plates, however, it seems they influence the response of the devices located downstream of them. The results obtained using the slotted plate and standard orifice combination are shown first followed by the results obtained using the slotted plate and Venturi meters.

β43-β467-β508 arrangement

The response of the β=0.43 and β=0.467 slotted plate and standard β=0.508 orifice plate combination in an air-water flow was investigated. It was observed that the ratio of ΔH_g for the standard orifice to the upstream orifice absolute pressure, (called $\Delta HgoP$ equation 54), exhibits a dependence on a term which is a function of the ratio of the orifice upstream density to the β=467 slotted plate upstream density minus the dP/P orifice ratio. This term is defined by equation 55 and is called Pρo. A correlation for the $\Delta HgoP$ term was obtained using TableCurve 2D and is presented in figure 41.

$$\Delta HgoP = \frac{\Delta H_g}{Pabs} \qquad\qquad (54)$$

$$P\rho o = \frac{\rho_{508}}{\rho_{467}} - dP/P_o \tag{55}$$

Knowing the ΔHgoP term for the standard orifice, ΔH_g can be estimated. Figure 42 presents the error in the ΔH_g computation. The standard deviation computed using equation (51) is 0.015. The gas Reynolds number, quality and upstream pressure range for these data is 115,000-360,000, 0.4-0.99 and 150-400 kPa (manometric) respectively. Once ΔH_g is obtained, it is possible to compute the gas velocity using equation 37.

Assuming $\alpha \approx 1$, the gas mass flow rate can also be calculated. Figure 43 shows the error obtained when estimating the gas mass flow rate; the error tends to increases as dP/P decreases reaching a maximum of 4.1% compared to the measured value. The standard deviation computed using equation (51) is 0.014. The results shown in figures 42 and 43 correspond to orifice plate pressure differentials of 12.4-96 kPa (50-385 in_H_2O).

$\beta43$-$\beta508$ arrangement

The response of the β=0.43 slotted plate and standard plate combination in an air-water flow was analyzed. As in the $\beta43$-$\beta467$-Standard plate case, the ΔHgoP of the orifice plate is represented as a function of Pρo as shown in figure 44. It is seen that the ΔH_g term can be directly estimated as in the previous case.

The error obtained when calculating ΔH_g and gas mass flow rate is presented in figures 45 and 46 respectively and corresponds to orifice plate pressure differentials of 6.7-81.1 kPa (27-326 in_H_2O). Using equation 52 the standard deviation for ΔHg and mass flow rate is 0.018 and 0.021 respectively.

It is observed in figure 46 that for dP/P less than 0.1 the error in the mass flow rate estimation using the standard plate in the $\beta43$-$\beta508$ arrangement is greater than in the $\beta43$-$\beta467$-$\beta508$ case. However, the differential pressure range for the standard plate of this last combination starts at 12.4 kPa (50 inH_2O) while the first case starts at 7.5 kPa (30 in_H_2O).

Applying the experimental equation method to the standard orifice plate, the standard deviation for the gas flow rate estimation is 0.07 while that using the differential pressure response is 0.021. The standard deviation for the mass flow rate estimation using the $\beta=43$ slotted plate is 0.014. It is important to know that the pressure drop in the standard orifice is not as low as in the $\beta43$ slotted plate.

<u>$\beta43$-$\beta467$-Venturi arrangement</u>

The previous technique applied to the standard orifice did not work for the Venturi meter. Thus, another method was tried. The Venturi differential (ΔP_v) and Venturi recovery pressures (Prv) were utilized to obtain a ΔH_g correlation. A combination of differential pressures in a Venturi meter (in the convergent zone, divergent zone and throat section) was used in the research done in ISA Solartron Inc [22] and the in the work developed by Fincke [21]. The way the recovery pressure is used in this work differs from these previous studies.

ΔP_v, Prv and ΔH_g were divided by the upstream absolute Venturi pressure and then plotted as shown in figure 47, where a standard deviation of 0.0016 is seen. This technique uses only the Venturi variables. The Venturi pressure drop range is 0.75-89.8 kPa (3-361 in_H_2O).

An increment of the error as the pressure drop decreases when estimating the ΔH_g and gas mass flow rate is seen in figure 48 and 49. For the ΔH_g case the error reaches 133% and a standard deviation of 0.246 while for the gas mass flow rate it reaches 62% and a standard deviation of 0.141.

An acceptable range for the gas mass flow rate computation is presented in figure 50 and corresponds to a pressure differential range of 12.4-90.6 kPa (50-364 inH_2O). The standard deviation for these data is 0.024. This value is greater than that shown by the slotted plate and the standard orifice.

Mixture density estimation by means of the computed velocity in the air water flow

A direct flow rate estimation based on the pressure drop response of the ΔH_m term, required to compute either the quality or the liquid density, was not found. To estimate the mixture density, the effect of the water on the gas flow was made comparing two phase flows to the 100% quality flow.

It was observed that in the single-phase flow, the non-dimensional velocity shown in equation 56, exhibits a dependence on the dP/P parameter as seen in figures 51 and 52 for the Venturi meter and the standard orifice. This parameter is called nU. It seems that this dependence is distorted by the presence of the water flow in the two-phase case (figures 53 and 54).

A three-dimensional plot was constructed to analyze the effect of the liquid in the gas flow. The non-dimensional velocity (nU_s) that would exist if only air were flowing, the gas non-dimensional velocity (nU_g, equation 56) for the two-phase flow, and, the gas non-dimensional velocity (nU_m,), defined by equation 57, were compared.

$$nU_g = \frac{\rho_g}{P_{abs}} \cdot U_g^2 \qquad\qquad (56)$$

$$nU_m = \frac{\rho_{mix}}{P_{abs}} \cdot U_g^2 \qquad\qquad (57)$$

A relationship of the three parameters was found for the Venturi meter and the standard plate. This is presented in figures 55 and 58. No relationship was found for the slotted plate. To compute nU_g in the two-phase flow, the velocity was calculated using the ΔH_g term obtained from the pressure differential response assuming $\alpha \approx 1$.

The non-dimensional velocity that would exist if only air were flowing (nU_s), was computed using the dP/P parameter. The non-dimensional velocity for the mixture flow can then be estimated and equation 37 can be solved for the mixture density.

Figure 56 presents the error in the mixture density estimation using the Venturi meter. The pressure differential range where the Venturi meter was tested was 0.75-89.8 kPa (3-361 in_H_2O). It is seen that the error increases considerable as dP/P decreases reaching 168% for pressure differential as low as 0.75 kPa (3 in_H_2O). The error lies between the ±10% for differential pressures greater than 24.9 kPa (100 in_H_2O) as shown in figure 57. The dispersion of the error points tends to reduce as the pressure increases.

The error for the mixture density computation using the standard orifice plate is observed in figure 59. The range where the orifice meter was tested is 12.4-96 kPa (50-386 in_H_2O). For this case the error tends to increases as the pressure differential decreases reaching 39% as seen in the Venturi meter, however, there is no a considerable reduction in the error dispersion as the pressure differential increases. The error lies between the ±14% interval for differential pressures greater than 24.9 kPa (100 in_H_2O) approximately.

Liquid and total mass flow rate estimation using the Venturi and standard plate in the air-water flow

It was seen in the previous paragraphs that the velocity and the mixture density can be estimated using the standard plate and the Venturi meter; it is then possible to calculate the total mass flow rate from equation 13 using these pressure differential devices. Figure 60 presents the error in the total mass flow rate computation using the Venturi meter.

It is observed in figure 60 that the computed total mass flow rate error increases beyond the ±10% limit for dP/P less than 0.07 approximately, reaching the 85% value at a differential pressure of 0.75 kPa (3 in_H_2O). Figure 61 shows the error computation for differential pressure greater than 24.9 kPa (100 in_H_2O); the maximum computed error in this region is 7% approximately.

Once having estimated the total and gas mass flow rate, only a subtraction is required to calculate the water mass flow. The error in the water mass flow rate computation is presented in figure 62; the plot shows an increase in the scatter for dP/P less than 0.1. In addition to the error due to the low differential pressure, it is magnified when quality approaches to 1.

The error in the water flow rate estimation can be as high as 700% at a pressure differential of 0.75 kPa (3 in_H_2O). The scatter in the error seems to reduce at differential pressures greater than 24.9 kPa (100 in_H_2O) as observed in figure 63. All but one point in this region, which correspond to a quality greater than 0.9, lies in the ±40% error limit.

Figure 64 shows the error in the total mass flow computation using the standard orifice plate. For this case, the scatter in the error lies in a range between –11% and 12% for dP/P from 0.1 to 0.3. To the left of this region the error reaches 34% and for dP/P beyond 0.3 the error lies in the ±5% limit.

The high error that results in the total mass computation using the standard orifice plate is reflected in the water flow rate estimation. The error is plotted against dP/P and shown in figure 65; an error as high as 1760% is observed. The higher error values corresponds to a pressure drop of about 12.4 kPa (50 in_H_2O) and qualities greater than 0.96.

Summary

The accuracy and the dynamic range for the methods employed to estimate the gas and liquid flow rates in the air-water flow using the slotted plate, the Venturi meter and the standard orifice are presented in table 1. Only the slotted plate was able to estimate under acceptable error the gas and liquid mass flow rates.

The standard orifice shows the best performance for the gas mass flow estimation using both the empirical equation and the pressure response methods. In spite of its best performance in the gas flow, poor results were obtained when computing the liquid flow rate. The Venturi meter did not show good results neither for the gas nor for the liquid flow estimation. However, its performance improves for differential pressures greater than 24.9 kPa (100 in_H_2O).

There is no difficulty in performing the calculations once the empirical correlation in the methods described before is known. Only algebraic computations are required to estimate the gas and liquid flow rates. The slotted plate seems to be the simplest configuration because no other element is used; the standard orifice needs the slotted plate to obtain a good performance while the Venturi meter requires the Venturi recovery pressure.

Figure 66 shows the error in the total mass flow rate computation assuming the quality is known. The results for the slotted plate, the Venturi meter and the standard orifice are shown. Under the homogeneous flow assumption, the total flow rate is then calculated using the estimated velocity obtained from the differential pressure devices.

All the computed errors except that from the Venturi meter at dP/P less than 0.08 approximately, lies within the ±4% limit. Although the slotted plate and the standard orifice data lie within the ±4% limit, the standard orifice exhibit a reduction in the scatter as dP/P increases. The slotted plate does not show this behavior.

The scatter in the Venturi meter data increases as dP/P decreases. The error computation reaches a value of 6.5% approximately at a dP/P value of 0.05. Compared to the error shown in figure 33, the slotted plate presents a greater scatter when using the true quality in the total flow estimation. It is probably due to the fact that in the correlation used to estimate the mixture density the estimated velocity was used instead of the true value.

For the standard orifice and the Venturi meter the error shown in figure 66 is considerable less than that of figures 60 and 64 respectively. Then, if the quality or the mixture density of the two-phase flow could be measured independently, the performance of these two differential pressure devices would increase.

Air-oil test results

Experiments with air-oil flows with qualities from 0.3 to 0.97, gas void fractions higher than 0.98 (wet gas) and line pressures from 24 to 78 psi were performed. The $\beta 43$-$\beta 467$-Venturi arrangement was used in the air-oil experiments. Results presented in the following paragraphs correspond to the velocity estimation based on Euler number applied to the slotted plate, and to the ΔH_g estimation based on the pressure drop response applied to the Venturi meter.

Air-oil flow visualization through a β=0.467 slotted plate were performed by Sparks [28] in the Turbomachinary laboratory at Texas A&M University. These videos show that, compared to the water in the air-water flow, the oil appears to move much slower in the air-oil flow and the oil tends to coat the pipe walls. The oil density and viscosity for this work was 910 kg/m^3 and 0.07 kg/m·s respectively.

If the gas moves faster than the liquid phase in the two-phase flow, then the ratio of the gas to the liquid velocity (slip velocity) is greater than 1. As a consequence, the gas void fraction tends to decrease and the mixture is not homogeneous. The performance of the multiphase flow meter is then affected and the homogeneous flow assumption becomes invalid. Another two-phase pattern where the oil flow is laminar is probably present. The results obtained for the air-oil flow seems to be influenced by these characteristics as shown in the next sections.

Results using the velocity estimation based on Euler number for the oil-air flow through the slotted plate

A simple quadratic equation for U_{gu} in terms of known quantities, which include polynomial terms of ρ_{gd}/ρ_{gu} and added terms of Eu_{dPs} and $Eu_{\Delta Hg}$, was obtained for the air-oil flow. Figure 67 shows the correlation that involves the gas velocity, the ΔH_g term, the pressure differential and the upstream and downstream gas densities for the $\beta 43$ slotted plate.

Figure 68 presents the error in the velocity computation using the Euler number approach. The results are not as good as in the air-water case showing a standard deviation of 0.087; however, it is seen that for dP/P greater than approximately 0.12, the error lies between the ±10% limit and the standard deviation is 0.05. The scatter to the left of this region comprises a –40% to 10% range. The root used for this plot is that defined by equation 44.

The pressure differential range for the $\beta 43$ slotted plate is 4.2-131.4 kPa (17-533 in_H_2O), greater than that of the air-water flow (7.4-104.3 kPa, 30-423 inH_2O). It is seen in figure 69 that the Lockhart-Martinelli parameter (LM) influences the computed error. At approximately LM=0.04 error starts to increases as LM decreases, reaching 10% at LM=0.0034.

Between LM=0.04 and LM=0.09, which corresponds to liquid flow rate of 5-10 lb/min (2.27-4.54 kg/min) the scatter lies between –8% and 2% error. Beyond LM=0.09 the error increases in a negative way reaching –40% at LM=0.22. This point corresponds to the lowest gas void fraction value and is then a consequence of the slower movement of the oil.

Figure 70 shows the computed error behavior as a function of the gas void fraction. The information presented in this plot is basically the same as those of figure 69. An increase in the error is observed as α approaches 1. The method used to compute the mixture density in the air-water flow using the slotted plate did not yield acceptable results for the air-oil case.

Results using the ΔH_g estimation based on pressure drop response

The Venturi pressure drop (dP_v) and Venturi recovery pressure (P_{rv}) were utilized to search for a ΔH_g correlation in the air-oil flow. ΔP_v, P_{rv} and ΔH_g were divided by the upstream absolute Venturi pressure and then plotted as seen in figure 71. This plot shows a standard deviation of 0.0024. The Venturi pressure differential range is 7.4-89 kPa (30-361 in_H_2O).

Figure 72 presents the error in the ΔH_g estimation as a function of dP/P. The maximum error in this plot is found at a pressure differential of approximately 3.21 kPa (13 in_H_2O). It was observed in the air-water case that when computing the mass flow rate, the error tends to be less than that of the ΔH_g term, however, as seen in figure 73 in the mass flow estimation the error reaches 36%.

The Lockhart-Martinelli parameter is used to analyze the error in the gas mass flow rate computation using the Venturi meter. Figure 74 shows that for LM greater than 0.05 the error tends to increase in a negative way. There is not a well-defined trend of the error but the scatter in this region is considerable and seems to depend on LM.

Figure 75 presents the error for Venturi pressure drop greater than 24.7 kPa (100 in_H_2O); it is seen that the points lie in the ±10% limit. In fact these trends occurs at a differential pressure of less than 19.73 kPa (80 in_H_2O). The reason for the Venturi performance improvement at differential pressures seems to be the mixture effect due to the turbulence.

Mixture density estimation using the Venturi meter (air-oil flow)

Non-dimensional velocity, computed by means of equations 56 and 57, was also utilized to estimate the mixture density in the Venturi meter in the same way as the air-water flow. The non-dimensional velocity that would exist if only air were flowing, the gas non-dimensional velocity for the two phase flow and the non-dimensional velocity for the mixture flow were compared in order to determine if a correlation to compute the mixture density was possible.

To compute the gas non-dimensional velocity in the two-phase flow, the velocity was calculated using the ΔH_g term obtained from the pressure drop response. The non-dimensional velocity that would exist if only air were flowing, is function of the dP/P parameter. The Non-dimensional velocity for the mixture flow can then be estimated and equation 37 solved for the mixture density.

The resulting correlation for the air-oil flow is shown in figure 76 for the Venturi meter. A standard deviation of 0.00020 is present in the plot. The error in the mixture density estimation is observed in figure 77. It is seen that the error increases as dP/P decreases reaching 50% for a pressure drop of 3.24 kPa (13 in_H_2O). There is also an increase in the scatter for dP/P between 0.15 and 0.22. Figure 78 shows that there is a dependence on the Lockhart-Martinelli parameter when computing the mixture density using the Venturi meter.

Liquid and total mass flow rate estimation by means of the Venturi meter

Total mass flow rate was estimated by means of equation 14 using the velocity and the mixture density obtained from the Venturi meter. Figure 79 presents the error in the total mass flow rate computation for the air-oil flow. It is observed that the behavior is similar to that of the mixture density computation, however, for this case the maximum error is about 34% and standard deviation of 0.09. As seen in figure 80, for Venturi pressure differentials greater than 24.9 kPa (100 inH$_2$O) most of the data lie in the ±10% limit. The scatter for this case is greater than that of the air-water flow (figure 60).

The estimated gas mass flow rate was subtracted from the estimated total mass flow rate to obtain the liquid flow. The error in the liquid mass flow rate computation is presented in figure 81; the plot shows an increase in the scatter for dP/P less than 0.05. The error reaches a maximum value of 150% approximately for 3.24 kPa (13 inH$_2$O) differential pressure. The quality effect on the liquid estimation is observed in figure 82.

Three-phase flow measurements

The procedure developed to estimate the mass flow rate of the components in a gas-liquid flow showed an acceptable accuracy at defined pressure differential limits. The experiments were carried out using air-water and air-oil mixtures. If two different liquids (water and oil) are present in the wet gas flow and the assumption that they act as a single liquid is made, then the resulting three-phase flow (air, oil, and water) could be considered as two-phase flow and the two-phase procedure applied.

If the last assumption is correct, U_g, ΔH_g and ρ_{mix} can be estimated since they depend only on ΔP, P_u, ρ_u and ρ_d; these parameters are obtained from direct measurement. What would remain is to estimate the oil and water flow. This estimation requires either the liquid density or the water cut, however these parameters are unknown in the three-phase flow since they depend on the amount of water and oil in the flow. The water cut is defined by equation 18.

Measurements, consisting of an oil-water-air mixture, were performed in a three-phase flow to test the validity of the two-phase assumption. Since a new variable is introduced in the analysis (the liquid density) a new relationship or a new metering element is required to know the water cut in the three-phase flow.

Two methods were used in the three-phase analysis: velocity estimation based on Euler number for the $\beta=0.43$ slotted plate and the ΔH_g estimation based on the differential pressure response for the Venturi meter. The differential pressure devices arrangement used in the study was $\beta 43$-$\beta 467$-Venturi. The water cut values are 0.0 0.2 to 0.5 and 1.0.

Results for correlations that include 0.0, 0.2, 0.5 and 1.0 water cut values

Using the empirical relation method the velocity in the air-water-oil flow was estimated for the 0.0, 0.2, 0.5 and 1.0 water cut values. The correlation shown in figure 83 was employed to calculate the flow velocity and the error in the estimation is presented in figure 84. A considerable scatter of the points is observed in the plot with the error lying within the –42%-32% limit exhibiting a poor performance; this behavior is reflected in the standard deviation which has a value of 0.123. The variation of viscosity and liquid density and the mixture effects seems to be the reasons of the poor results.

The differential and recovery pressures in the Venturi meter were used to obtain a correlation for the flow velocity. Figure 85 presents the relation of the differential and recovery pressure and the ΔH_g term in the Venturi meter. The standard deviation shown in the plot is 0.029. Figure 86 shows the estimate gas mass flow rate using the Venturi meter.

A better performance is observed for the Venturi meter probably due to the mixture effects of the β=0.43 and β=0.467 slotted plates located upstream of the Venturi. For pressure drops less than 12.33 kPa (50 in_H_2O) the scatter of the points increases considerably reaching the error a value of 80% with a standard deviation of 0.182. However, as seen in figure 87, there is a reduction of the scatter for differential pressures greater than 24.7 kPa (100 in_H_2O) lying within the $\pm10\%$ limit.

No correlations were found for the 0.0-1.0 water cut range flow when trying to estimate the mixture density. The points did not collapse into a surface for the slotted plate case while a set of different surfaces due to the water cut is seen in the Venturi meter (figure 88). New correlations were performed using only the 0.2 and 0.5 water cut values. The results are presented in the next section.

Results using the velocity estimation based on Euler number for the air-oil-water flow through the slotted plate

A quadratic equation for U_{gu} in terms of known quantities was obtained for the air-oil-water flow. Figure 89 shows the correlation that involves the gas velocity, the ΔHg term, the pressure drop and the upstream and downstream gas densities for the β43 slotted plate in a 4.93-127.25 kPa (20-516 in_H_2O) pressure differential range. Only the 0.2 and 0.5 water cut values were used.

Using the Euler number approach in the air-oil-water flow, the error in the velocity computation is presented in figure 90. The root used for this plot is that defined by equation 46. It is seen that the scatter at low-pressure drop is between the −31% to 26% limits with a standard deviation of 0.123.

The error band tends to be narrower as dP/P increases. As seen in figure 91 the data exhibit a tendency to converge to zero; only 1 point is out of the ±10% error at differential pressures greater than 39.8 kPa (160 in_H$_2$O). Considering only the points with differential pressure greater than 49.8 kPa (200 in_H$_2$O) the standard deviation is 0.054.

The computed velocity error was plotted against the Lockhard-Martinelli parameter (LM) and the result is presented in figure 92. The behavior shown in figure 92 is similar to that of the air-oil flow (figure 74), however the scatter of the data is greater in this case; the LM range for the air-oil flow is greater than that of the air-oil-water case.

The LM region where the air-oil flow velocity error was less dispersed correspond to the region where the air-oil-water flow reaches the greatest error. These points correspond to gas void fractions less than 0.998 as shown in figure 93. The estimated velocity for the air-oil-water flow did not show acceptable results when trying to estimate the mixture density as in the air-water case.

Assuming homogeneous oil-water mixture in the liquid flow, equation 58 is used to estimate an equivalent viscosity for the liquid flow. WMF is the ratio of the water to the total liquid flow rate. An equivalent multiphase viscosity is estimated using equation 59. Reynolds number is then computed for the multiphase flow.

$$\mu_l = \mu_w \cdot \text{WMF} + \mu_o \cdot (1 - \text{WMF}) \tag{58}$$

$$\mu_m = \mu_g \cdot \text{Qual} + \mu_l \cdot (1 - \text{Qual}) \tag{59}$$

Figure 94, 95 and 96 show the error in the estimated velocity as function of the Reynolds number for the air-water, air-oil and air-water-oil respectively. The Reynolds number values for the air-oil and air-water-oil cases are much less compared to the air-water flow. An apparent laminar flow is then present in these cases.

Results using the ΔHg estimation based on pressure drop response (air-oil-water flow)

The Venturi differential pressure (dP_v) and Venturi recovery pressure (P_{rv}) were utilized to search a ΔH_g correlation in the air-oil-water flow. ΔP_v, Prv and ΔH_g were divided by the upstream absolute Venturi pressure and then plotted as seen in figure 97. This plot shows a standard deviation of 0.0024 for a Venturi pressure differential range is 3.5-86.3 kPa (14-350 in_H_2O).

The ΔH_g term was computed from the $\Delta HgoP$ correlation. The error resulting from the ΔH_g estimation is shown in figure 98. The scatter in the error exhibits an increase at dP/P less than 0.1. It reaches 29% error at a pressure differential of 5.43 kPa (22 in_H_2O). Figure 99 presents the error for the gas mass flow rate estimation. The standard deviation is 0.18. As seen in the air-oil case, the error for this parameter tends to be greater than that of the ΔH_g term.

The plot in figure 100 shows the effect of the LM parameter in the gas mass flow rate computation. It exhibits a tendency to increases negatively as LM increases. There are 8 points that are out of this trend corresponding to low differential pressure. It is observed in figure 101 that for pressure drop greater than 24.7 kPa (100 in_H_2O) the error is located in the –8% to 6% limit and presents a tendency to converge to zero. The standard deviation for this range is 0.034. Actually, these behavior starts at 17.3 kPa (70 in_H_2O) pressure drop.

Figure 102 presents a comparison of the gas flow rate error estimation for the air-water-oil, air-oil and air-water cases. It is seen that except for the scatter of the point at low LM values in the air-water-oil flow, a similar dependence is observed in the three cases. The wider range for the LM parameter in the air-oil flow is due to the less liquid density value.

Mixture density estimation using the Venturi meter in the air-oil-water flow

The non-dimensional velocity defined by equations 55 and 56, were also utilized to estimate the mixture density in the air-oil-water flow using the Venturi meter. To compute the gas non-dimensional velocity in the air-oil-water flow, the velocity was calculated using the ΔH_g term obtained from the pressure drop response.

The non-dimensional velocity that would exist if only air were flowing, was computed using the dP/P parameter. The non-dimensional velocity for the mixture flow can then be estimated and then equation 56 is solved for the mixture density.

The resulting plot for the air-oil-water flow is shown in figure 103 for the Venturi meter. The standard deviation for this correlation is 0.00034. Figure 104 presents the error in the mixture density estimation. An increase in the error as dP/P decreases is observed. The plot shows a tendency to converge to zero as dP/P increases.

Figure 105 shows the influence of the Lockhard-Martinelli parameter when computing the mixture density using the Venturi meter. At LM=0.02 the error increases linearly as LM increases; this region corresponds to low mixture Reynolds number. The error in mixture density estimation for differential pressure greater than 24.7 kPa (100 in_H_2O) is presented in figure 106. All points at differential pressures greater than 24.7 kPa (100 in_H_2O) lie within the $\pm 10\%$ limit.

Liquid and total mass flow rate estimation by means of the Venturi meter

Total mass flow rate was estimated by means of equation 13 using the velocity and the mixture density obtained from the Venturi meter in the air-oil-water flow. Results for this estimation are shown in figures 107 and 108. A maximum error of 51% at low differential pressure is seen in figure 107 with a standard deviation of 0.16; the scatter tends to converge to zero as dP/P increases.

Figure 108 presents the error in the total mass flow computation for pressure drops greater than 24.7 kPa (100 in_H_2O). The computed standard deviation is 0.053. Although all but one point lie in the ±10% error limit and there is a tendency to converge to zero, the dispersion of the points is considerable. For pressure drops greater than 86.31 kPa (350 in_H_2O) the convergence to zero would be probably more remarkable.

The estimated gas mass flow rate was subtracted from the estimated total mass flow rate to obtain the liquid flow in the air-oil-water flow. Figure 109 and 110 present the results for this computation. It can be observed in figure 109 that most of the error points lie in a ±100% range. At lower pressure drops the error reaches a 158% value

Figure 110 presents the error in the liquid mass flow rate estimation for pressure drops greater than 24.7 kPa (100 in_H_2O). All but one point lie in a ±50% error in this region. Compared to the total mass flow rate estimation, the error for the liquid computation is approximately five times greater at pressure drops beyond 24.7 kPa (100 inH_2O).

Euler number correlation assuming known quality

During the course of this research it was determined that for the air water flows, the flow rates could be accurately calculated if the quality of the flow was given. Then the Euler number was expressed as a function of quality and dP/P. The effectiveness of this relationship will be evaluated for the air-water-oil flow in this section

Assuming a known quality in the multiphase flow, the Euler number (equation 60) was plotted against dP/P and quality. An empirical Euler number correlation was obtained and solved for the flow velocity. Knowing the quality, the gas and liquid densities, the mixture density can be computed and finally, the total mass flow rate is estimated applying the continuity equation to the homogeneous multiphase flow.

$$Eu = \frac{\Delta P}{\rho_g \cdot U_g^2} \tag{60}$$

The procedure mentioned in the previous paragraph was applied to the slotted plate and the Venturi meter for the air-water, air-water-oil and air-oil flows. Figures 111 to 116 present the resulting plots. The response of the β=0.43 slotted plate is shown in figures 111, 112 and 113 where, despite of the different residuals in the plots, a similar trend is observed.

As seen in figure 111, a considerable number of data points do not lie in the generated surface. This behavior is mainly observed at low differential pressures. For the air-water-oil case, the residual increases considerably at low differential pressures. A similar behavior is seen in the air-oil flow at low quality and low differential pressures.

Figures 114, 115 and 116 show the resulting plots for the Venturi meter. The air-water flow exhibits less residual values compared to the air-water-oil and air-oil flows. The worse performance is observed in the air-water-oil case. It probably suggests that, in addition to the viscosity effects seen in the air-oil flow, the liquid mixture process influence the performance of the meter.

The behavior described in the previous paragraphs is reflected in the error of the total mass flow rate computation as shown in figures 117 and 118. The slotted plate and the Venturi meter exhibit better results in the air-water flow. The performance of the meters to the air-oil and air-water-oil improves as the pressure differential increases.

Summary

The results for the air-water-oil flow exhibit a greater error compared to the air-water flow. The error in the estimated velocity using the empirical equation method in the slotted plate and the recovery pressure method in the Venturi meter show a dependence in the pressure differential and in the mixture Reynolds number.

For low differential pressures and low mixture Reynolds numbers the error increases considerably. The methods used in this work to estimate the velocity did not show favorable results at these conditions. Turbulent mixture Reynolds numbers and differential pressures greater than 24.7 kPa (100 in_H_2O) will probably increase the accuracy of the measuring process in the air-water-oil flow.

The Venturi meter exhibits a better performance than the slotted plate in the air-water-oil flow. The flow velocity and the mixture density were estimated using the Venturi meter; only the velocity was estimated using the slotted plate. This meter can then be used to estimate the flow velocity and the mixture density at Reynolds number greater than 5000 and differential pressures greater than 24.7 kPa (100 in_H_2O).

If the quality can be obtained independently, then the error of the estimate velocity would be reduced. Since the homogeneous assumption does not work at low differential pressures and low mixture Reynolds numbers, the viscosity of the fluid seems to be an important parameter when using differential pressure devices. The performance of the meters would probably increase at higher line pressures using the same pipe size and β ratios.

Low differential pressure results

A study of the gas mass flow rate measurement using a differential pressure device was undertaken. The behavior of the discharge coefficient, defined by equation 23, was analyzed in a 0.11-5 kPa (0.43-20 in_H_2O) pressure differential range. The differential pressure was produced by a β=0.467 slotted plate.

The parameters that define the discharge coefficient in equation 23 are the mass flow rate, the differential pressure, the upstream gas density, the β ratio and the pipe cross section.

The last two parameters are geometrically measured and are constant, while instrumentation is required for the first two. In the gas density case, a perfect gas is assumed and equation 6 is used to calculate it.

Pressure and temperature were measured upstream of the slotted plate to compute the gas density. The slotted plate differential pressure was measured with a 0-14 kPa (0-2 psi) range Honeywell multivariable transducer. The gas flow rate was measured by means of two sonic nozzles (critical Venturis).

The discharge coefficient was also measured in the 6-350 in_H_2O range to compare the C_d behavior in both cases. The pressure differential for the 1.5-86.8 kPa (6-350 in_H_2O) range was measured with a 0-68.95 kPa (0-10 psi) range Honeywell multivariable transducer while the gas flow rate was measured with the Daniel turbine meter, which had been calibrated using the sonic nozzle bank.

Figure 119 shows the coefficient C_d behavior as a function of dP/P in the 1.5-86.8 kPa (6-350 in_H_2O) range. A linear equation that empirically expresses the C_d behavior as a function of dP/P was chosen. The expansion factor obtained from the correlation is 0.692 while the incompressible factor is 0.925.

Conceptually, the C_d coefficient is the ratio of the computed mass flow rate with no head losses or density changes to the actual mass flow rate. This concept is defined in equation 61. If the differential pressure from the slotted plate were zero (dP/P=0), the coefficient C_d value would be 0.925 according to the data obtained using the turbine meter as reference meter. The minimum dP/P value for this case is 0.004.

$$C_d = \frac{\dot{m}_{nl}}{\dot{m}_{actual}}$$ (61)

A less well defined relation is seen for the coefficient C_d as a function of dP/P in the 0.11-5 kPa (0-20 inH_2O) differential pressure range. A set of dispersed C_d points between dP/P=0.0005 and dP/P=0.015 is observed is figure 120. Two parallel lines showing a dependence on dP/P seems to emerge for dP/P greater than 0.015. Not a convergence to 0.925 is present as might be expected from the larger flow rate results shown in figure 119

To compare the behavior of C_d for both pressure ranges, a plot is presented in figure 121. It is seen that the points obtained using the sonic nozzles as a reference meter have a value less than that of the points obtained using the turbine meter as reference. Despite the dispersion of C_d, a tendency to linearly depend on dP/P can be deduced for the sonic nozzle points at dP/P greater than 0.015 as previously mentioned. This figure illustrates that there is another parameter that is important when calculating C_d, especially at the lower flow rates.

Reynolds number is computed using equation 60 to analyze the Coefficient C_d behavior. The parameters utilized to compute the Reynolds number correspond to the upstream slotted plate location. The Reynolds number varies between 14000 and 76000 for the low differential pressure data. This would indicate a turbulent flow is present in the pipe.

In contrast to the high Reynolds number obtained using equation 62, the length scale for the slot is smaller and the Reynolds numbers based upon the slot width vary from 2600 to14000. These low Reynolds numbers accompanied by the laminarizing effect of the fluid accelerating into the slot may indicate transitional Reynolds number.

$$\text{Re ynolds} = \frac{\rho \cdot U \cdot D}{\mu} \qquad (62)$$

Figure 122 presents the coefficient C_d as a function of Reynolds number and dP/P. A Reynolds number effect is seen as the coefficient C_d increases and dP/P decreases for a defined upstream absolute pressure. The Reynolds number is comprised between 80000 and 750000 for these data.

A plot of C_d as function of Reynolds number and dP/P for the low differential pressure data is presented in figure 123 to extend the information obtained from the 1.5-86.8 kPa (6-350 in_H_2O) differential pressure range. A scatter of points is seen in the plot and despite the information obtained from figure 122, no apparent relation exists on Reynolds number.

The data from the 1.5-86.8 kPa (6-350 in_H_2O) differential pressure range and the low differential analysis were include in figure 124. These data show the coefficient C_d as function of Reynolds number and dP/P. Regarding the Reynolds number effect, a similitude with the 1.5-86.8 kPa range data is observed for some low differential pressure points.

No relationship between Reynolds number or dP/P and coefficient C_d was found. The upstream velocity was then employed to analyze the behavior of the low differential pressure flow. The ideal velocity computed using equation 63 was compared with the velocity obtained from the mass flow rate as expressed by equation 64. The mass flow rate present in equation 64 corresponds to the measured flow using the sonic nozzle bank.

$$U_{id} = \frac{\beta^2}{\sqrt{1-\beta^4}} \cdot \sqrt{\frac{2}{\rho} \cdot \Delta P} \qquad (63)$$

$$U = \frac{m_{meas}}{A \cdot \rho} \qquad (64)$$

A linear relationship between the ideal and real velocity is seen in figure 125. The upstream velocity can then be estimated using equation 61. Equation 65 is used to set the estimated velocity with a zero value as ΔP tends to zero. A constant C_d coefficient is then present in equation 3.

$$U_{es} = \theta \cdot U_{ideal} \qquad (65)$$

The slope of the plot shown in figure 125 (θ) is the average of C_d values observed in figure 120. This average has a value of 0.865516. No compressible effects are considered under this assumption. The upstream and downstream densities are computed neglecting temperature changes in the slotted orifice plate to see the density change. The results are shown in figure 126.

It is observed in figure 126 that for dP/P less than 0.01 (1 kPa, 4 in_H_2O) the density change is less than 1%. The maximum density change for the low differential pressure data is 4.6%. Compressible effects can then be ignored and equation 65 be used to estimate the upstream velocity.

Figure 127 present the error in the velocity estimation neglecting expansion effects. A maximum error of 4.5% at approximately dP/P=0.08 is observed. Most of the points are within the ±2% limit for dP/P less than 0.01. A dependence on dP/P can be regarded for dP/P greater than 0.01, which indicates expansion effects.

Summary

Low differential pressure results did not show dependence on the Reynolds number as might be expected from the information of the larger flow rate. The plot of the coefficient C_d as a function of dP/P exhibited a set of scatter points and no relationship was found to estimate this coefficient.

The ideal velocity computed using equation 61 was used to estimate the upstream velocity. The linear relationship observed in figure 125 indicates that the mass flow rate can be computed in a simple way assuming a constant coefficient in equation 63 which is the average of the computed C_d values.

Since the density change for dP/P is less than 1%, compressibility effects can be neglected. The maximum error in the velocity estimation was 4.5% found at dP/P≈0.08 (differential pressure of 1.5 kPa, 6 in_H_2O). It is then possible to estimate the gas mass flow rate using a slotted plate at differential pressures below 1.24 kPa (5 in_H_2O) where the expansion factor can be neglected.

CHAPTER VI
CONCLUSIONS AND RECOMMENDATIONS

Conclusions

The response of slotted plate, Venturi meter and standard orifice to the presence of two phase, three phase and low differential flows was investigated. Two mixtures (air-water and air-oil) were used in the two-phase analysis while a mixture of air, water and oil was employed in the three-phase all of them in a wet gas flow. A slotted plate was utilized in the low differential pressure analysis.

The best results were obtained for the slotted plate and standard orifice using the empirical equation technique in the air water flow. Good performance was also exhibited by the standard orifice using the pressure response technique. The Venturi meter did not show good performance; however, better results are obtained for differential pressures greater than 12.4 kPa (50 in_H_2O) using the recovery Venturi pressure.

For the liquid flow rate estimation in the air-water flow, the best results were obtained using the slotted plate. Due to the tendency to a zero value for the liquid flow, the error of the estimation increases reaching values of more than 500% at high qualities. The Venturi meter exhibited the poorest accuracy. The results of the air-water flow are summarized in table 1.

Air-oil two phase flow did show that viscosity influences the response of the differential pressure meters. The performance improved only a high differential pressure. The best results were obtained in the Venturi meter using the recovery pressure for the gas flow estimation at differential pressures greater than 24.9 kPa (100 in_H_2O); the accuracy was ±9.5% with a standard deviation of 0.037. This is presented in table 2.

Applying the empirical relation to the air-oil flow for the gas flow estimation, accuracy of $\pm14\%$ with a standard deviation of 0.05 was obtained at differential pressure greater than 49.8 kPa (200 in_H_2O). This technique was used only with the slotted plates, no relationship was found when using it with the other meters. A relationship to estimate the liquid flow rate was only obtained using the Venturi meter. Results show no a good performance.

An improvement of the differential meter performance was observed for the air-water-oil flow as seen in table 3. The same techniques as in the air-oil flow were employed. Using the recovery pressure, an accuracy of ±8.7 with a standard deviation of 0.034 was exhibited by the Venturi meter in the gas flow estimation at differential pressure greater than 19.91 kPa (80 in_H_2O).

At differential pressures greater than 37.3 kPa (150 in_H_2O) the accuracy of the slotted plate was ±9.5 with a standard deviation of 0.054. The empirical equation technique was used in this case. A relationship to estimate the liquid flow rate was found for the Venturi meter; the accuracy in the liquid estimation was ±32 with a standard deviation of 0.262, which indicates poor performance.

The results using the homogeneous assumption exhibit good performance for air-water flow, i.e. low liquid viscosity while high differential pressure is required as liquid viscosity increases. The best performance of the Venturi meter in the air-oil and the air-water-oil flow seems to be due to the mixing effect of the slotted plates located upstream.

A constant coefficient C_d was used for the low differential pressure analysis and results did show that for differential pressure less than 1.24 kPa (5 in_H_2O) density changes are less than 1% making possible the incompressible flow assumption. The average of the computed coefficients is the value of C_d.

Recommendations

It has been shown the feasibility to use differential pressure devices as multiphase flow meters. An upstream mixer element that induces homogeneous flow is recommended. Differential pressures greater than 24.9 kPa (100 in_H$_2$O) are suggested at high liquid viscosity together with a study of the cost derived by the increasing of the permanent head loss. The use of an independent way to estimate the liquid flow rate or the mixture density would increases the performance of the multiphase meter.

Further work is necessary to know the flow pattern present in the wet gas flow as well to know how this pattern change as line pressure, quality and water cut vary. The response of the meters to the presence of wet gas at line pressures above 1 MPa is another subject recommended to investigate.

With respect to the low differential pressure analysis, it is recommend the use of a different element as reference meter (such as a turbine meter) to study the C_d behavior. It is also suggested to investigate the possible laminar flow through the slots in the slotted plate as well further work on the compressibility effects. Finally, the turbulent dynamic properties of the gas flow that cause fluctuations in differential pressure should be analyzed.

REFERENCES

[1]   G.L. Morrison, K. R. Hall, J. C. Holste, M. L. Macek, L. M. Ihfe, R. E. Deotte, D. P. Terracina, Comparison of orifice and slotted plate flowmeters, Flow Measurements and Instrumentation 5 (1994) 71-92.

[2]   G.L. Morrison, Euler number based orifice discharge coefficient relationship, Journal of Fluid Engineering 125 (2003) 189-191.

[3]   J. Amdal, Handbook of Multiphase Metering. The Norwegian Society for Oil and Gas Measurement, Oslo, Norway,1995

[4]   R. Northedge, Three phase flow measurements for both subsea and platform applications, in: International Conference on Multiphase Flow, Technology and Consequences for Field Development, Stavanger, Norway, 1987

[5]   A.W. Jamieson, Multiphase metering, the challenge of implementation in: 16th North Sea Flow Measurement Workshop, London, 1998.

[6]   P. Mehdizadeh, State of the art multiphase flow metering, API 2002-100094 report, 2002

[7]   R.N. Steven, Wet gas metering with a horizontally mounted Venturi meter, Flow Measurements and Instrumentation 12 (2002) 361-372.

[8]   R.G Teyssandier, Flow measurements and metering requirements in the oil and gas industry, ASME FED Devices for Flow Measurement and Control 159 (1993) 51-54.

[9]   D.L. George, T. B. Morrow, Orifice meter flow measurements at low differential pressures, SwRI 18-8890 report, 2001.

[10]   D.P. Terracina, The experimental and numerical development of a slotted orifice meter and its design parameters, PhD dissertation, Texas A&M University, 1996.

[11]   D.C.G Lewis, J. Singer, A new development in low loss flow metering, in: First Symposium on Flow, Its Measurement and Control in Science and Industry, ISA, Pittsburgh, 1971

[12]   M.J Reader-Harris, J.A Sattary, E. P. Spearman, The orifice plate discharge coefficient equation. Further work, Flow Measurement and Instrumentation, 6 (1995) 101-114.

[13] M.J Reader-Harris, J.A Sattary, The orifice plate discharge coefficient equation, Flow Measurement and Instrumentation 1 (1990) 67-76

[14] Z.D. Husain, R. G. Teyssandier, Effects of flow-induced disturbances and the frequency response of pressure transducers on the measurement of the differential pressure at the flange taps in: Symposium on Differential Pressure Type Fluid Meters, ASME/Winter Annual Meeting, Washington, D.C. 1984.

[15] D.L. George, T. B. Morrow and M. G. Nored, Operational factors that affect orifice meter accuracy, SwRI 18-8890 report, 2002.

[16] R.C Martinelli, M. K. Boelter, T.H.M. Taylor, E.G. Thomsen and E.H. Morrin, Isothermal pressure drop for two phase two component flow in a horizontal pipe, Transactions ASME, 66 (1944) 139-151.

[17] R.W. Lockhart, R. C. Martinelli, Proposed correlation of data for isothermal two-phase, two-components flow in pipes, Chemical Engineering Progress, 45 (1949) 39-48.

[18] S.M. Zivi, Estimation of steady state steam void-fraction by means of the principle of minimum entropy production, Journal of Heat Transfer, 86 (1964) 247-252.

[19] J.W. Murdock, Two phase flow measurements with orifices, ASME Journal of Basic Engineering, 84 (1962) 419-433.

[20] D. Chisholm, Two-phase flow through sharp-edged orifices, Journal of Mechanical Engineering Science, 19 (1977) 128-130

[21] J.R. Fincke, C. Ronnenkamp, D. Kruse, J. Krogue. D. Householder, Performance characteristics of an extended throat flow nozzle for the measurement of high void fraction multi-phase flows, in: 4th International Symposium on Fluid Flow Measurement, Denver, 1999

[22] A. Downing, Development of a new intelligent wet gas meter, Solartron ISA, Durham UK, 2001

[23] G.A. Johansen, P. Jackson, Salinity independent measurement of gas volume fraction in oil/gas/water pipe flows, Applied Radiation and Isotopes, 53 (2000) 595-601.

[24] C. Fischer, Development of a metering system for total mass flow and compositional measurements of multiphase/multicomponent flows such as oil/water/air mixtures, Flow Measurement and Instrumentation, 5 (1994) 34-42

[25] G. Oddie, H. Shi, L.J. Durlofsky, K. Aziz, B. Pfeffer, J. A. Holmes, Experimental study of two and three phases flows in large diameter inclined pipes, International Journal of Multiphase Flow, 29 (2003) 527-558.

[26] N. Petalas, K. Aziz, A mechanistic model for multiphase flow in pipe, Journal of Petroleum Technology, 39 (2000) 43-55.

[27] A.R. W. Hall, M. J. Reader-Harris and B. C. Millington, A study of the performance of Venturi meters in multiphase flows, in: Second North American Conference on Multiphase Technology, Banff, Canada, 2000

[28] S. Sparks, Air-oil flow visualization through slotted plates, MS thesis, Turbomachinary Laboratory Mechanichal Engineering Department, Texas A&M University 2004.

APPENDIX A

FIGURES

$$P_1 \qquad\qquad P_2$$
$$U_1 \qquad\qquad U_2$$
$$\rho_1 \qquad\qquad \rho_2$$

Pressure drop device
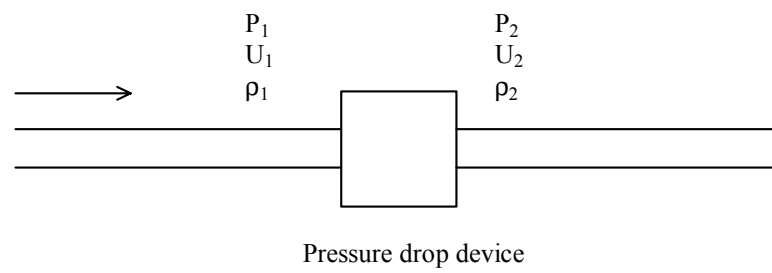
Figure 1. Differential pressure device.

Figure 2. General facilities.
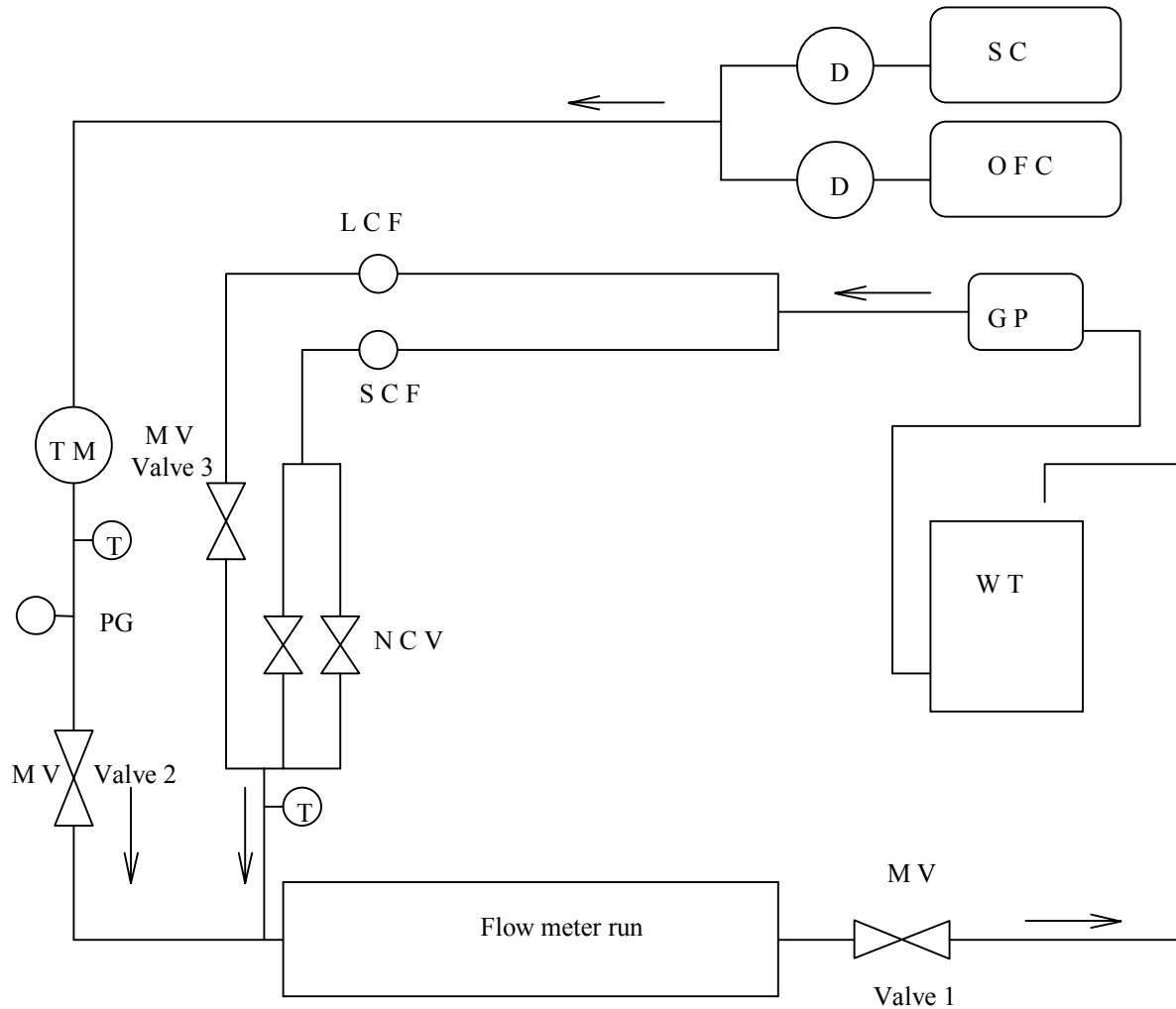
D   Dryer
G P   Gear Pump
L C F   Large Coriollis Flow meter
M   Mixer
N C   Needle Control Valves
O F C   Oil Free Compressor
O P   Orifice Plate
P D T   Pressure Differential
P G   Pressure Gage
S C   Sullair Compressor
S C F   Small Coriollis Flow meter
T   Thermocouple
T M   Turbine Meter
W T   Water Tank
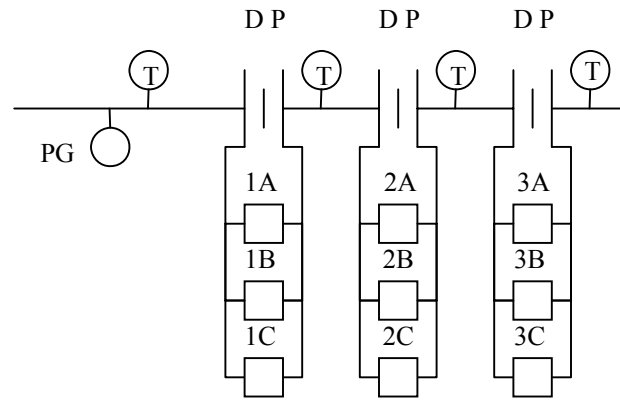
Figure 3. Schematic of the test zone for two-phase measurement work.
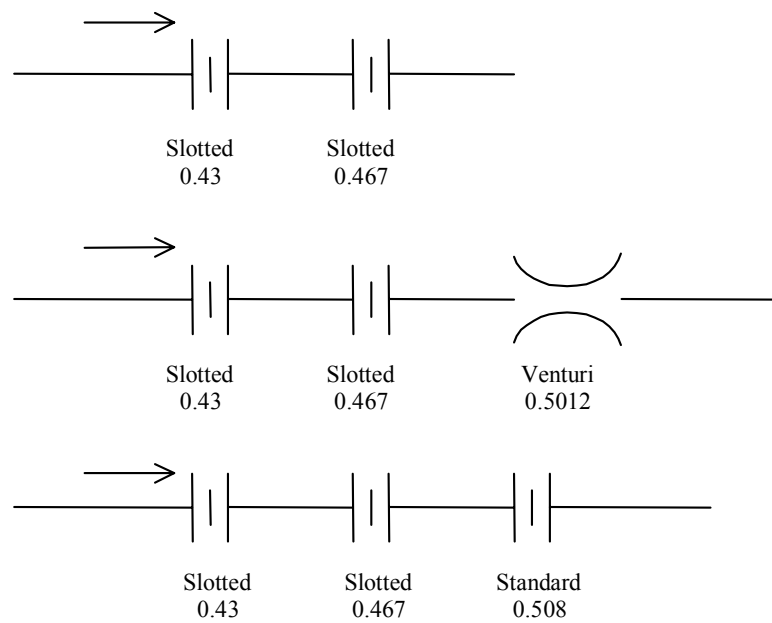
Figure 4. Differential pressure meters arrangement for two-phase air-water flow.
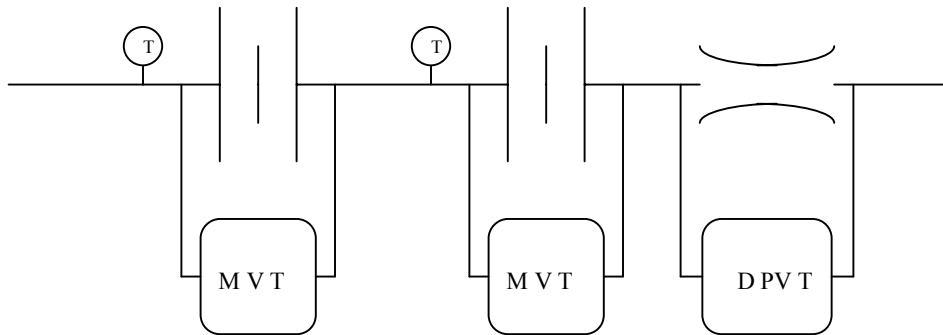
Figure 5. Differential pressure meters arrangement for two-phase air-oil flow.
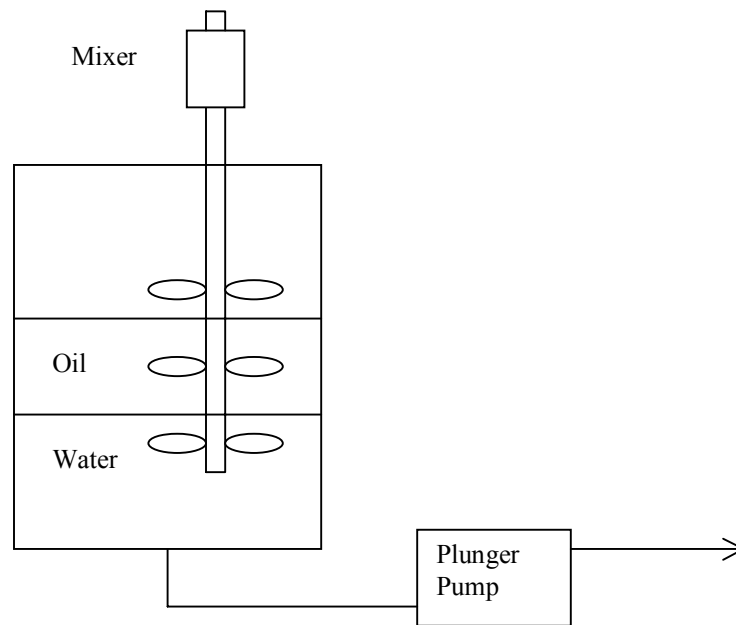
Figure 6. Oil-water mixing system.

Figure 7. Sonic nozzle bank.
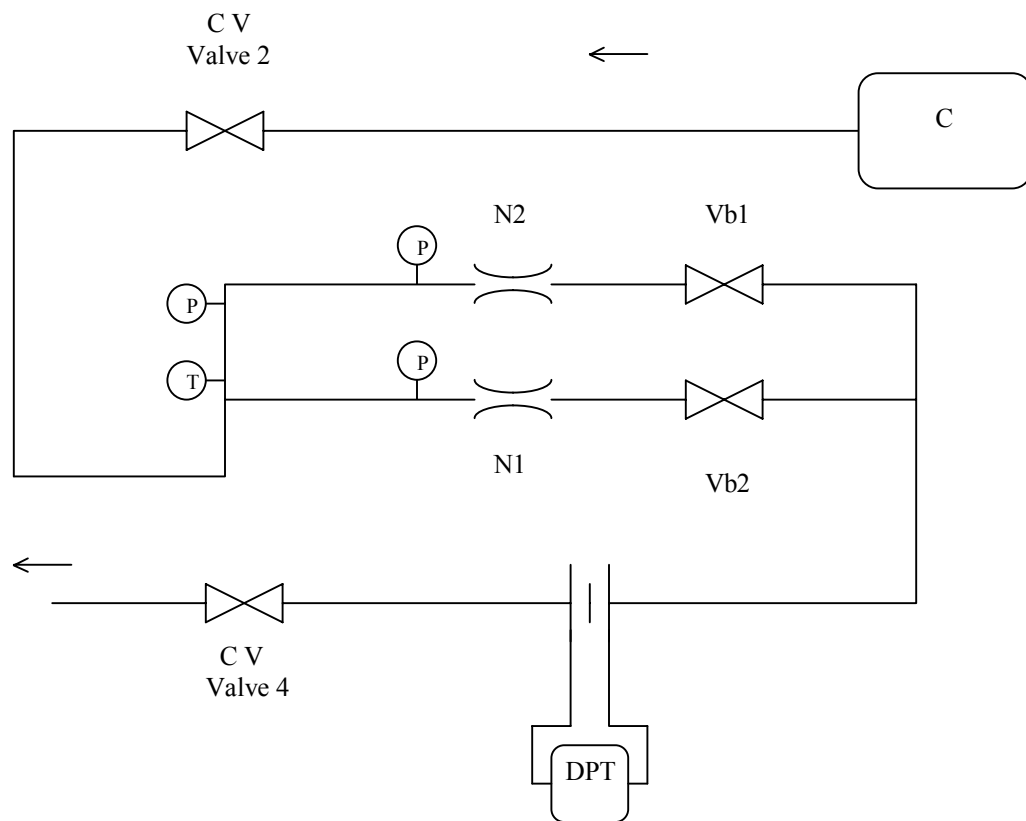
C	Compressor
CV	Control Valve
DPT	Differential Pressure Transducer
N	Nozzle
P	Pressure Transducer
T	Temperature Transducer
V	Ball Valve
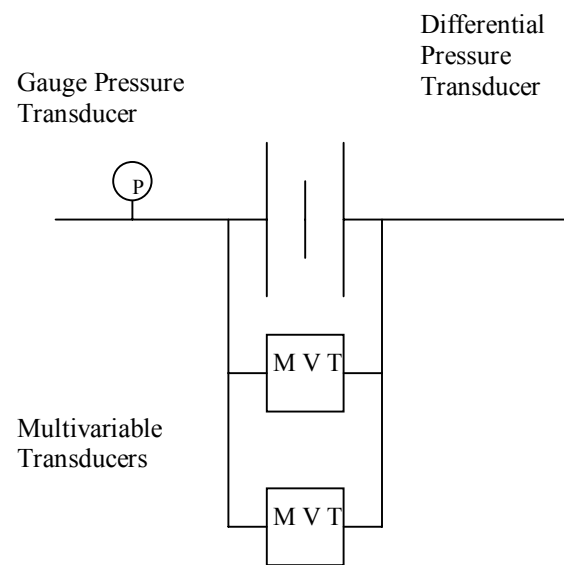
Figure 8. Schematic of the test zone for low differential pressure measurements.

a) β=0.43
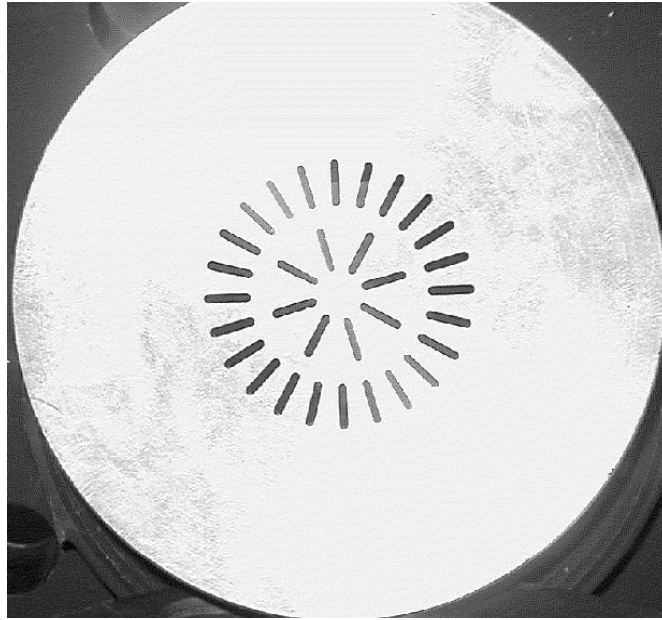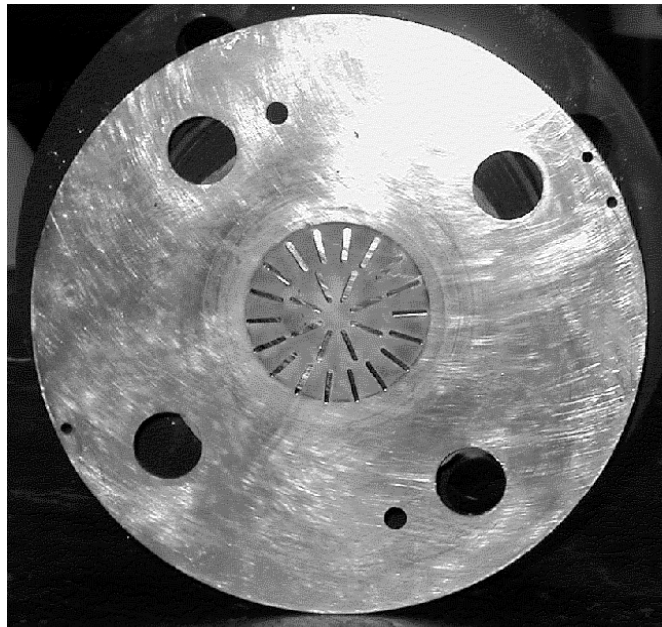
b) β=0.467

Figure 9. Slotted plates.

0.252 in

D = 0.0625 in

β = 0.43

0.374 in

D = 0.0625 in

β = 0.467
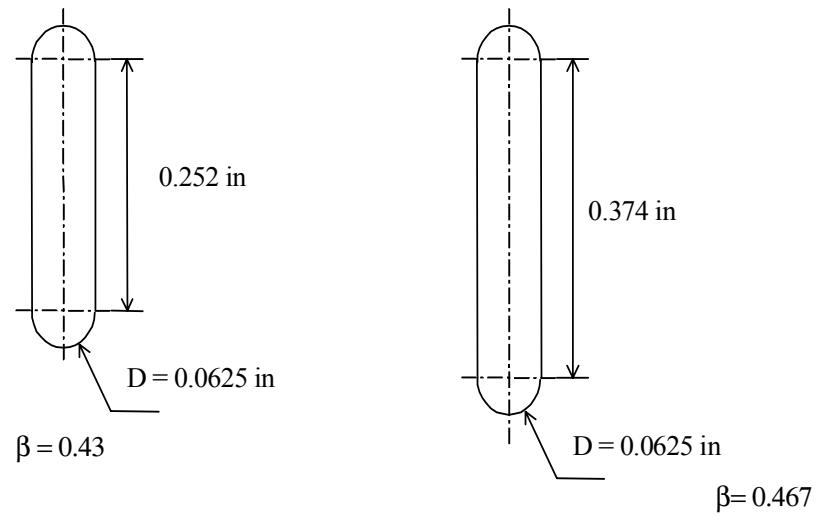
Figure 10. Slot details.
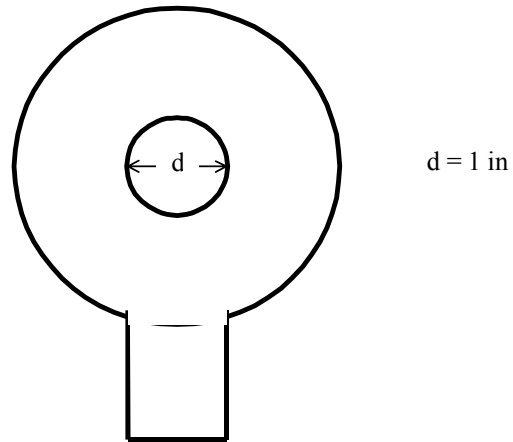
Figure 11. Standard plate β=0.508.

d = 1 in

$\alpha_1 = 9.50°$
$\alpha_2 = 3.6°$
d = 1.054 in
D = 2 in
t = 3.5 in
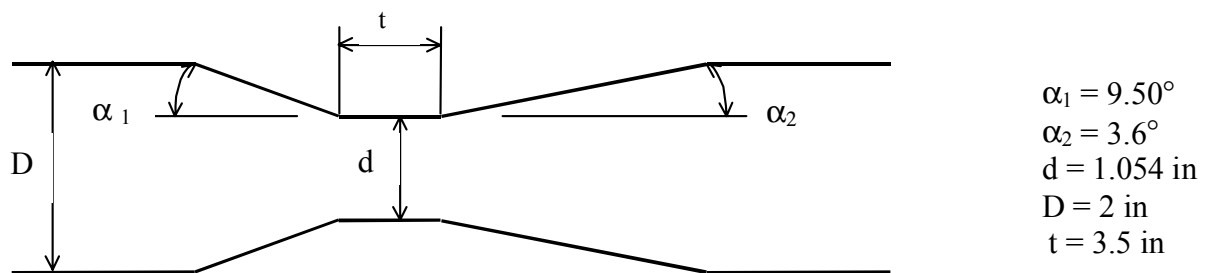
Figure 12. Venturi meter β=0.5271.
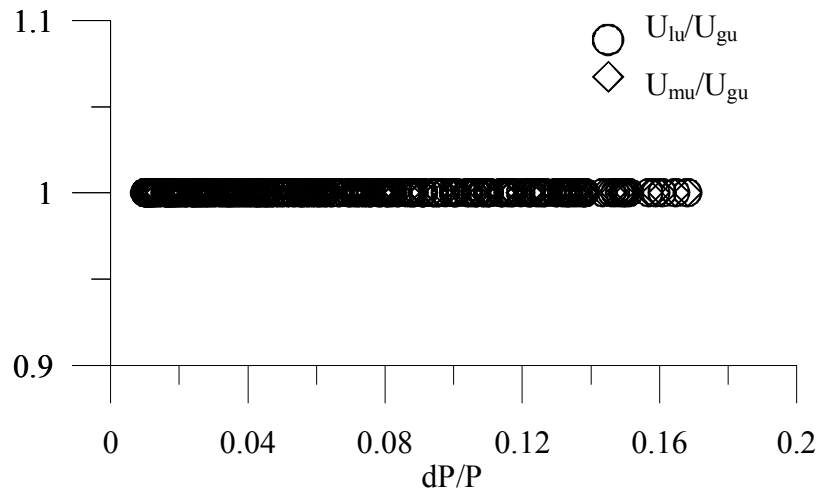
a) Upstream velocity ratio.
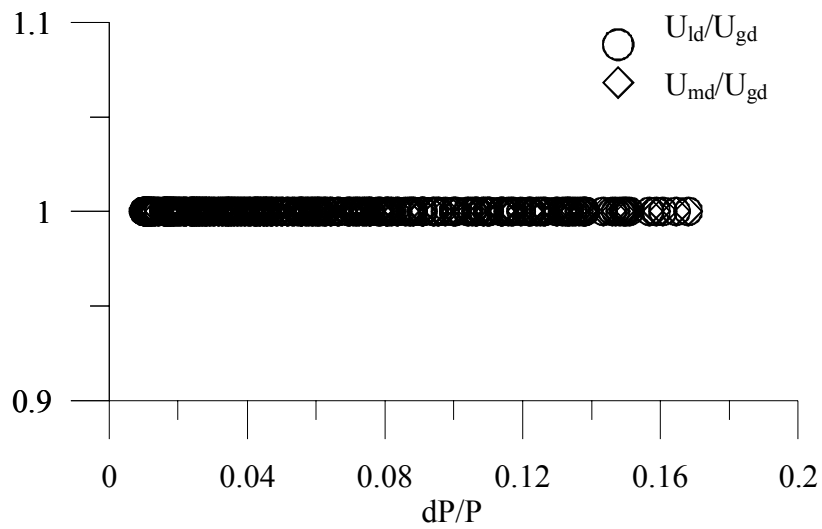
b) Down stream velocity ratio.

Figure 13. Gas, liquid and mixture velocity comparison. Air-water flow. Slotted plate
β=0.43.
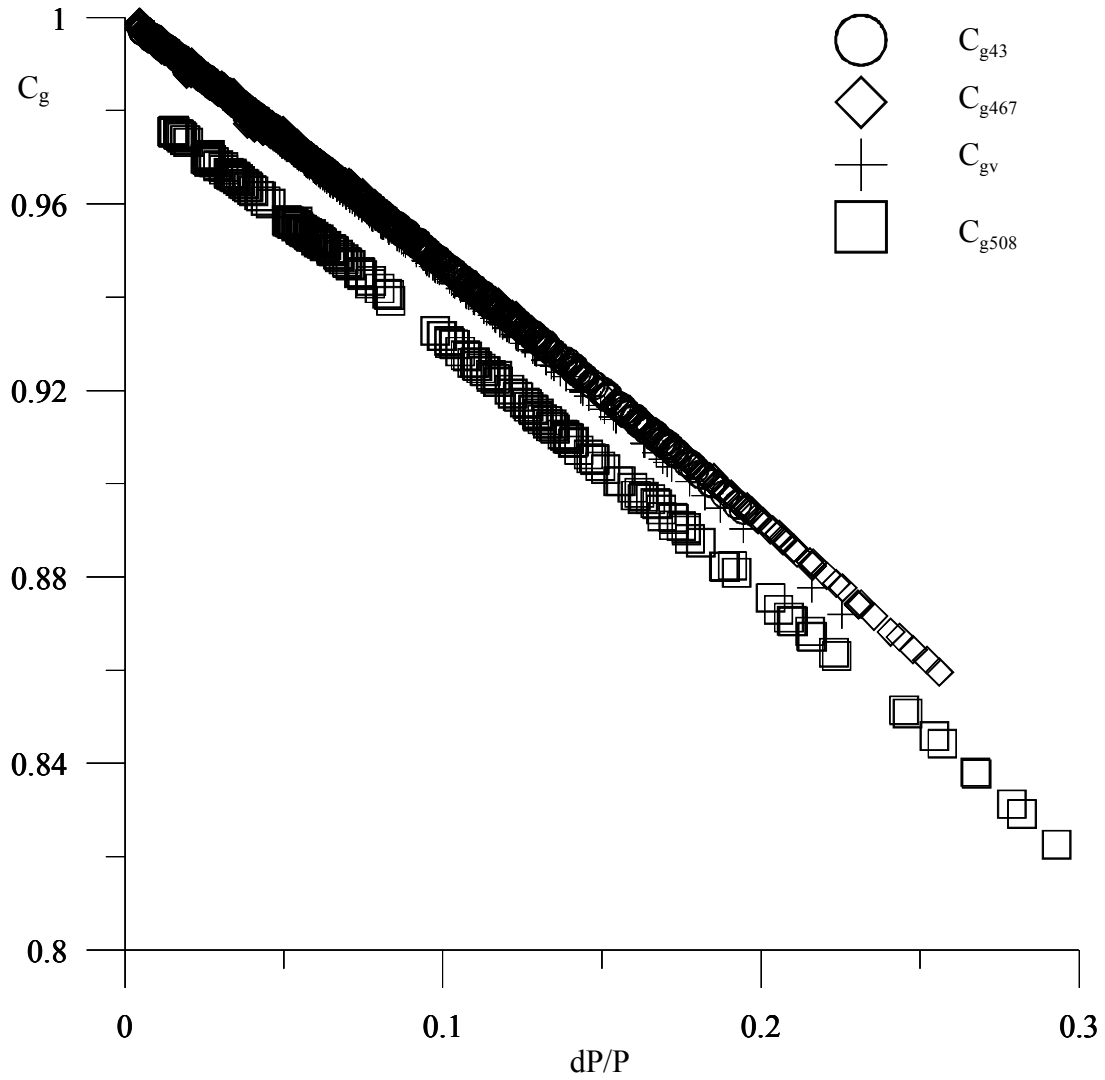
Figure 14. Coefficients C_g for the slotted plates, the Venturi meter and the standard orifice.
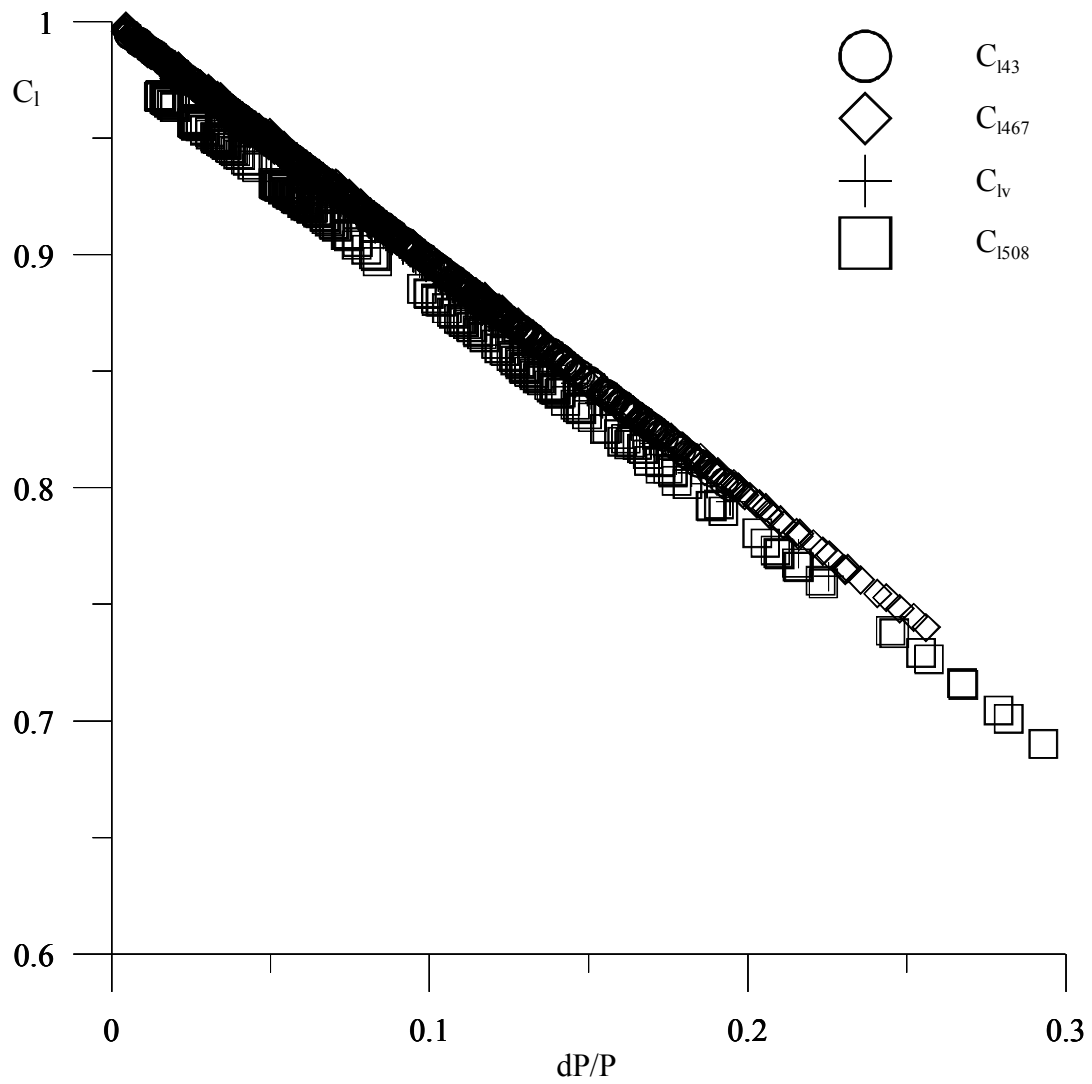
Figure 15. Coefficients C_l for the slotted plates, the Venturi meter and the standard orifice.
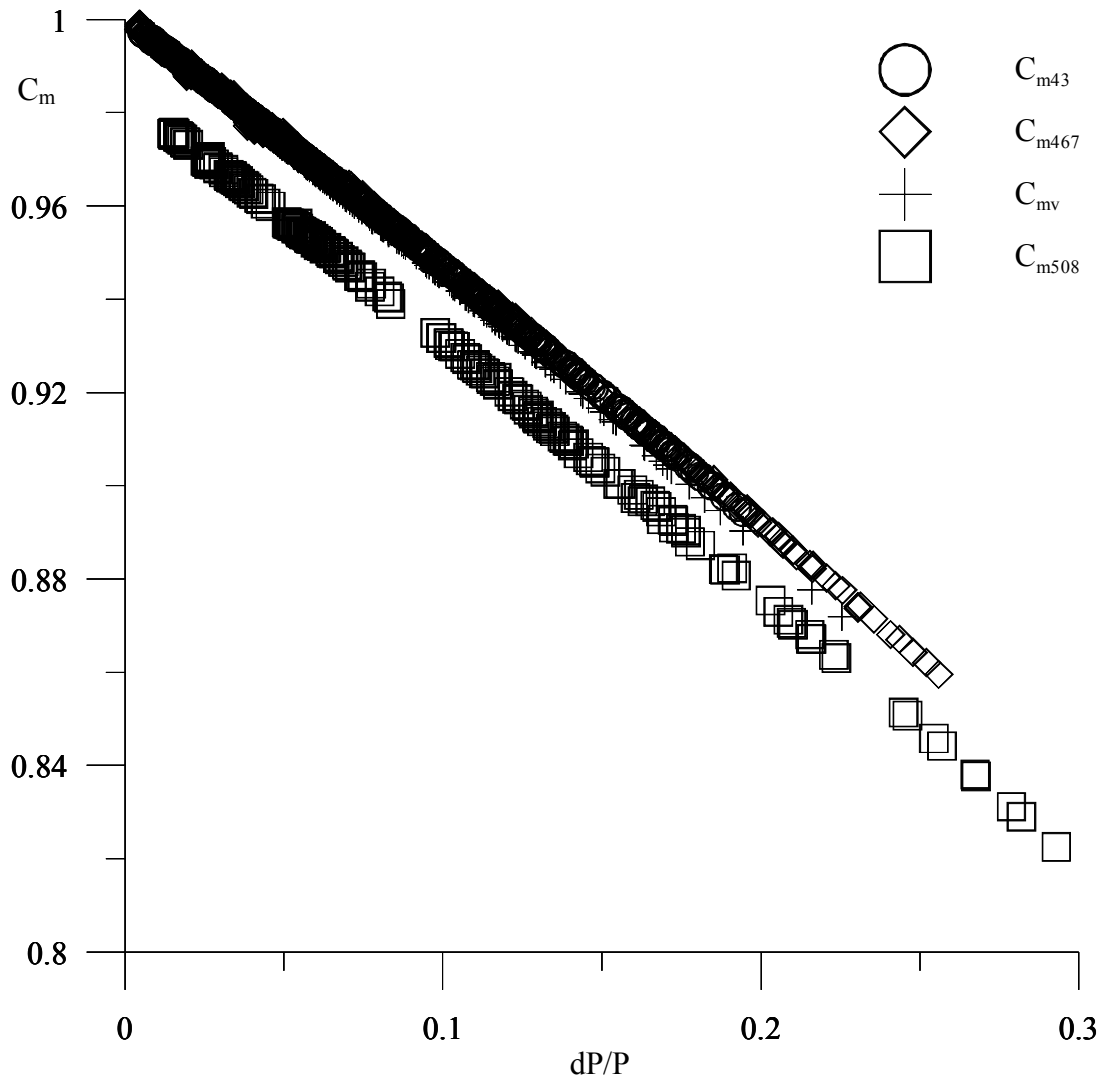
Figure 16. Coefficients C_m for the slotted plates, the Venturi meter and the standard orifice.
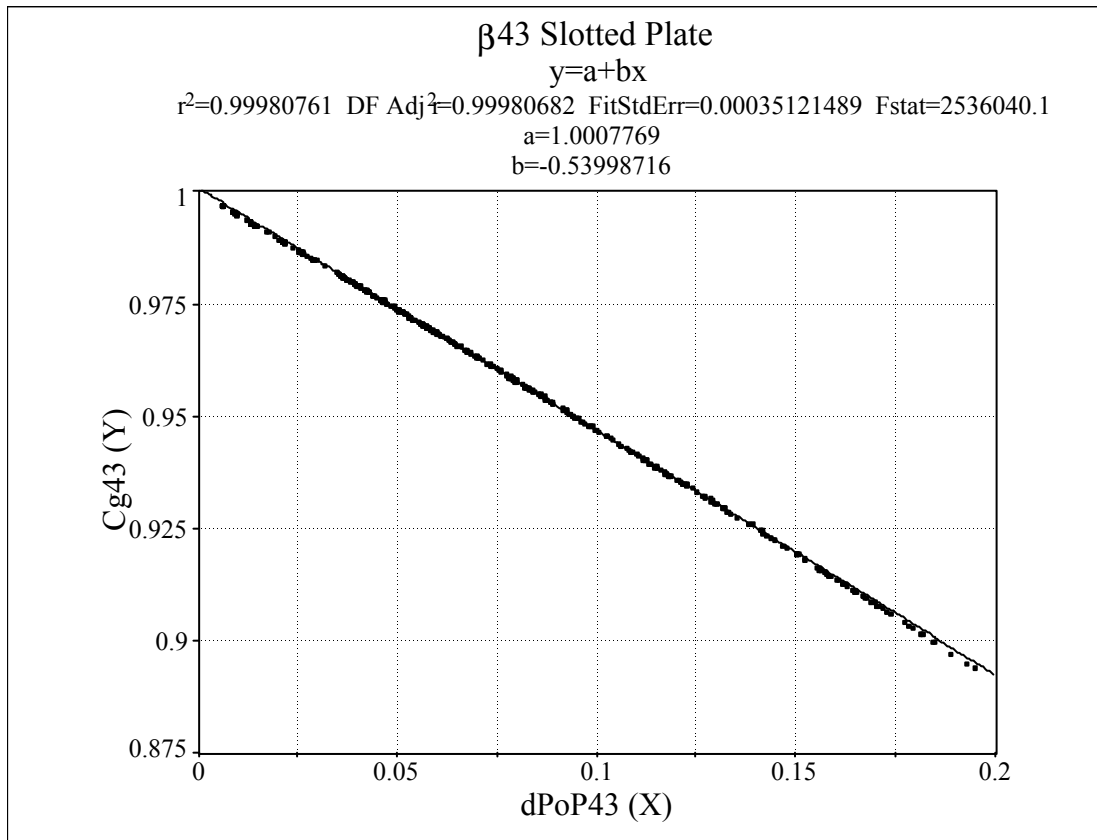
Figure 17. C_g curve fitting. $\beta=0.43$ slotted plate.
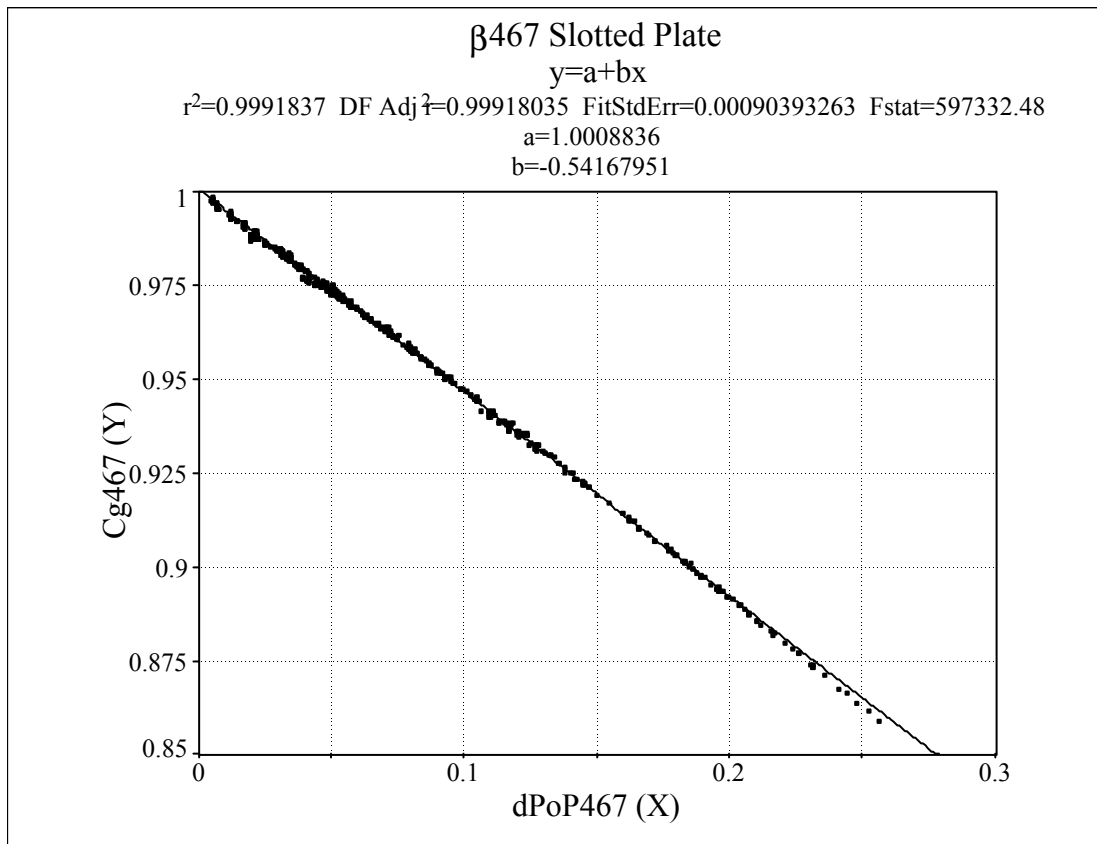
Figure 18. C$_g$ curve fitting. β=0.467 slotted plate.

Figure 19. C_g curve fitting. Venturi meter.
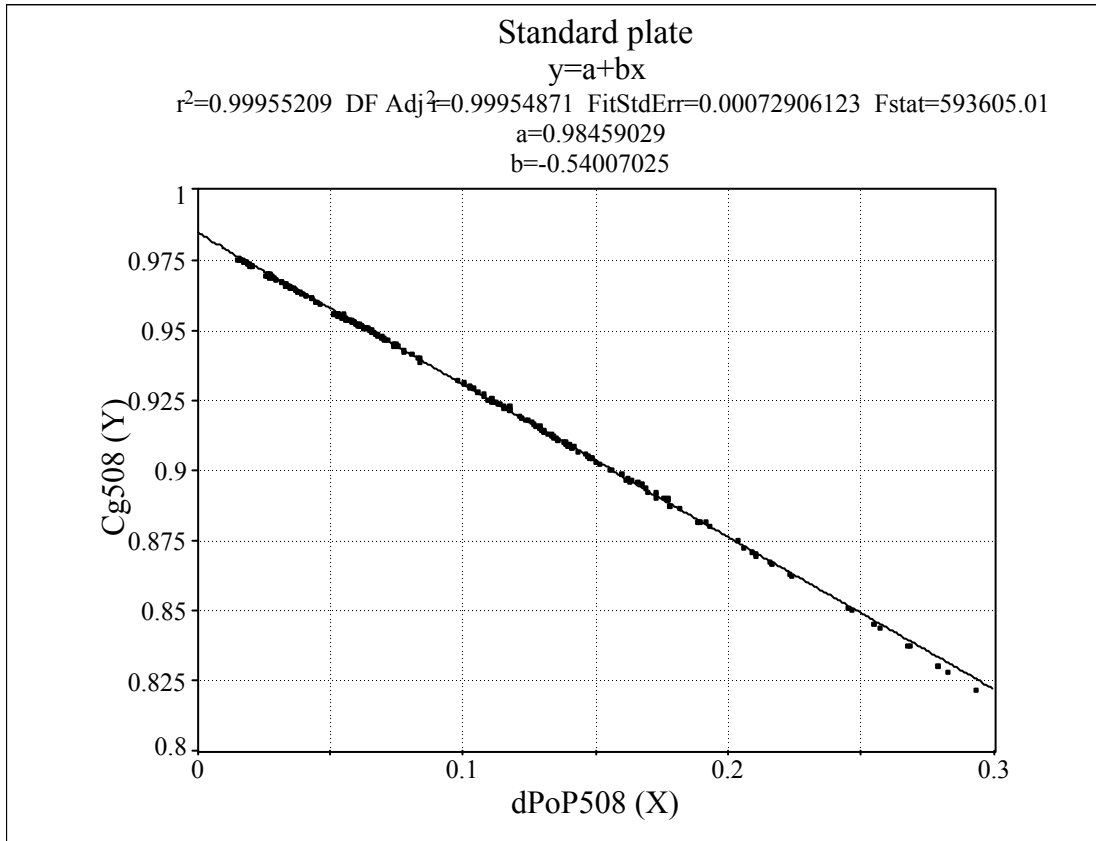
Figure 20. C_g curve fitting. Standard plate.
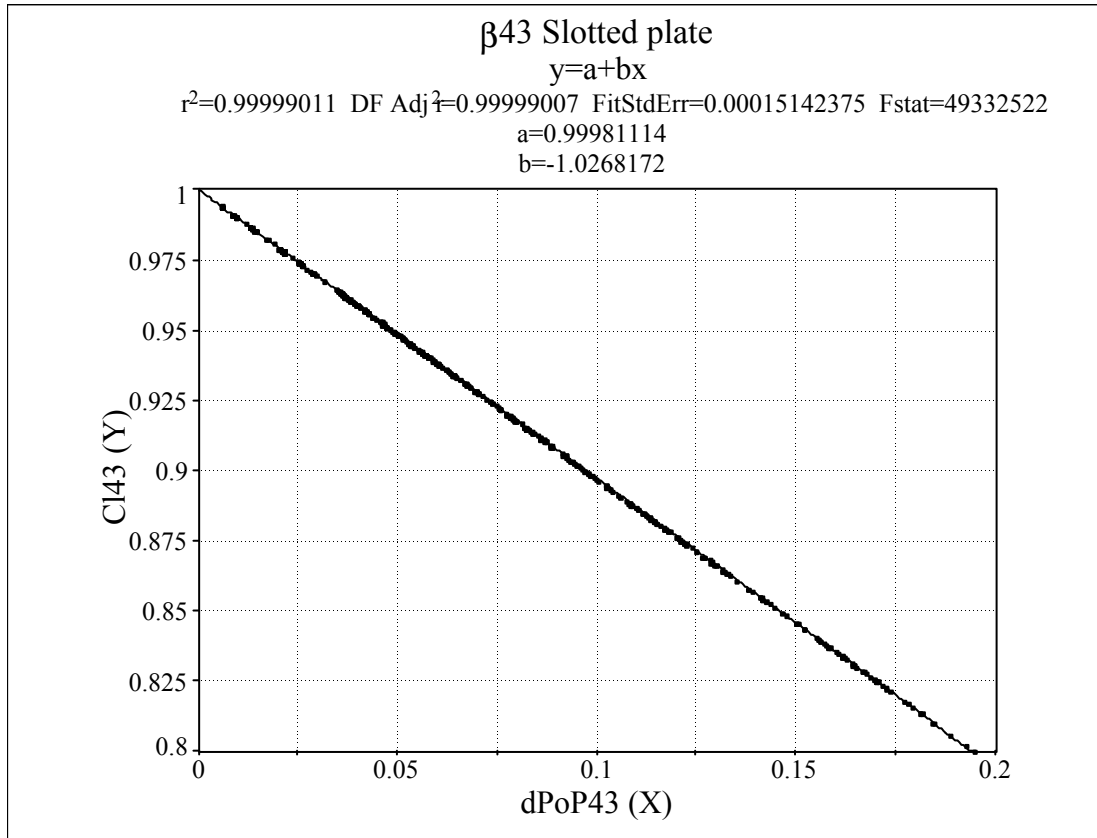
Figure 21. C_l curve fitting. β=0.43 slotted plate.

Figure 22. C$_l$ curve fitting. β=0.467 slotted plate.

Figure 23. C_l curve fitting. Venturi meter.
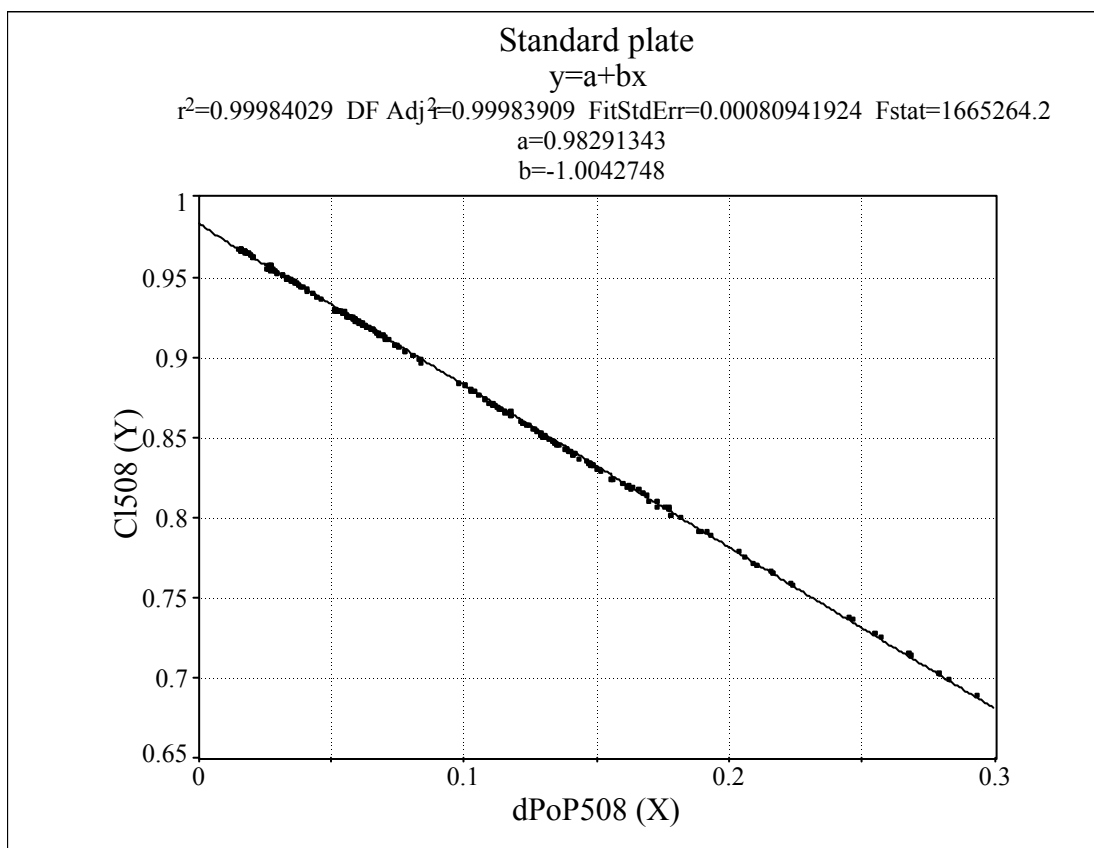
Figure 24. C_l curve fitting. Standard plate.
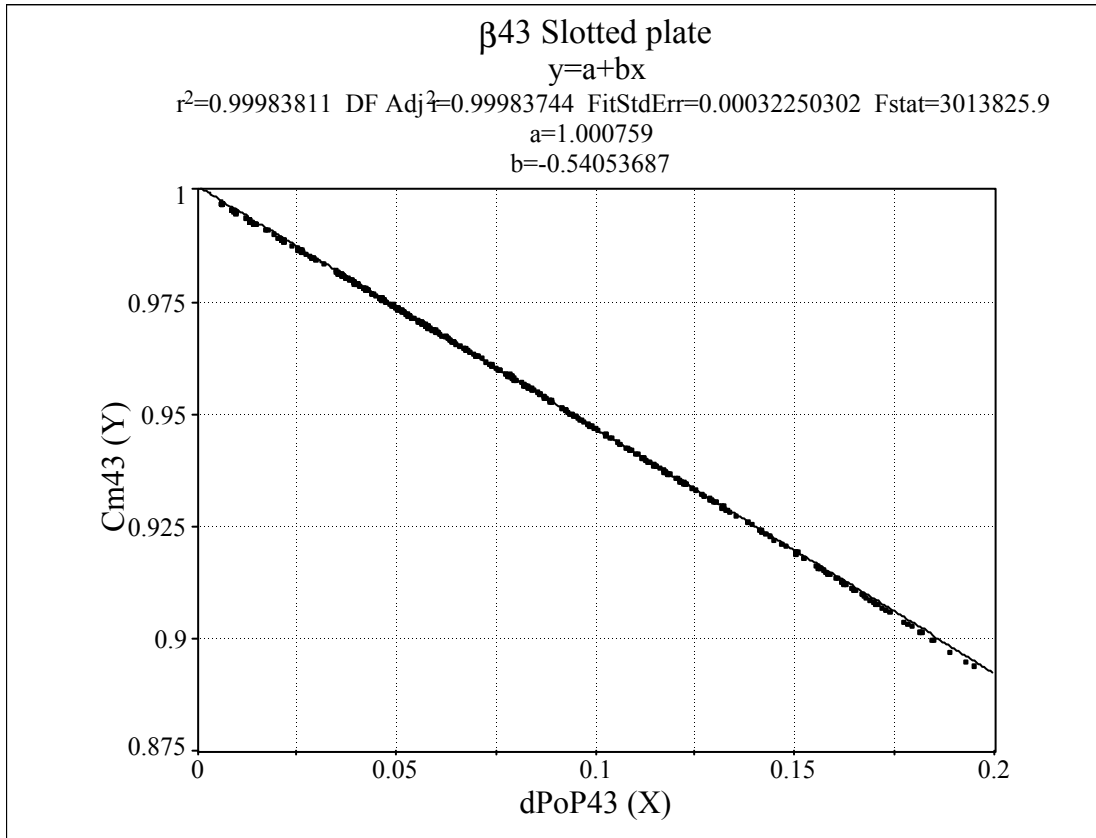
Figure 25. C_m curve fitting. $\beta=0.43$ slotted plate.
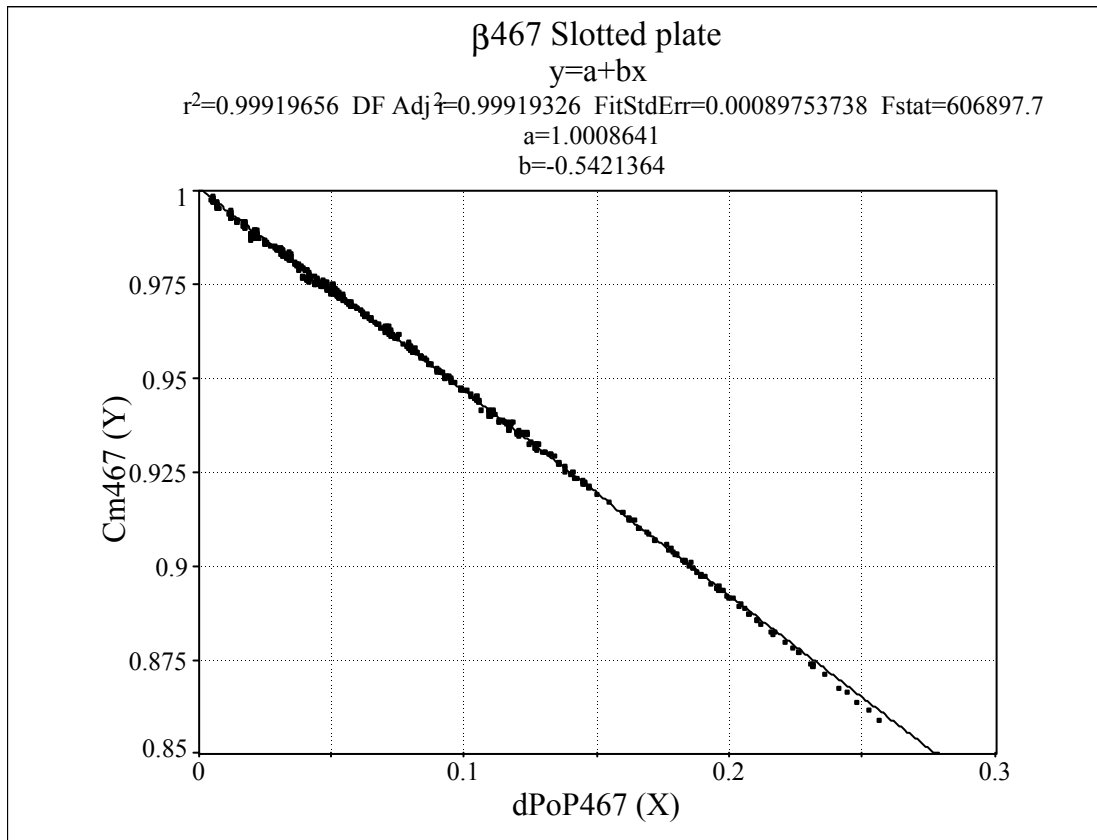
Figure 26. C_m curve fitting. $\beta=0.467$ slotted plate.
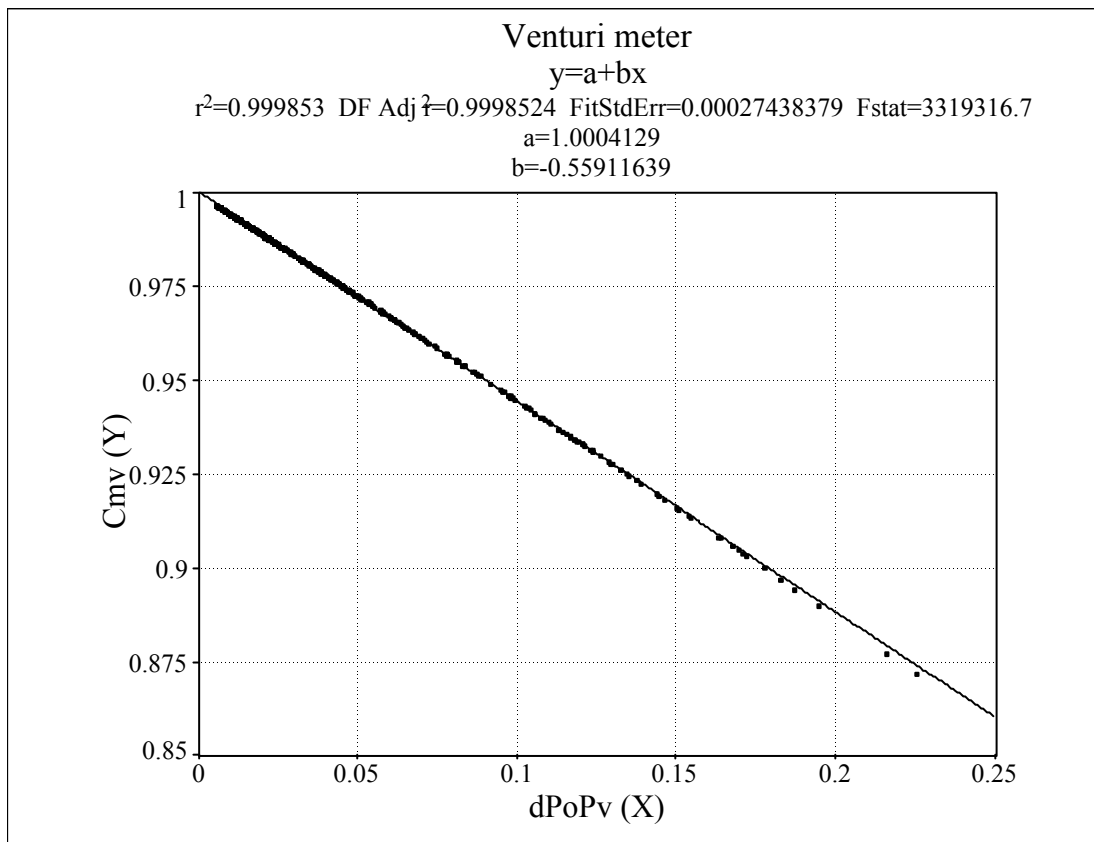
Figure 27. C_m curve fitting. Venturi meter.
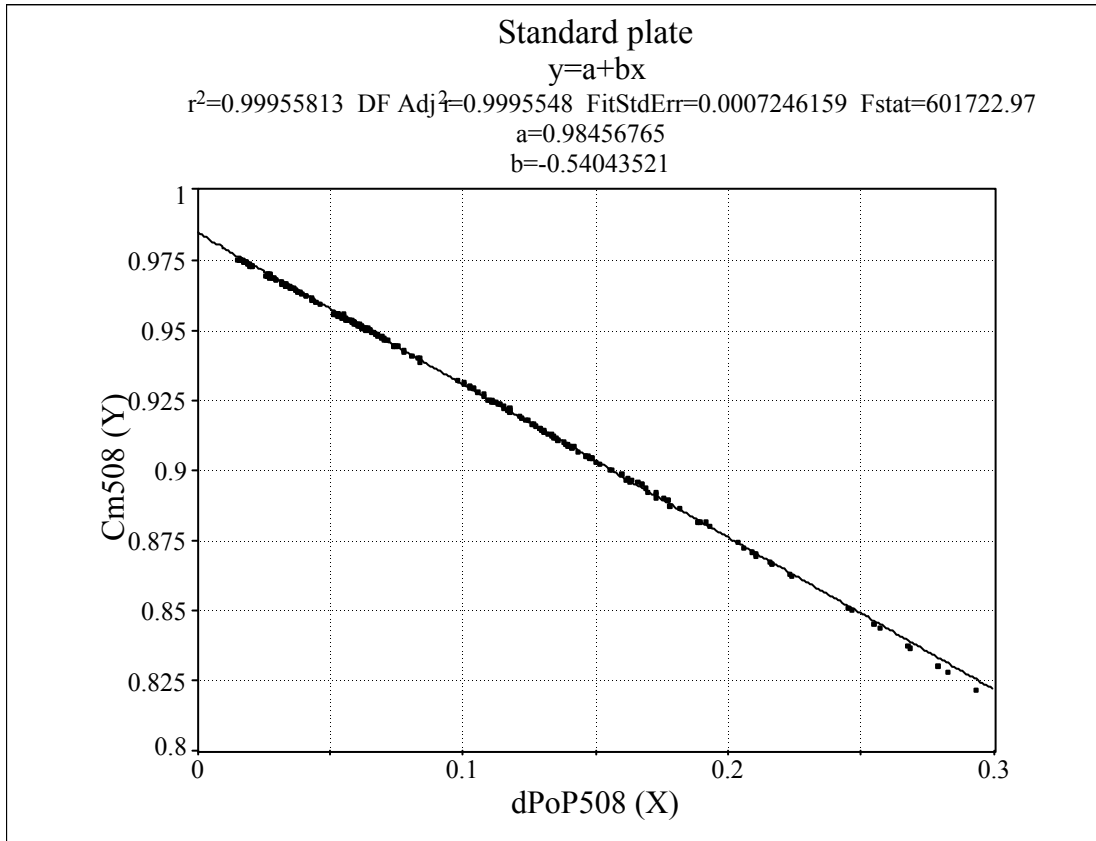
Figure 28. C_m curve fitting. Standard plate.
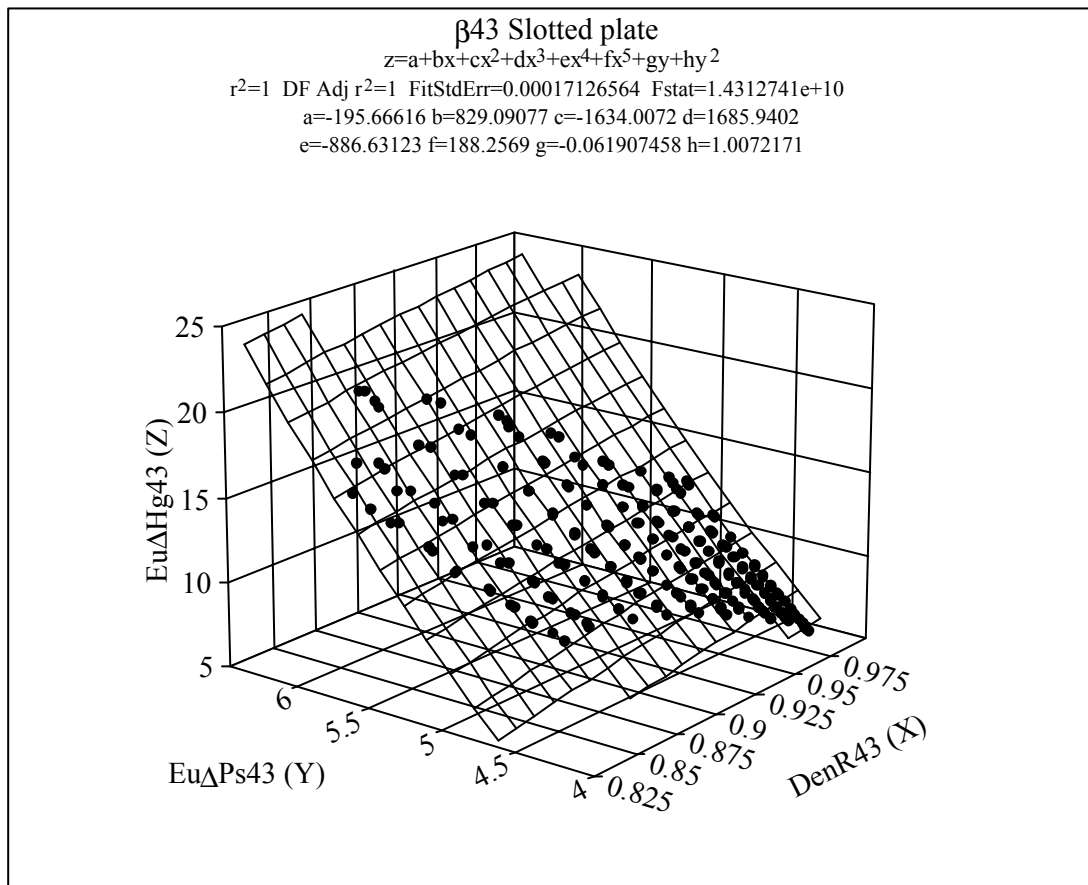
Figure 29. Empirical relation of ΔHg as a function of the upstream and downstream

pressure, the gas velocity and the differential pressure.
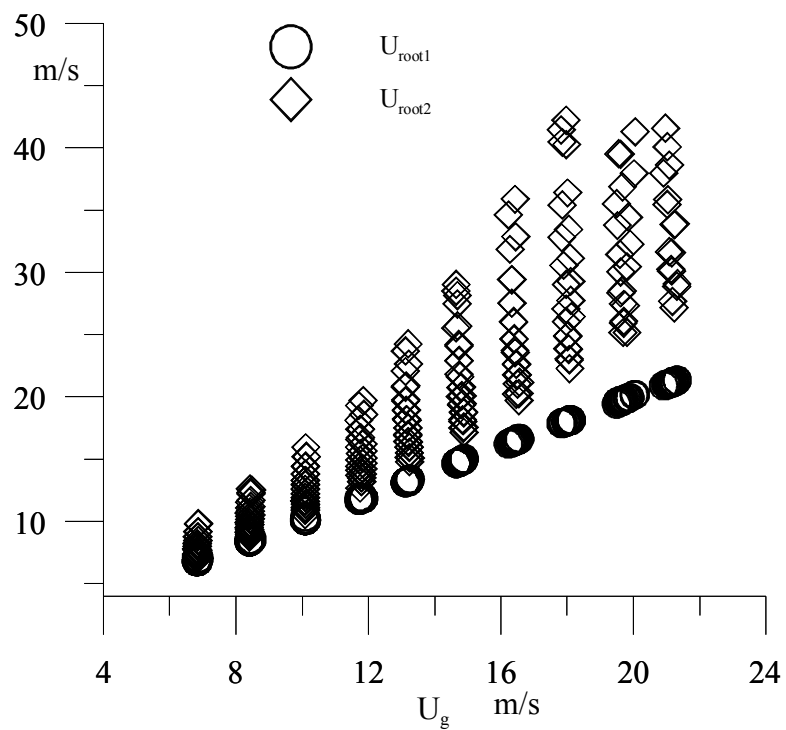
Figure 30. Solutions obtained from the combination of an empirical relation and equation 26.
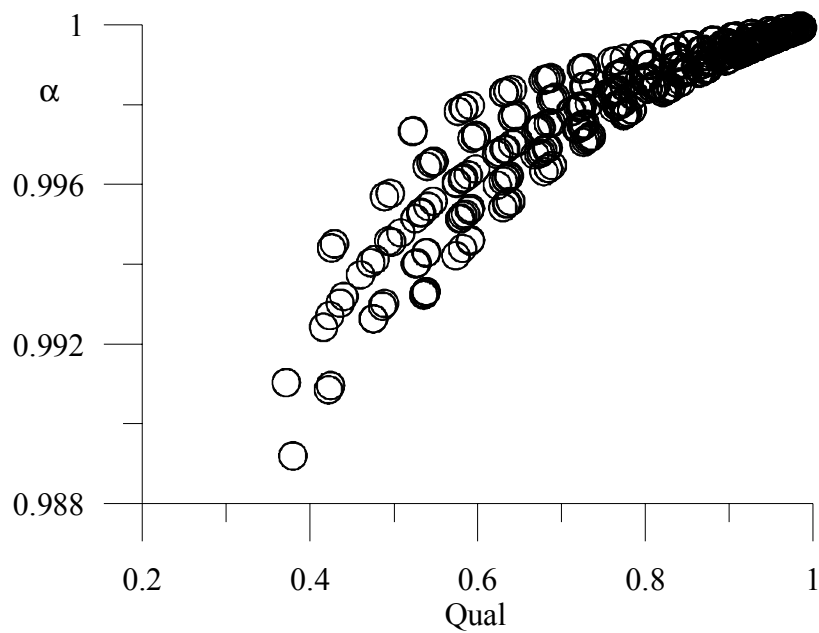
Figure 31. Gas void fraction range.
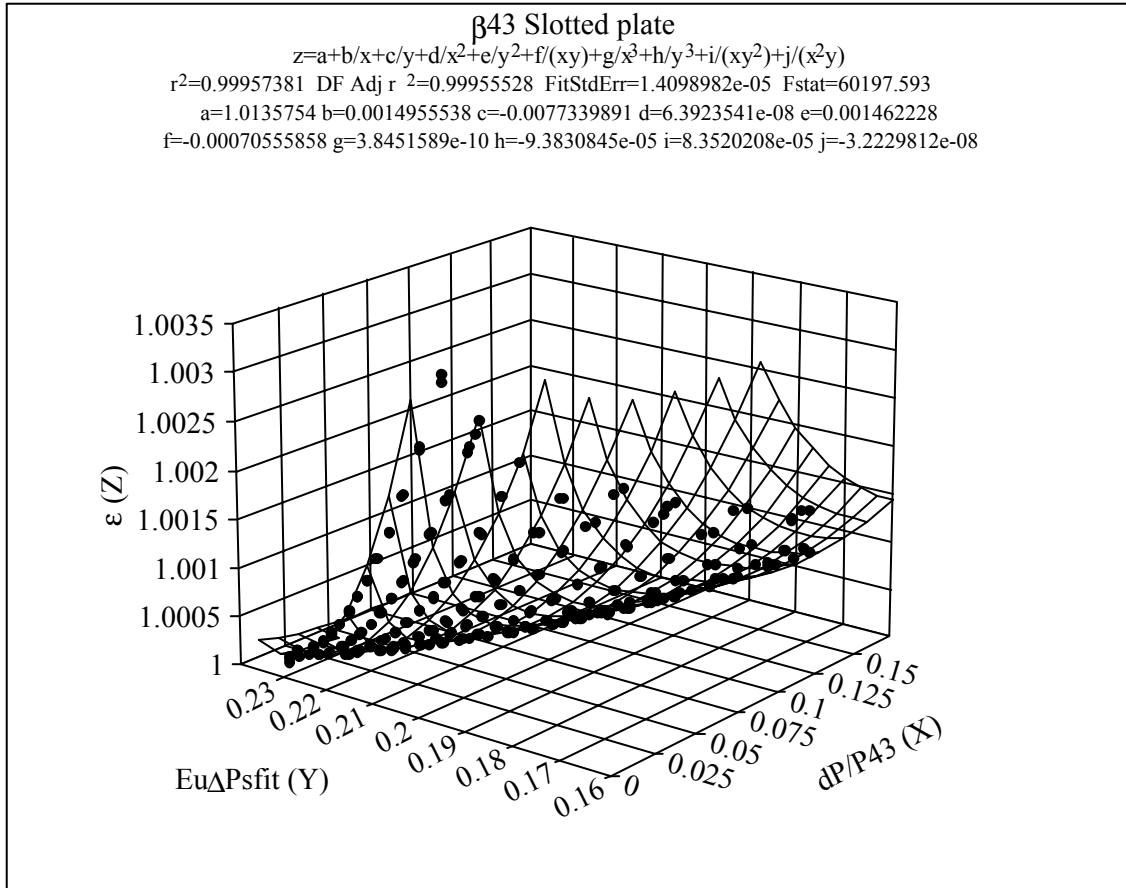
Figure 32. Gas void fraction as a function of velocity U_{root}, the differential and upstream pressures and the upstream gas density.
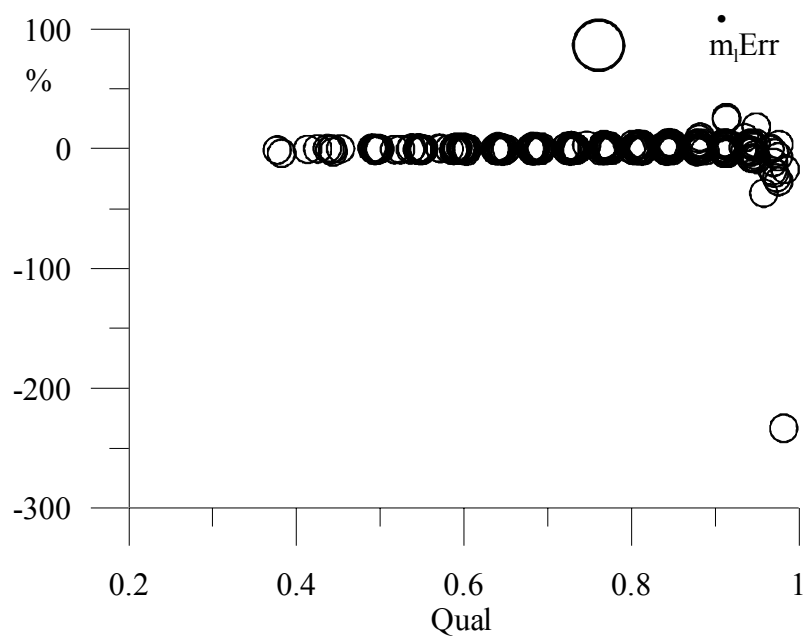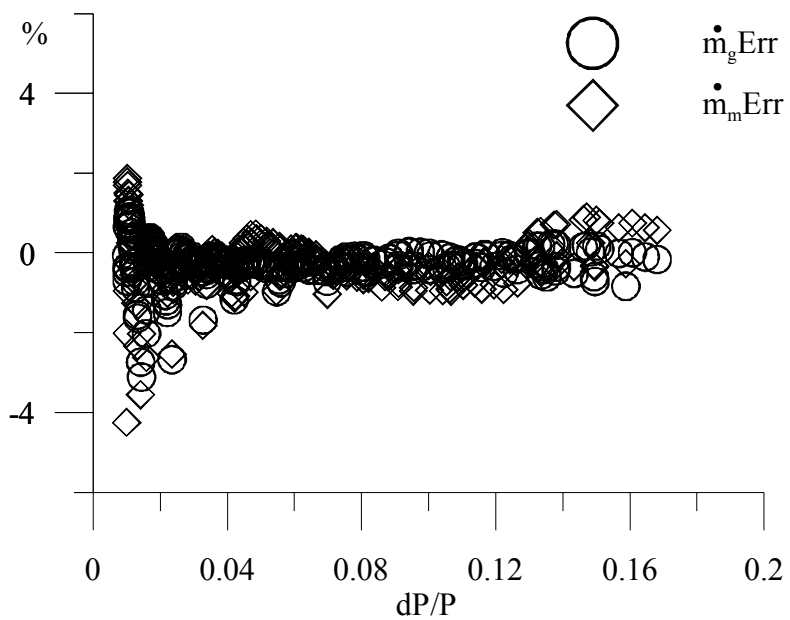
Figure 33. Error in gas, liquid and total flow rate using the slotted plate.
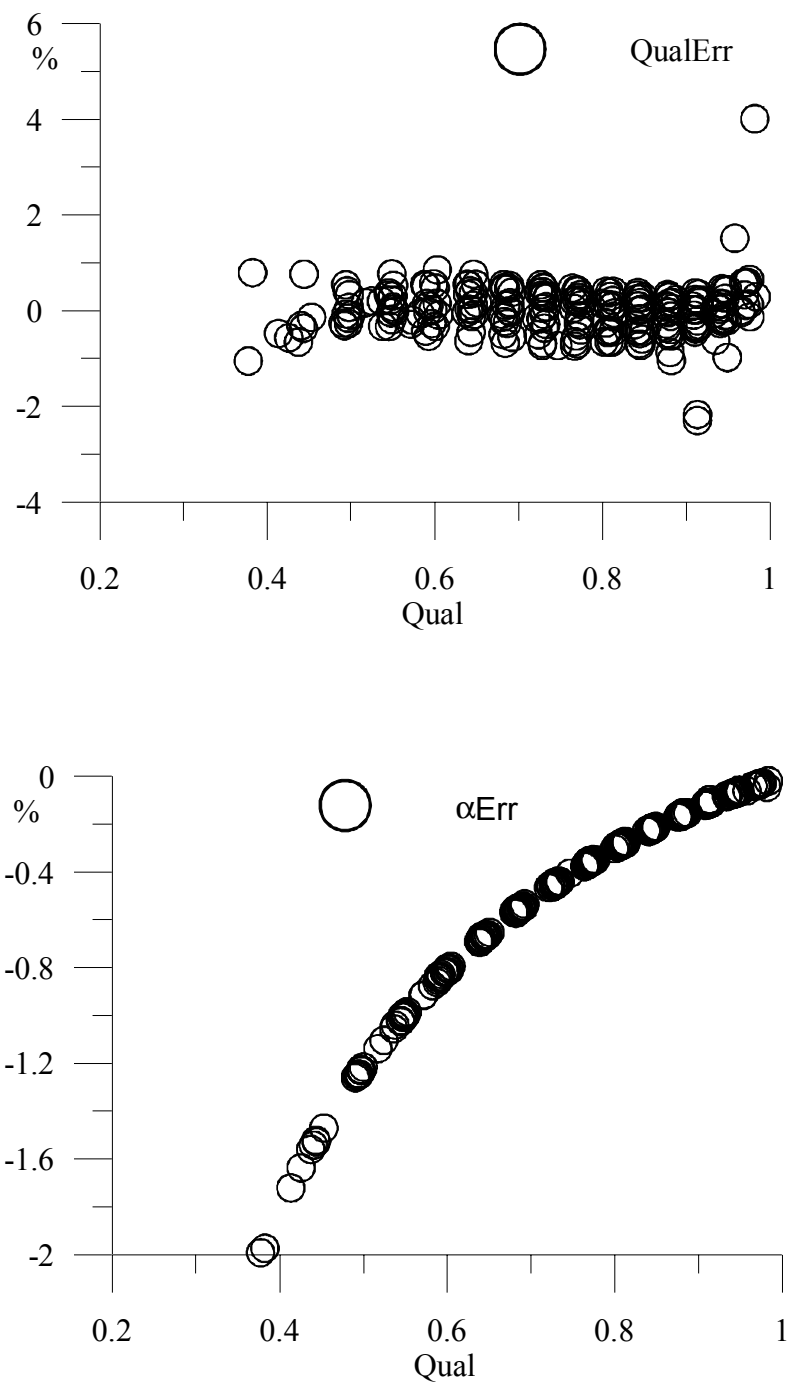
Figure 34. Error in mixture density, and gas void fraction using the slotted plate.
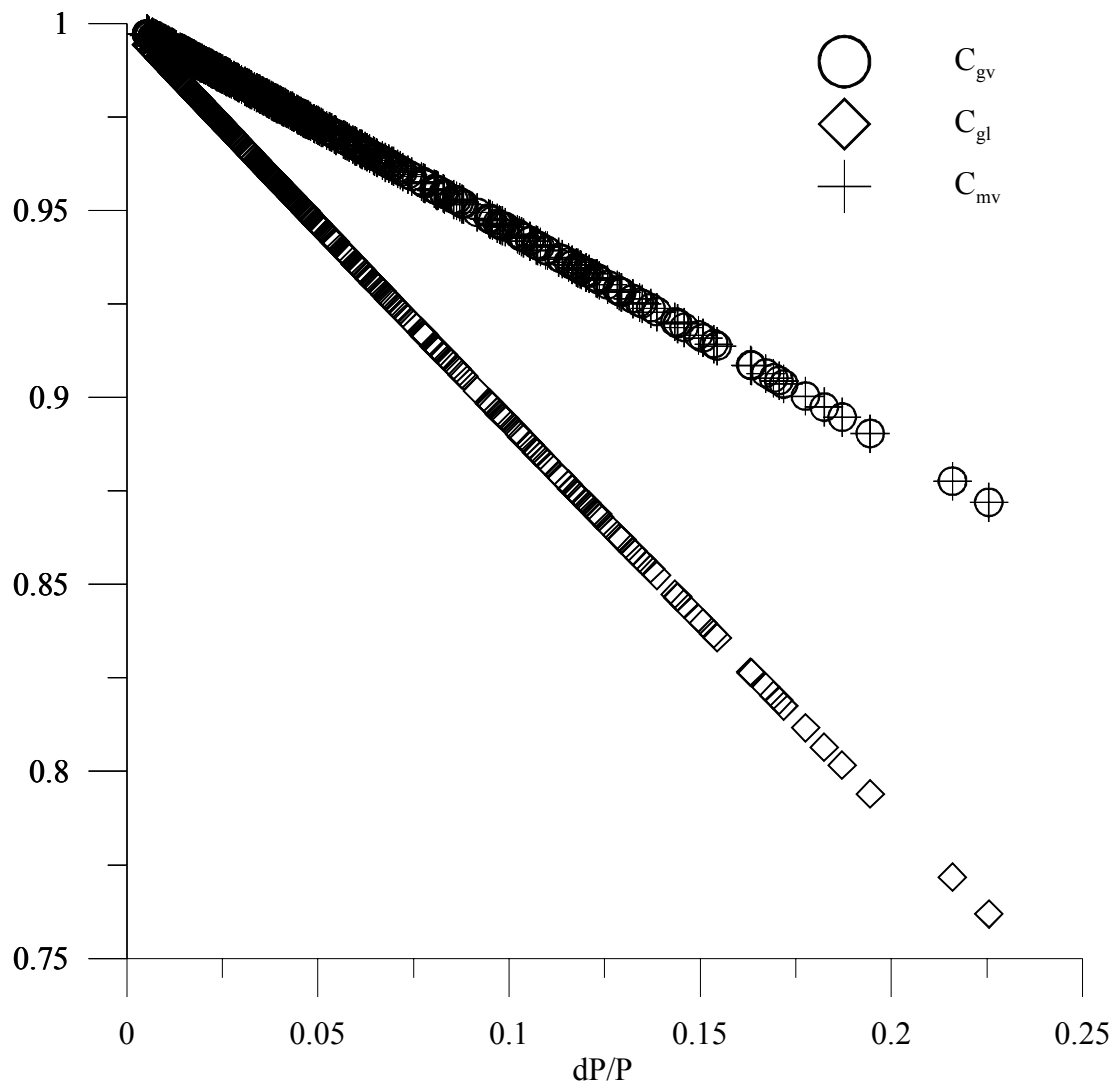
Figure 35. Discharge coefficient for the Venturi meter.
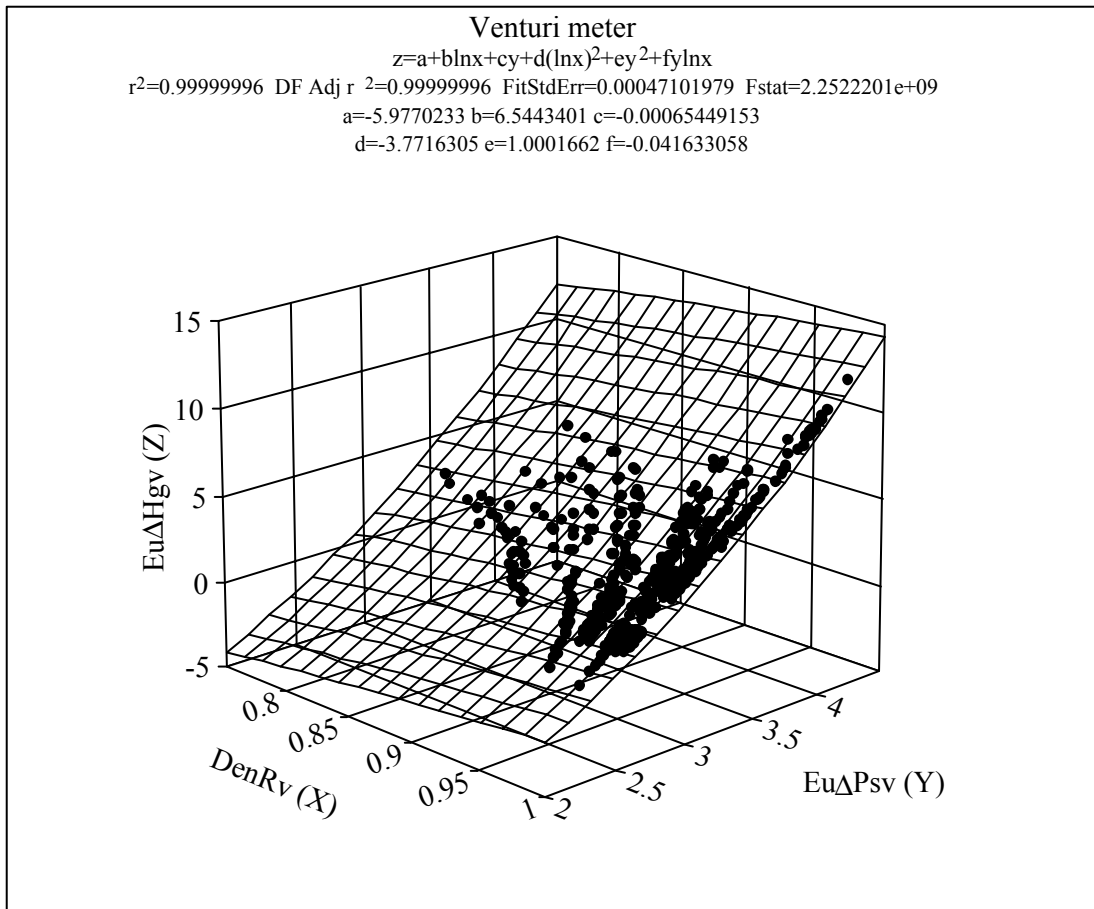
Figure 36. Euler ΔH_g number correlation for Venturi meter.
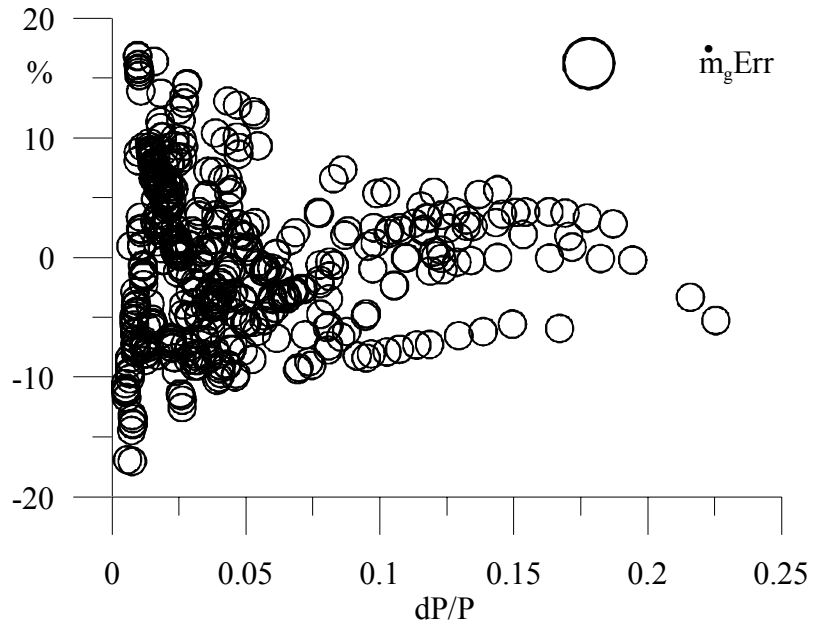
Figure 37. Gas mass flow rate computation error using Venturi meter
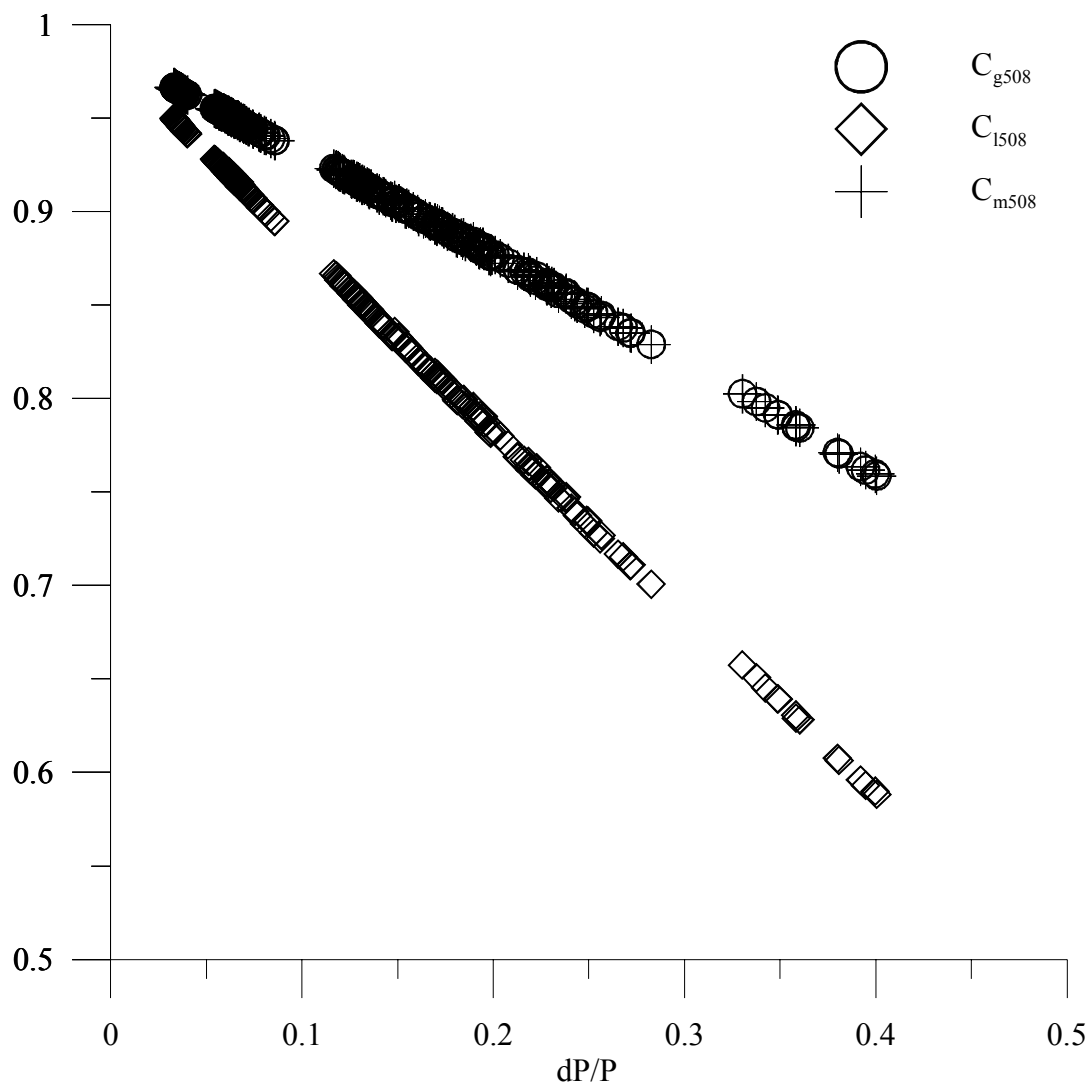
Figure 38. Discharge coefficient for the standard plate.

Standard Plate

$z=a+b/x+cy+d/x^2+ey^2+fy/x$

$r^2=0.9999996$ DF Adj r $^2=0.99999959$ FitStdErr=0.00060955569 Fstat=1.3022607e+08

a=0.90725522 b=-7.8434369 c=-0.1617181

d=-0.066298112 e=1.012262 f=0.051495134
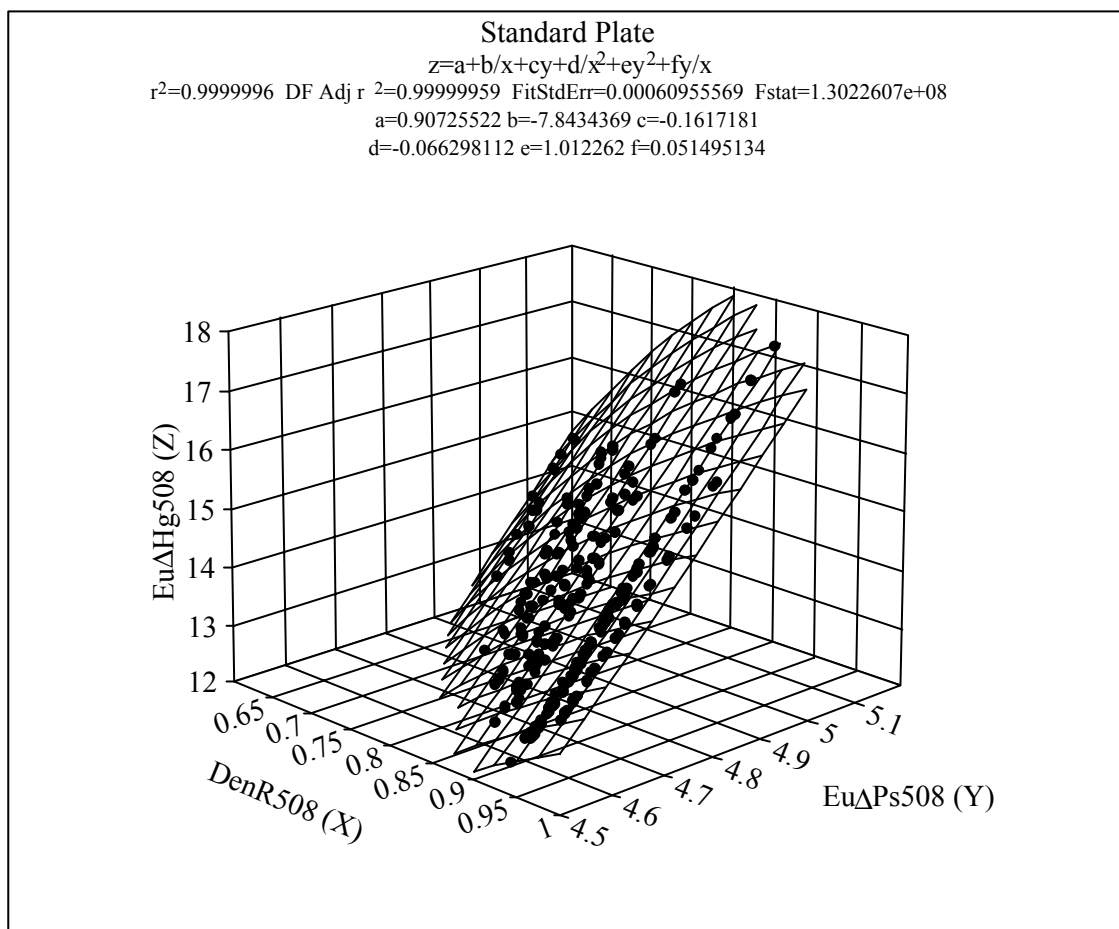
Figure 39. Euler ΔH_g number correlation for the standard plate.
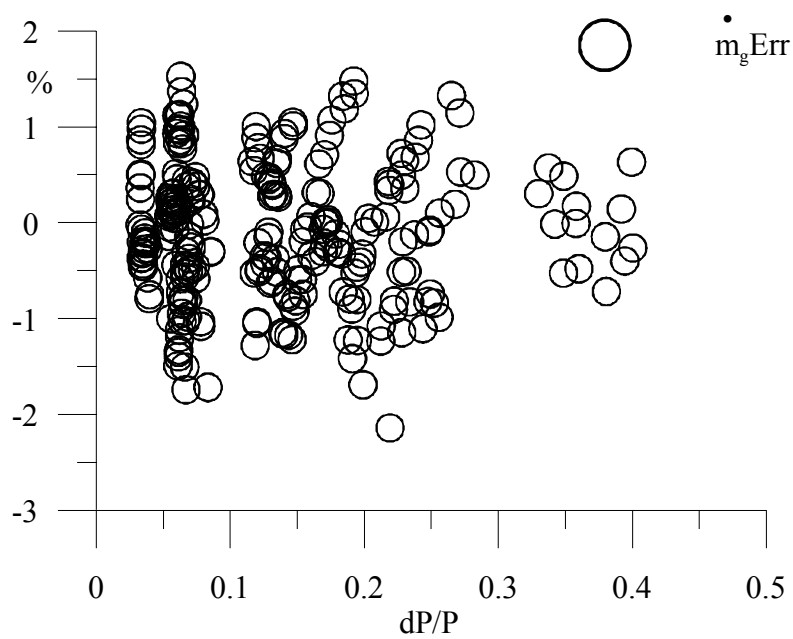
Figure 40. Gas mass flow rate computation error using the standard orifice plate.
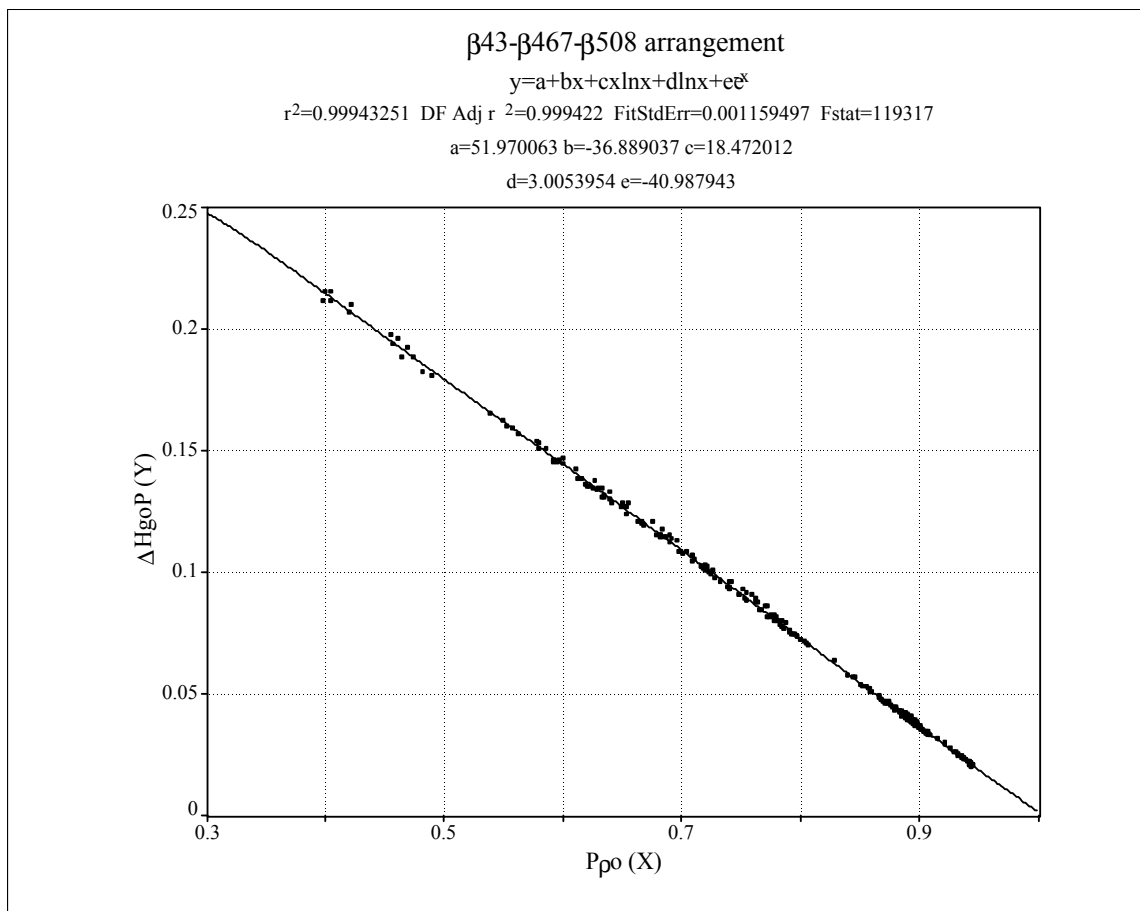
Figure 41. Standard plate ΔHgoP correlation using the β43-β467-β508 arrangement.
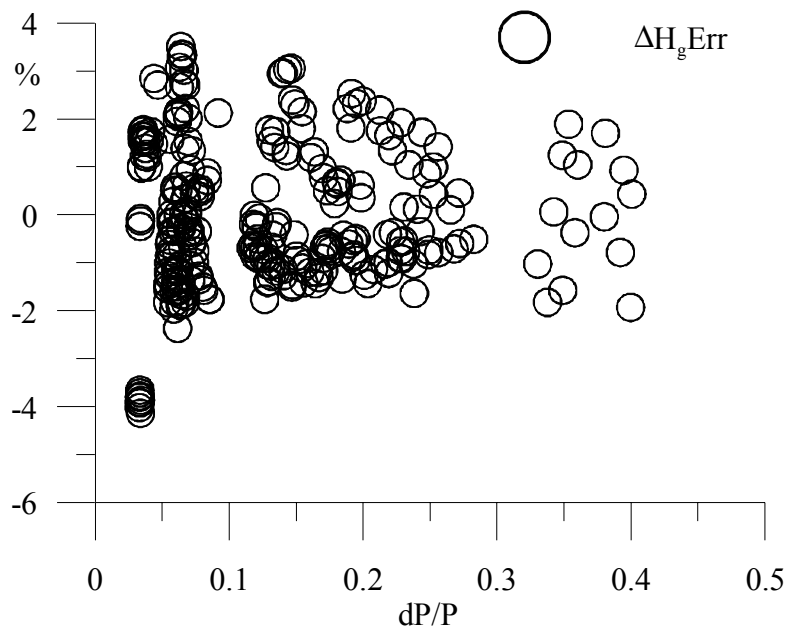
Figure 42. Standard plate ΔHg computation using the β43-β467-β508 arrangement.
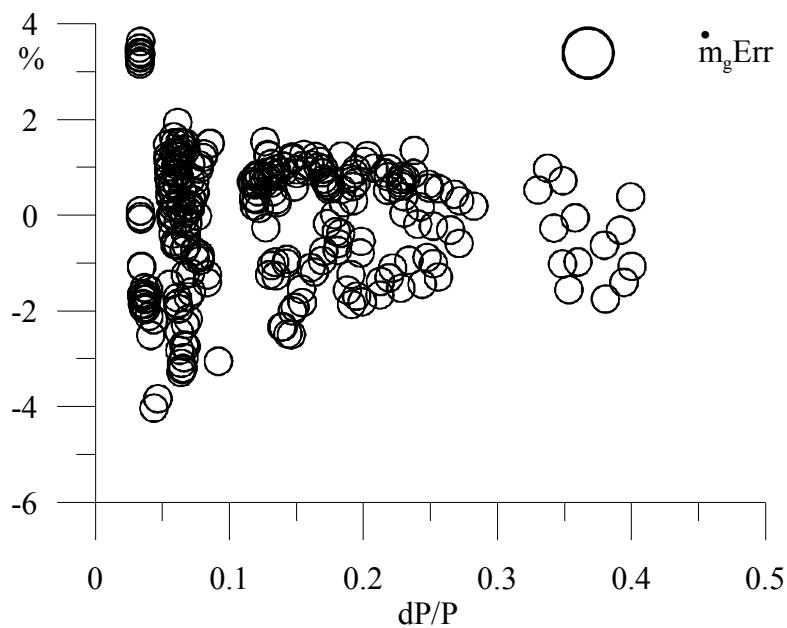
Figure 43. Standard plate gas mass flow rate estimation using the β43-β467-β508 arrangement.
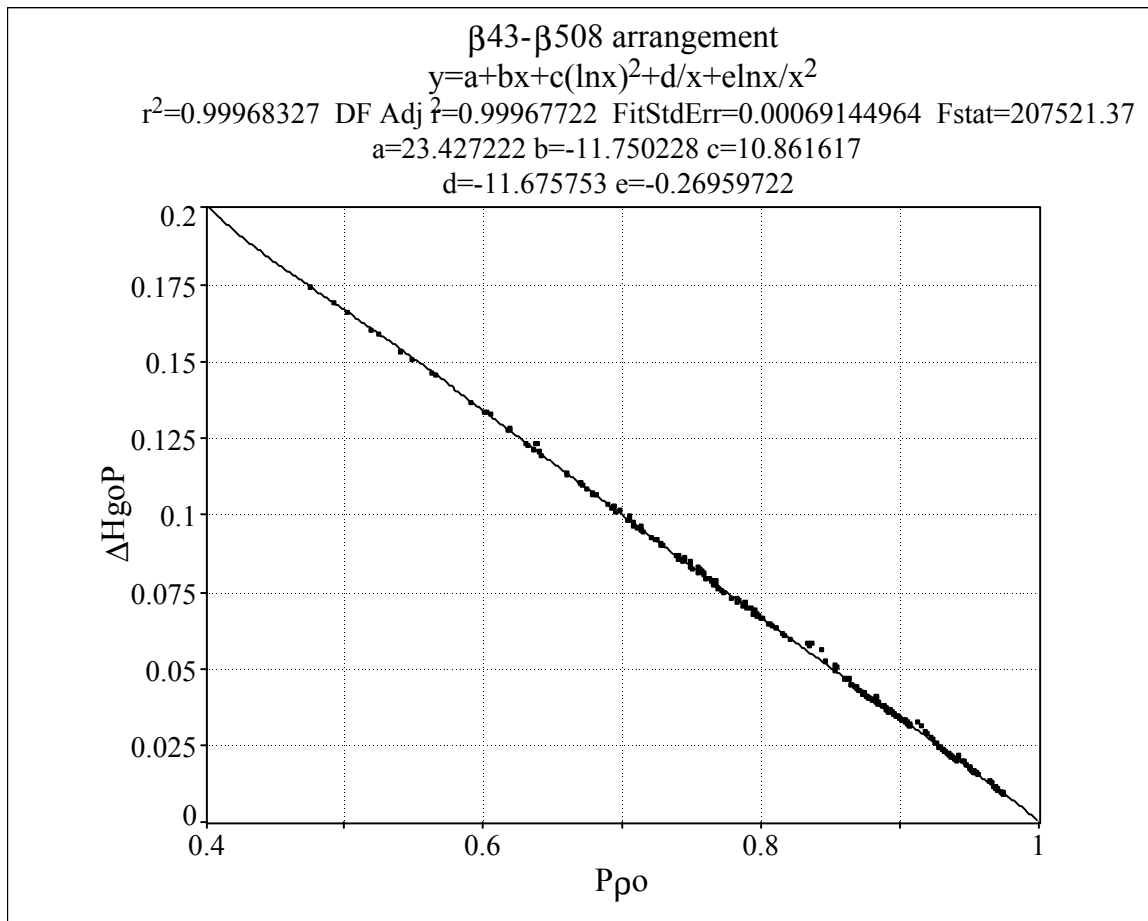
Figure 44. Standard plate ΔHgoP correlation using the β43-β508 arrangement.
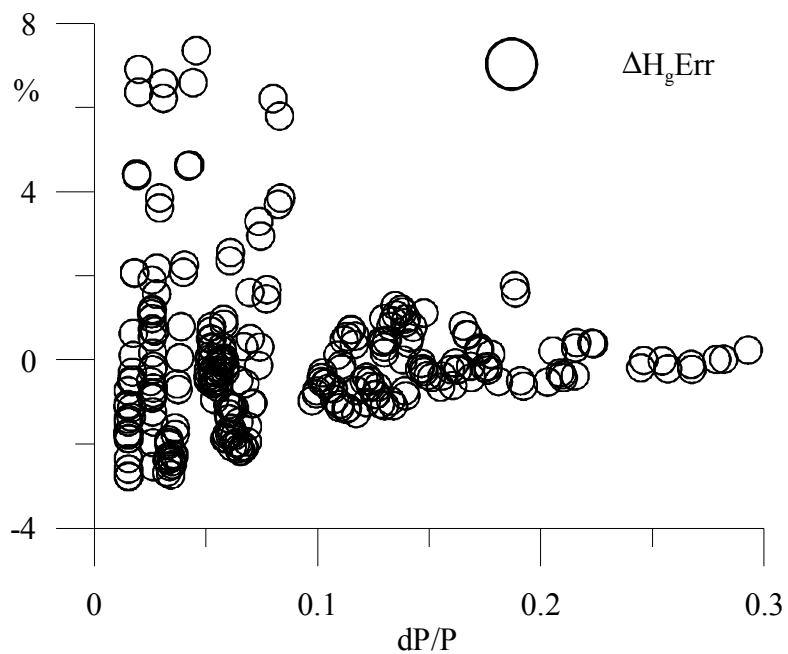
Figure 45. Standard plate ΔHg computation using the β43-β508 arrangement.
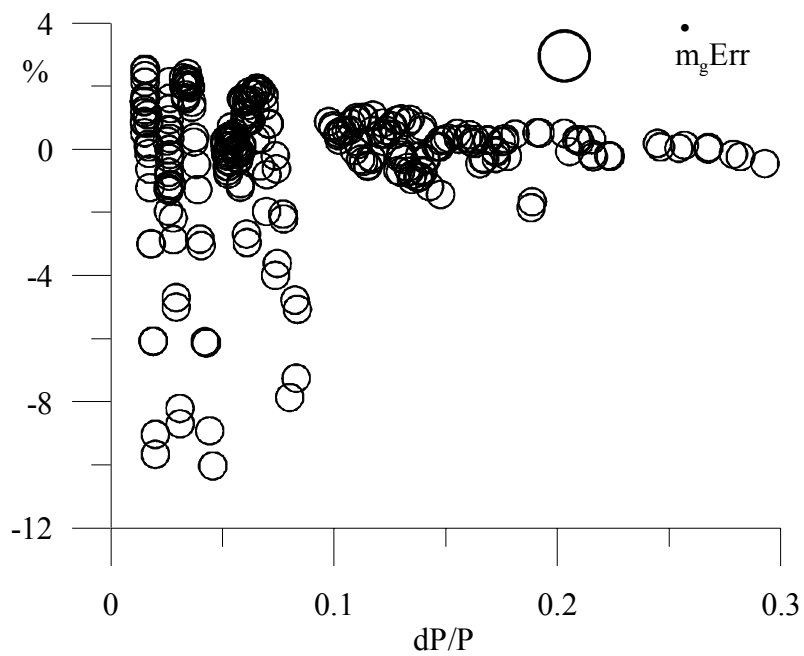
Figure 46. Standard plate gas mass flow rate estimation using the β43-β508 arrangement.
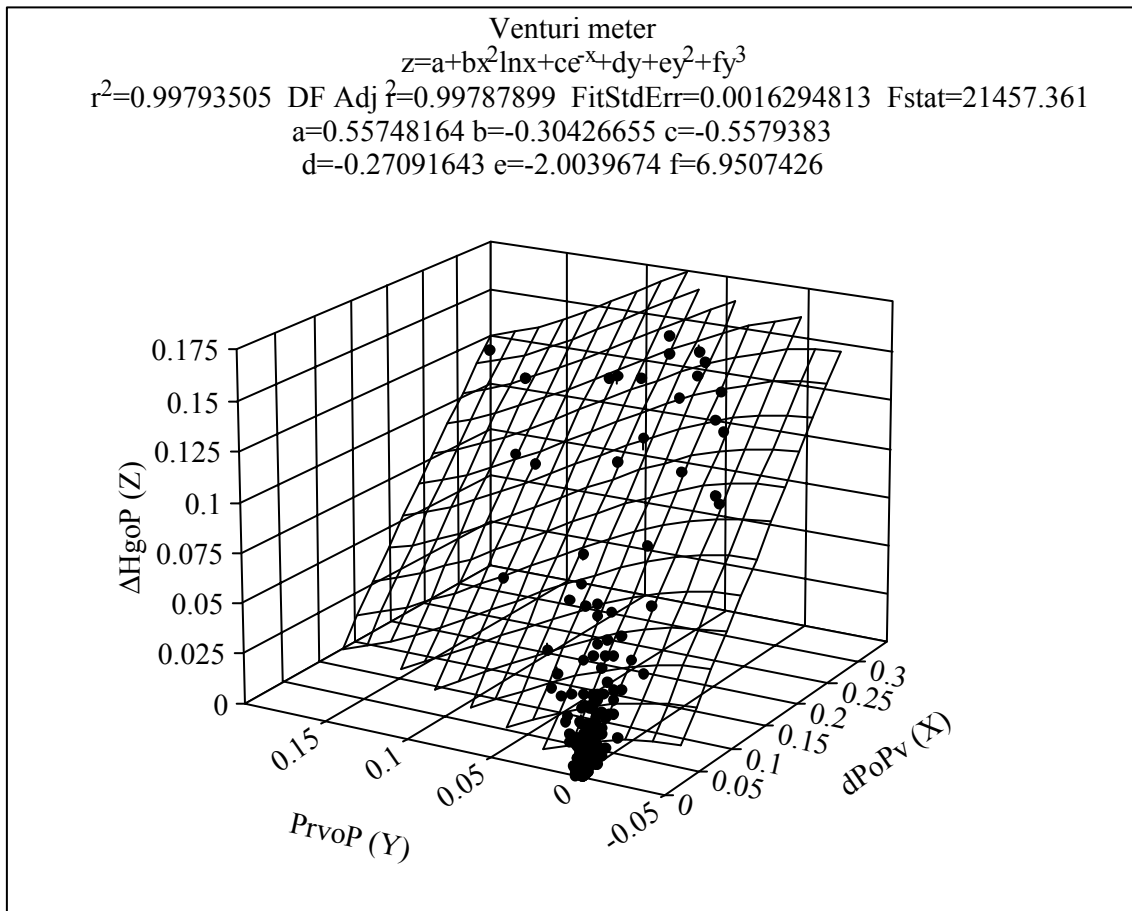
Figure 47. Venturi ΔHgoP as a function of Venturi pressure drop and Venturi recovery pressure.
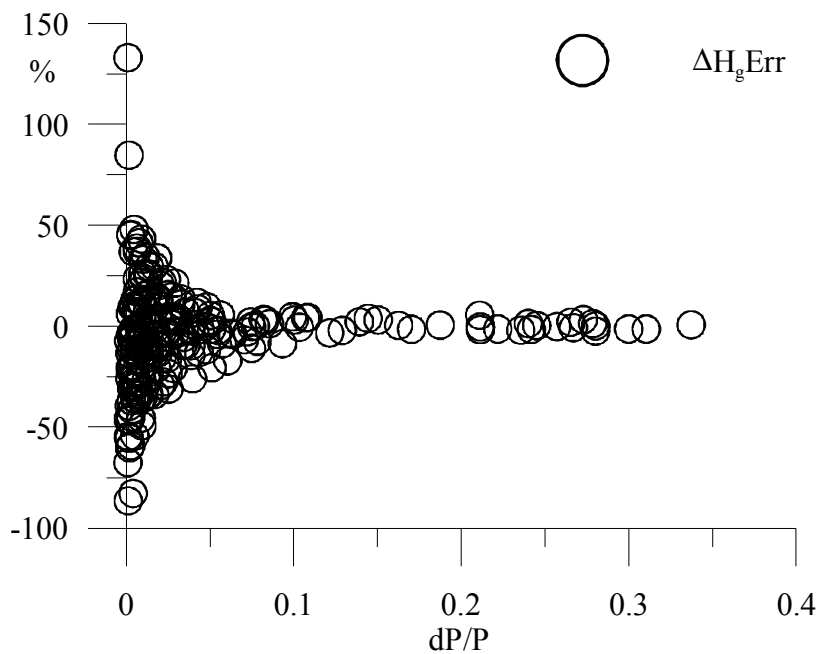
Figure 48. Venturi ΔHg computation using the Venturi pressure drop and Venturi recovery pressure
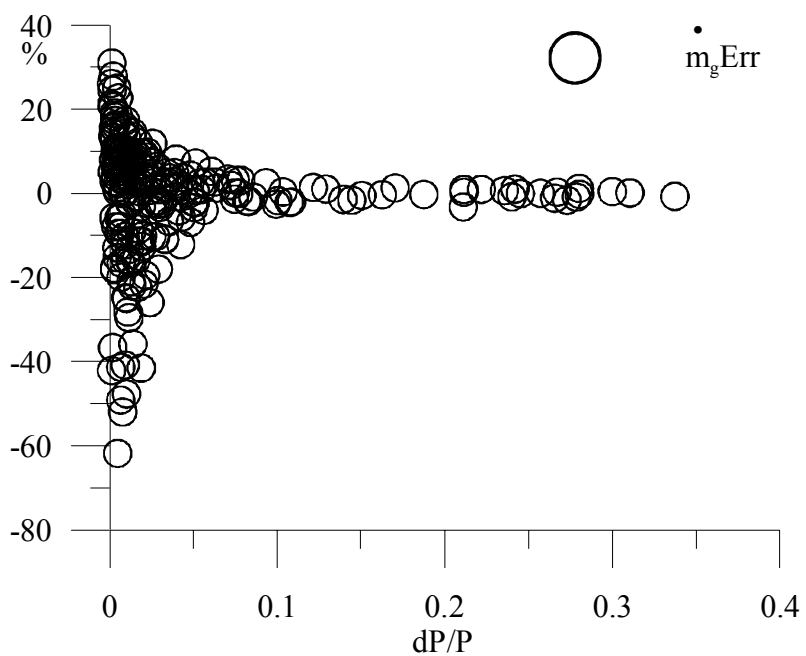
Figure 49. Gas mass flow rate estimation using the Venturi pressure drop and Venturi recovery pressure.
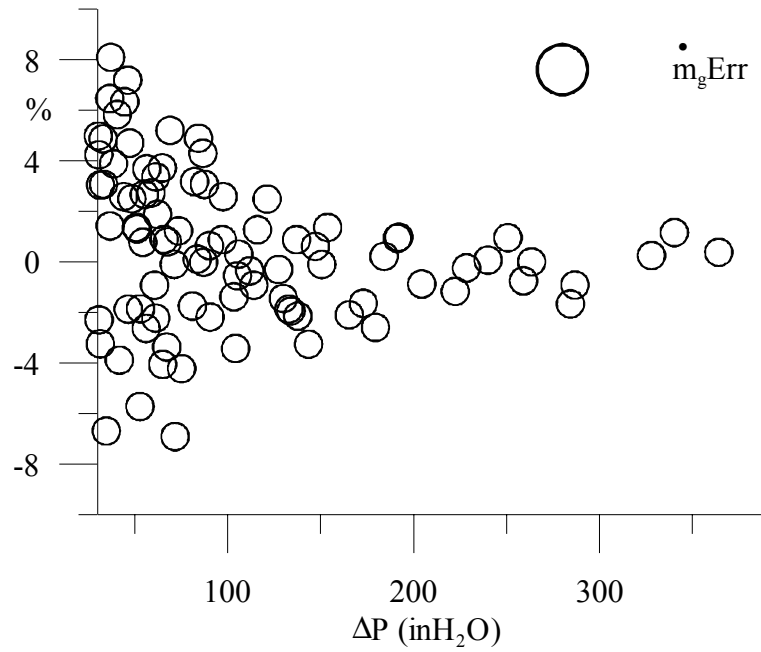
Figure 50. Gas mass flow rate estimation using the Venturi pressure differential and Venturi recovery pressure in the 30-365 inH$_2$O pressure drop range.
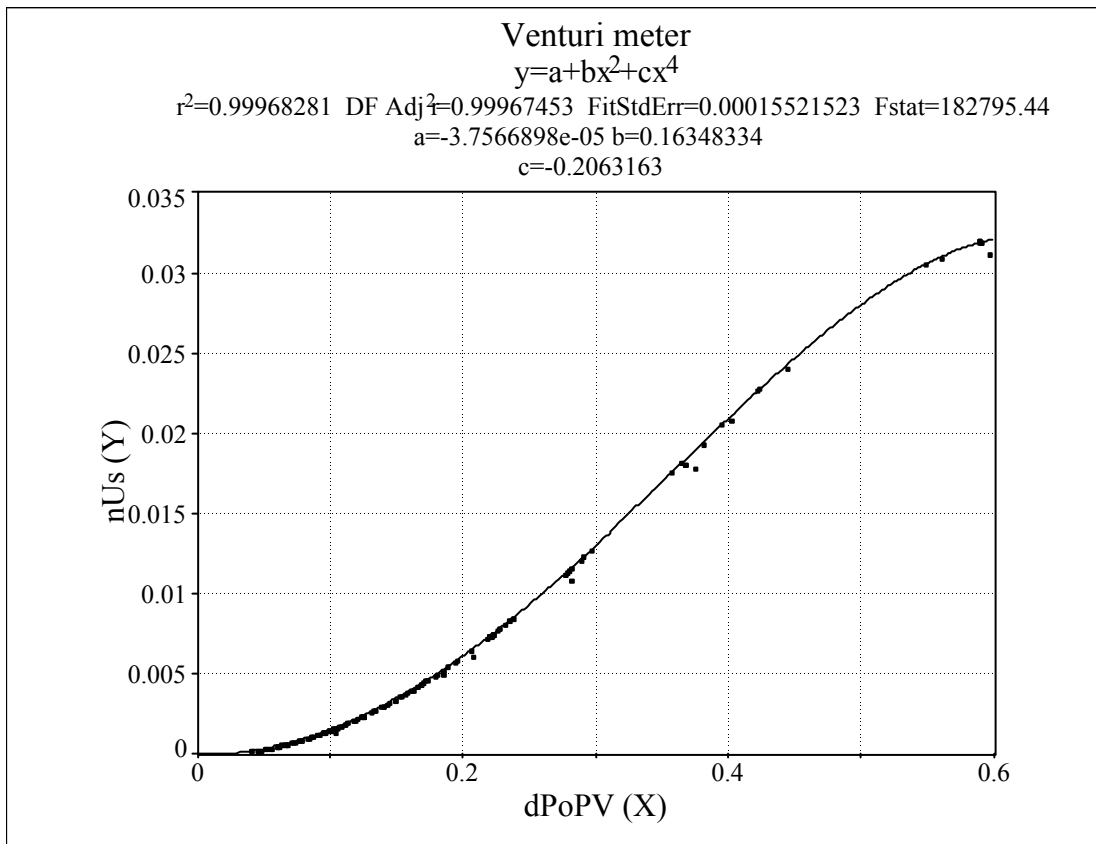
Figure 51. Non-dimensional velocity number for the Venturi meter. Air flow.
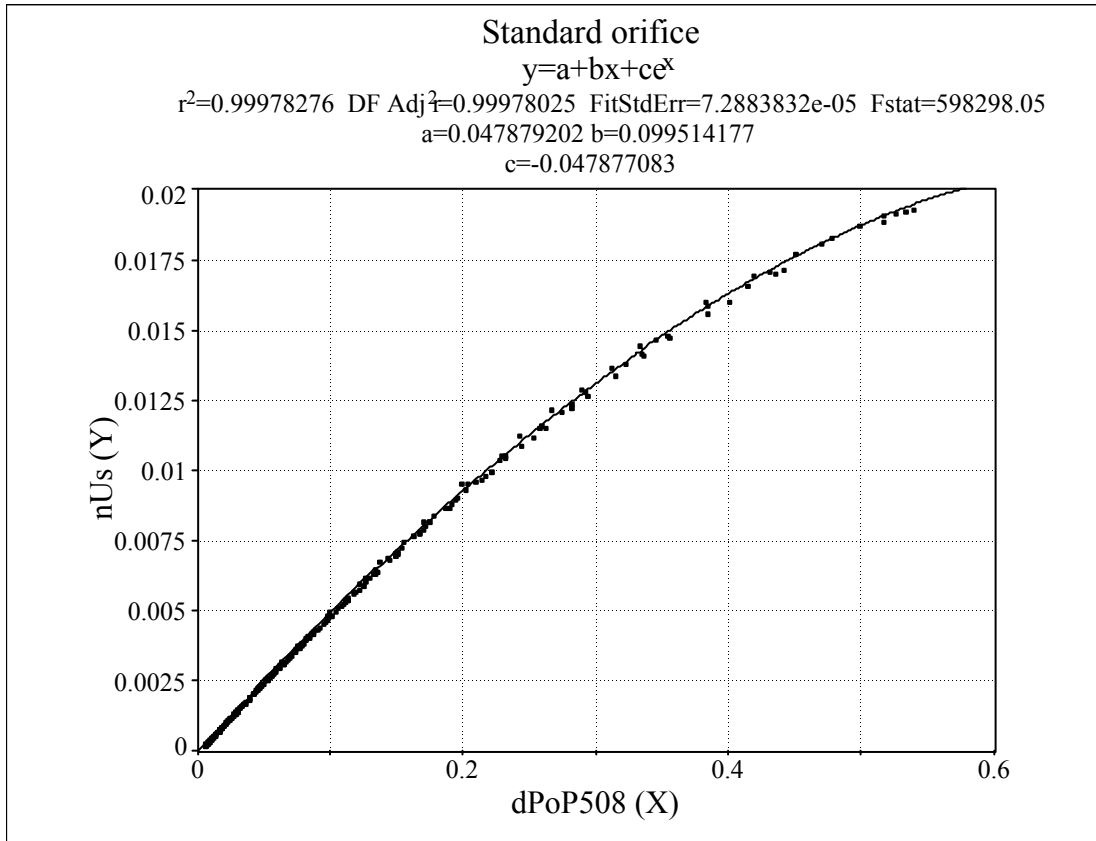
Figure 52. Non-dimensional velocity for the standard orifice plate. Air flow.
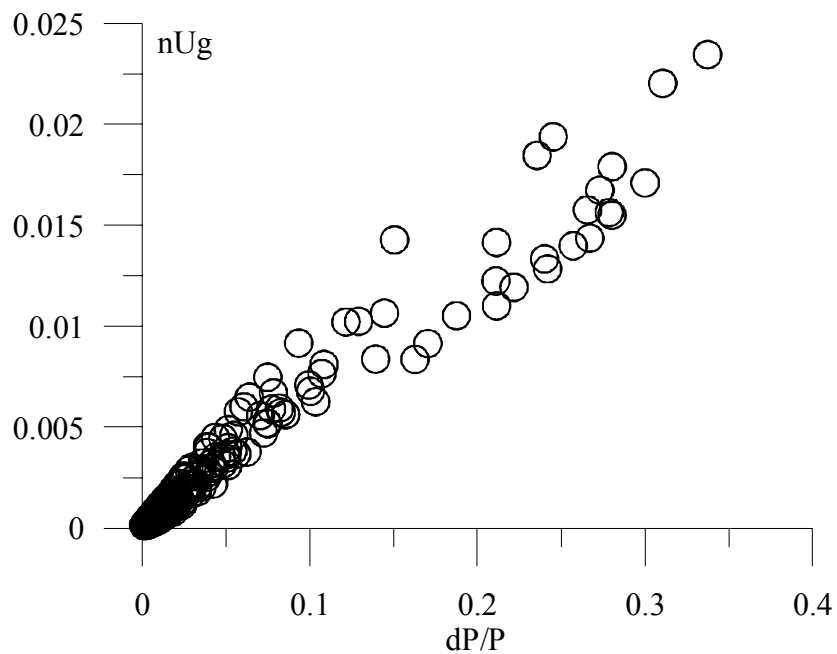
Figure 53. Non-dimensional velocity for the Venturi meter. Air water flow.
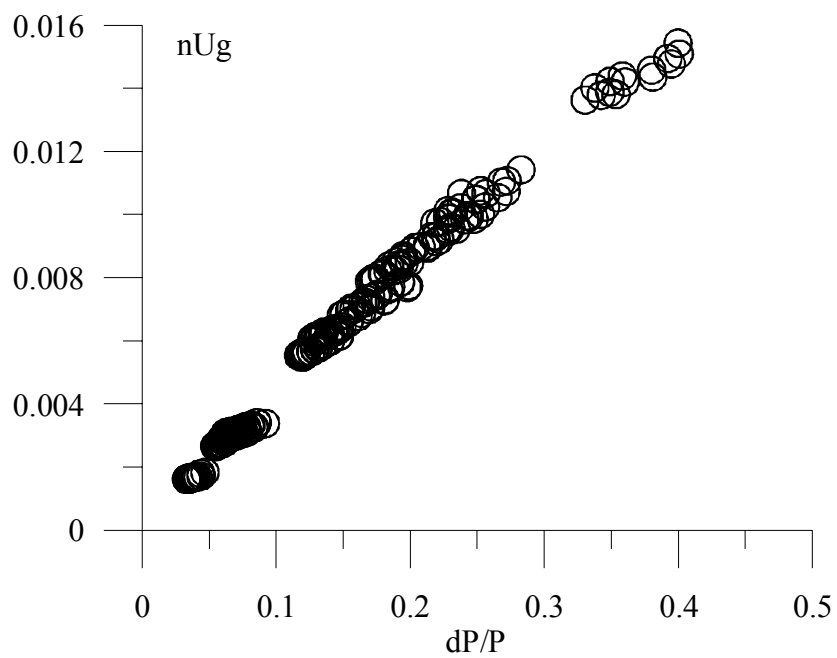
Figure 54. Non-dimensional velocity for the standard plate. Air water flow.
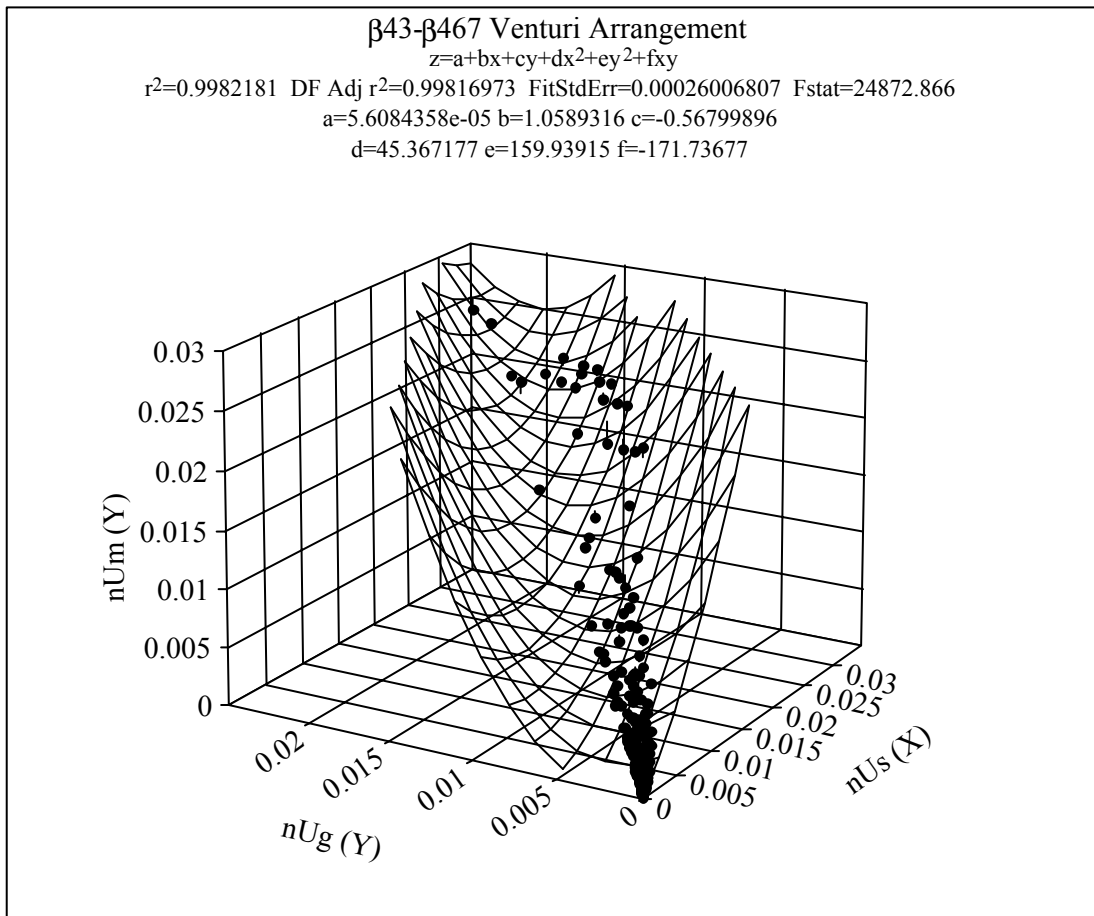
Figure 55. Correlation for the mixture density using the Venturi meter.
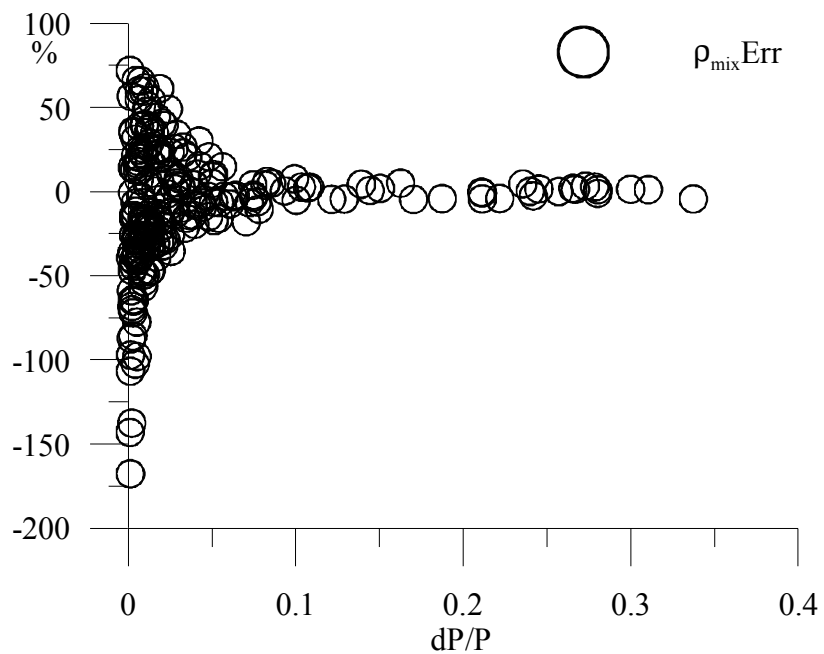
Figure 56. Mixture density estimation using the Venturi meter.
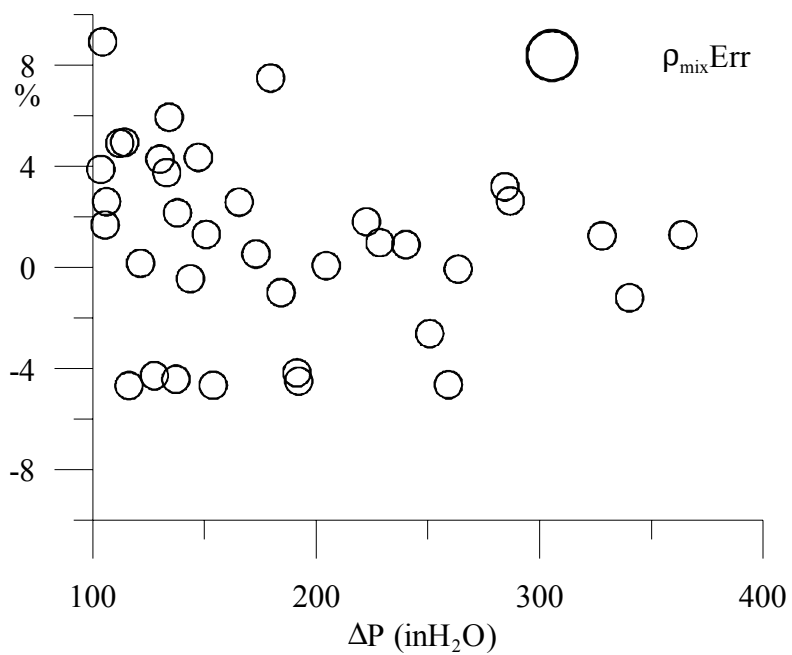
Figure 57. Mixture density estimation using the Venturi meter in the 100-361 inH$_2$O differential pressure range.
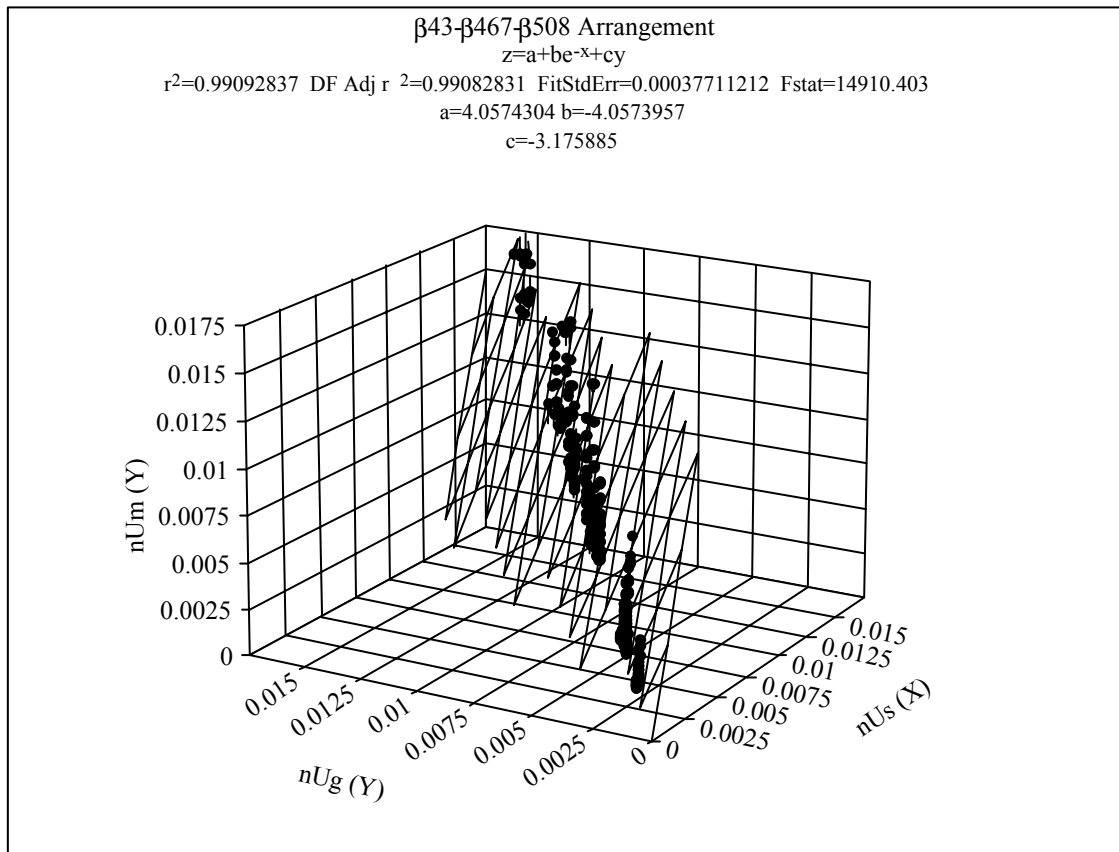
Figure 58. Correlation for the mixture density using the standard orifice.
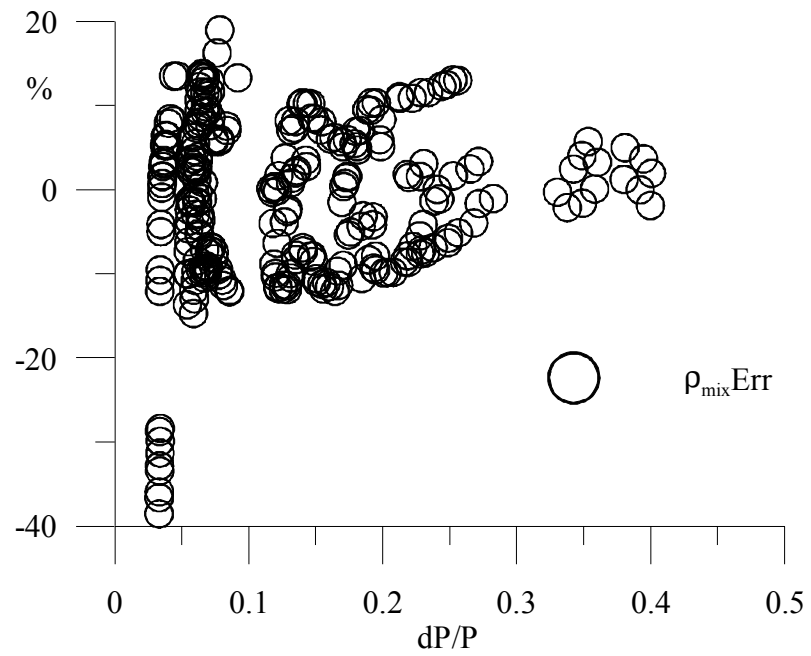
Figure 59. Mixture density estimation using the standard plate.
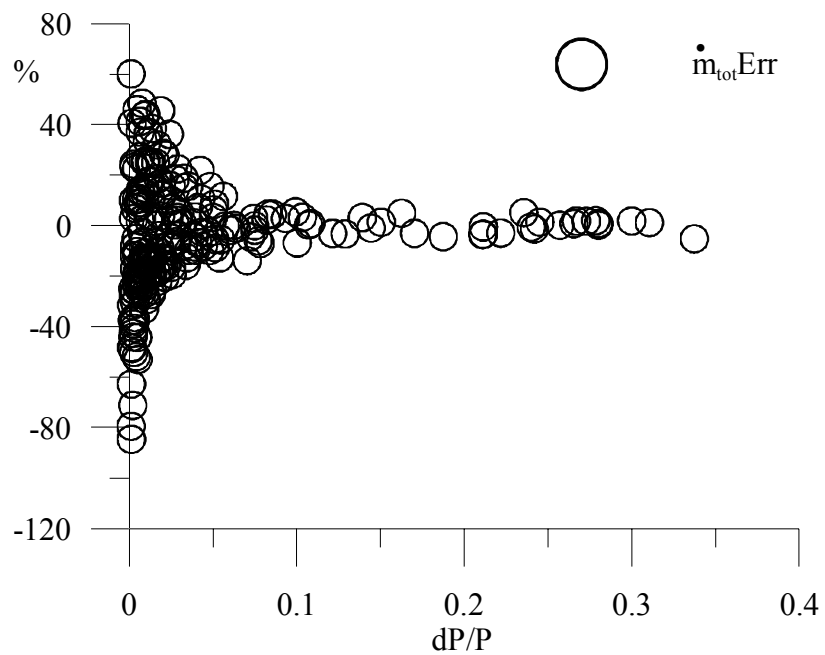
Figure 60. Total mass flow rate computation using the Venturi meter.
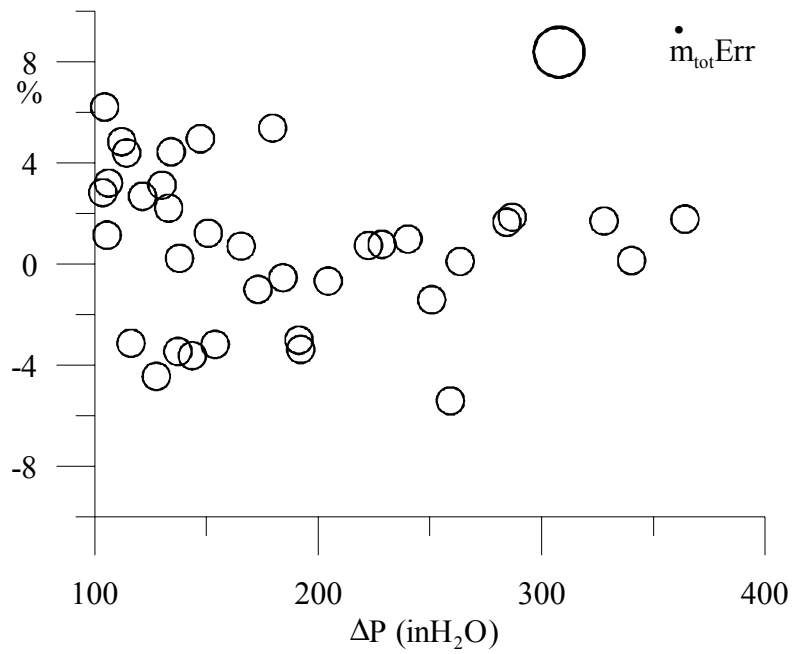
Figure 61. Total mass flow rate computation using the Venturi meter in the
100-361 in_H₂O pressure drop range.
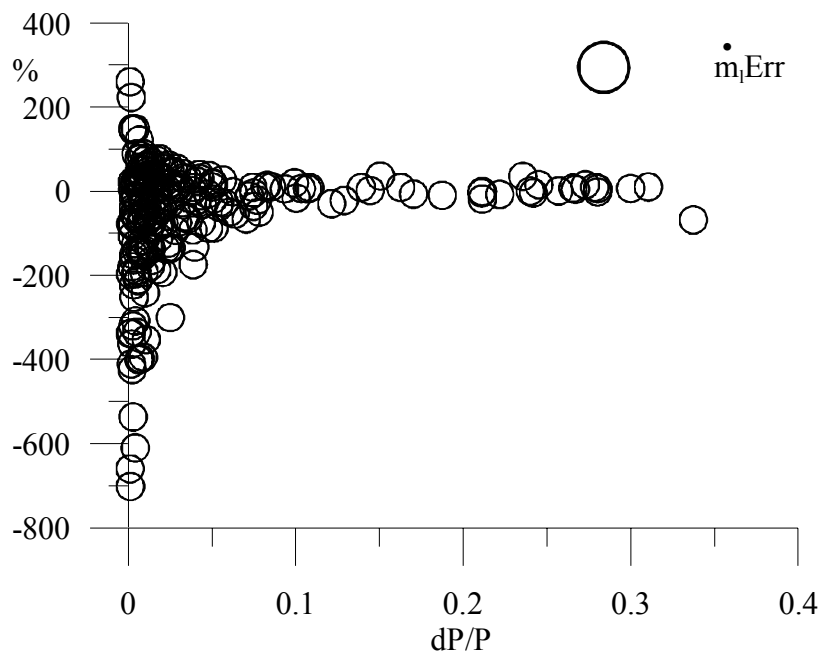
Figure 62. Water mass flow rate computation using the Venturi meter.
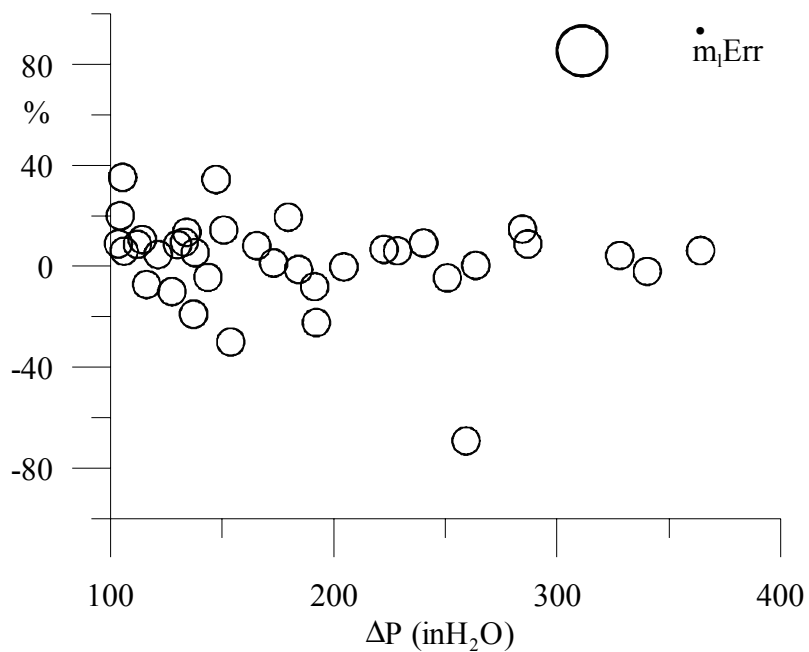
Figure 63. Water mass flow rate computation using the Venturi meter in the 100-361 inH₂O pressure differential range.
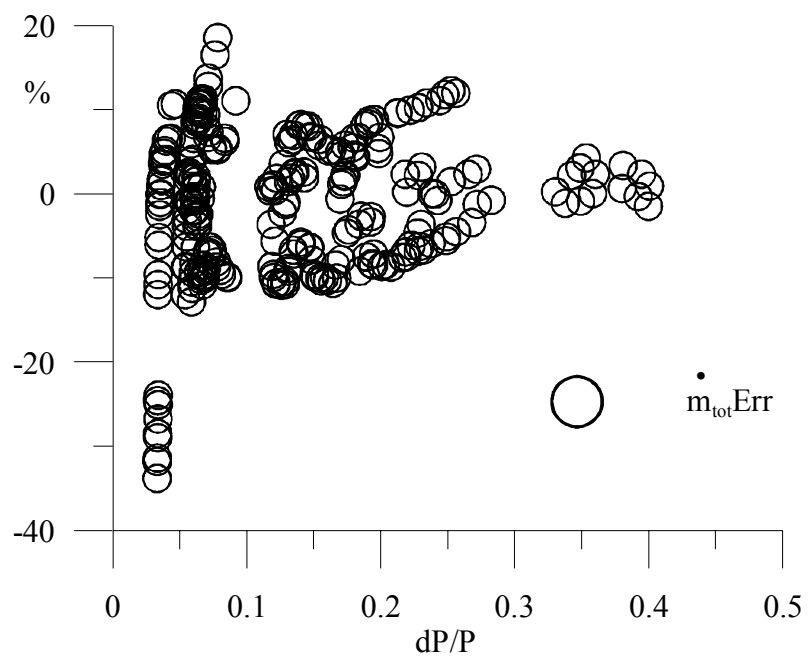
Figure 64. Total mass flow rate computation using the standard plate.
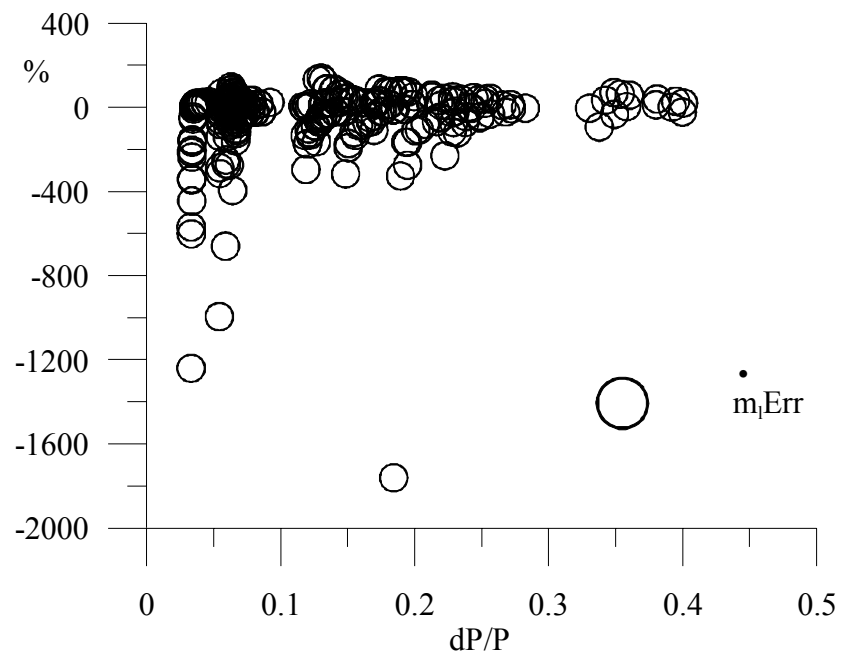
Figure 65. Water mass flow rate computation using the standard plate
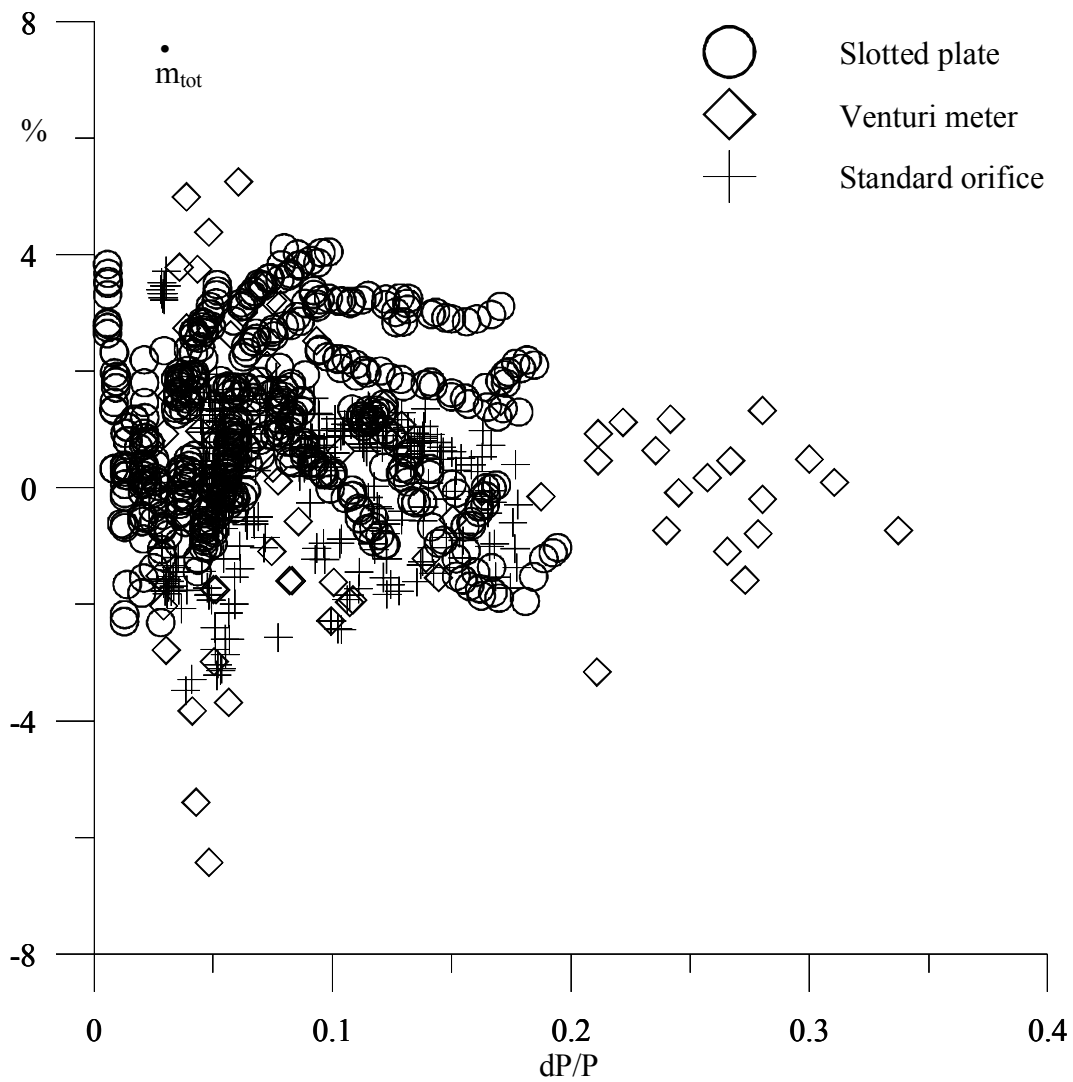
Figure 66. Estimated total mass flow rate assuming the correct quality is known.
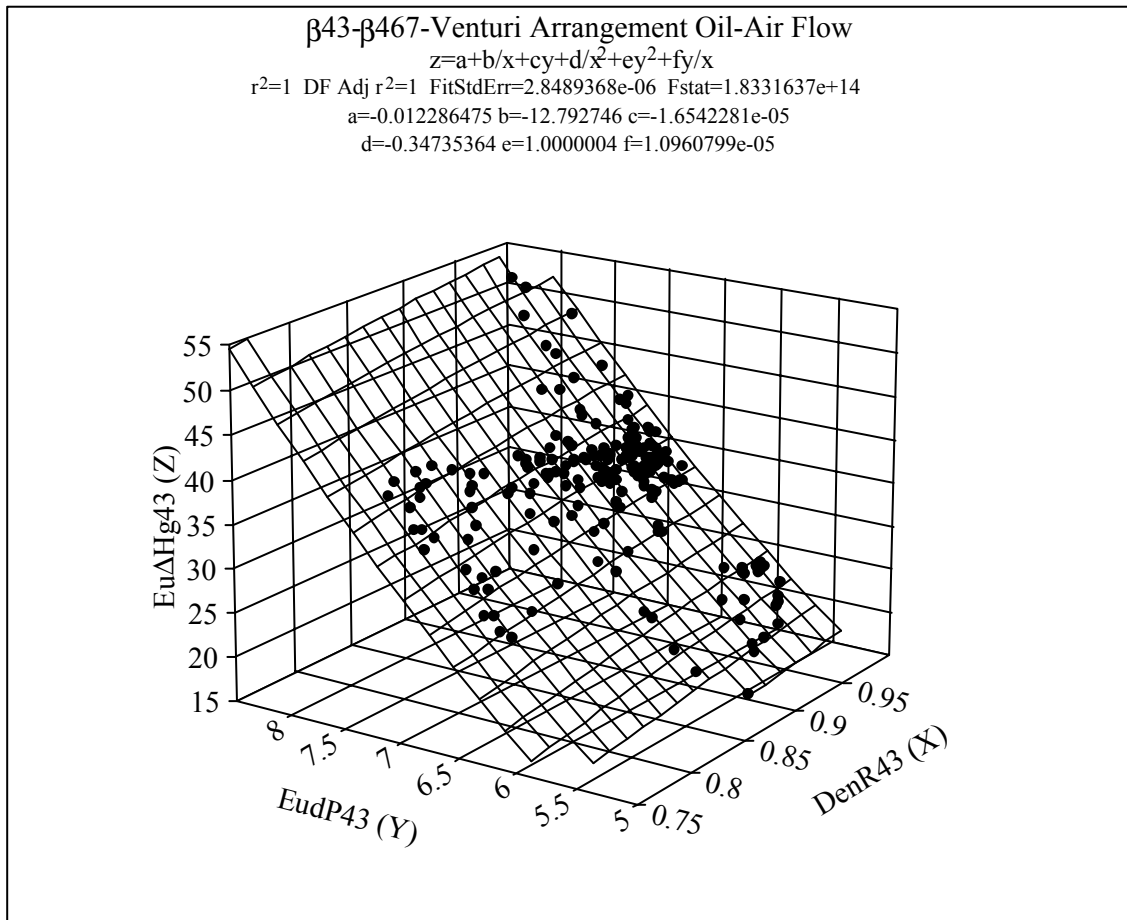
Figure 67. Euler ΔH_g number correlation for the β43 slotted plate. Air-oil flow.
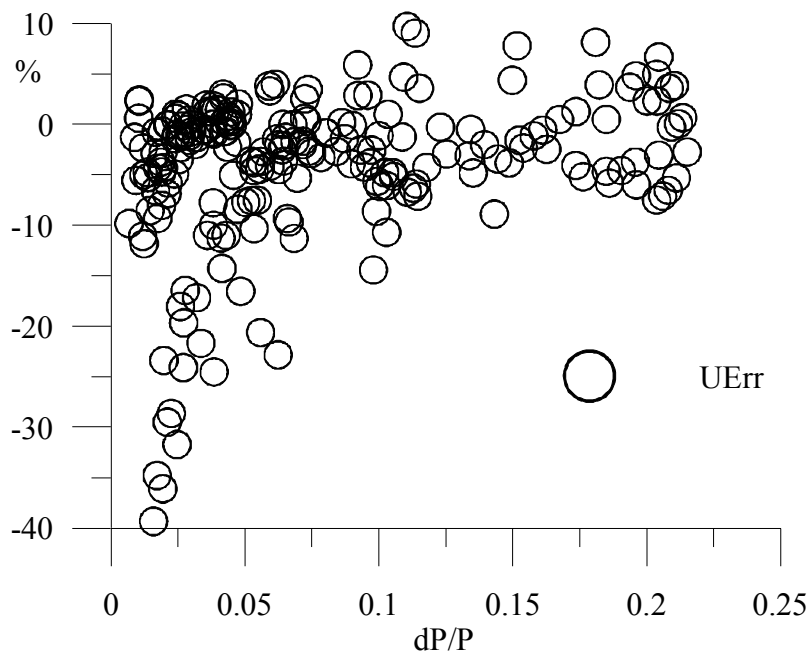
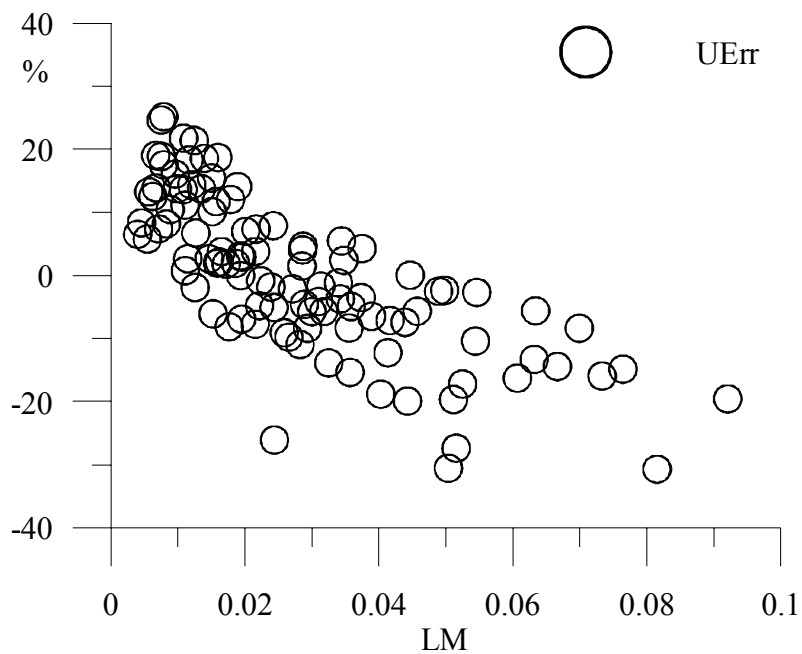Figure 68. Error in velocity estimation for the β43 slotted plate. Air-oil flow.
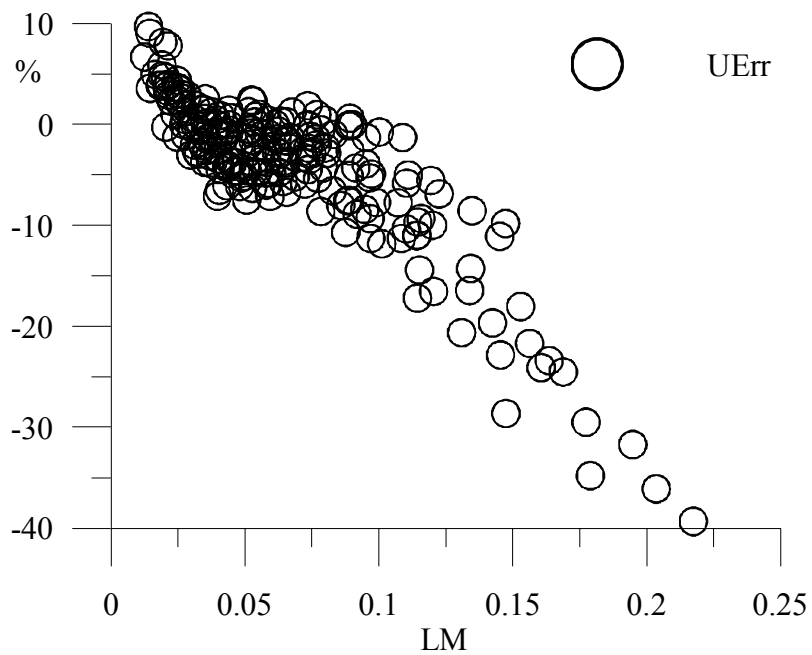
Figure 69. Error dependence on the Lockhart-Martinelli parameter for the velocity estimation using the β43 slotted plate. Air-oil flow.
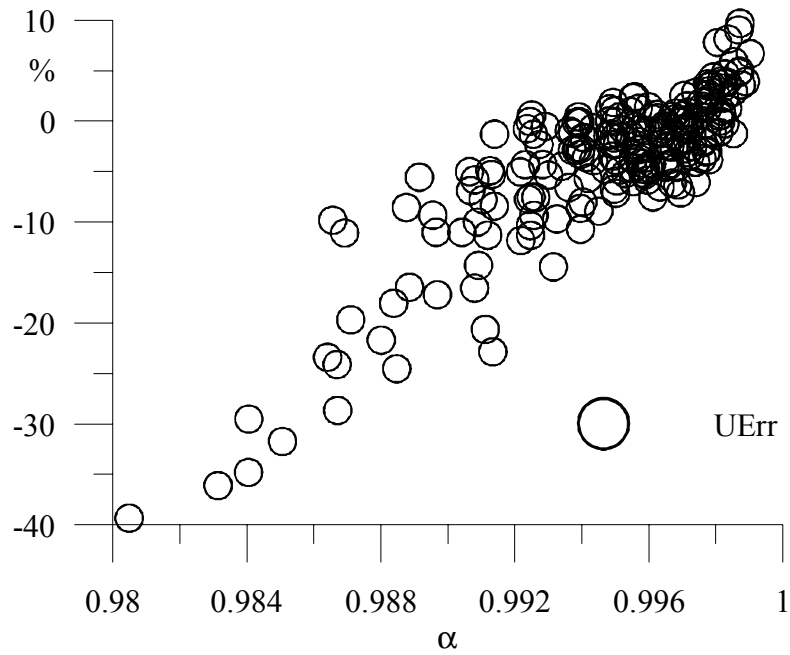
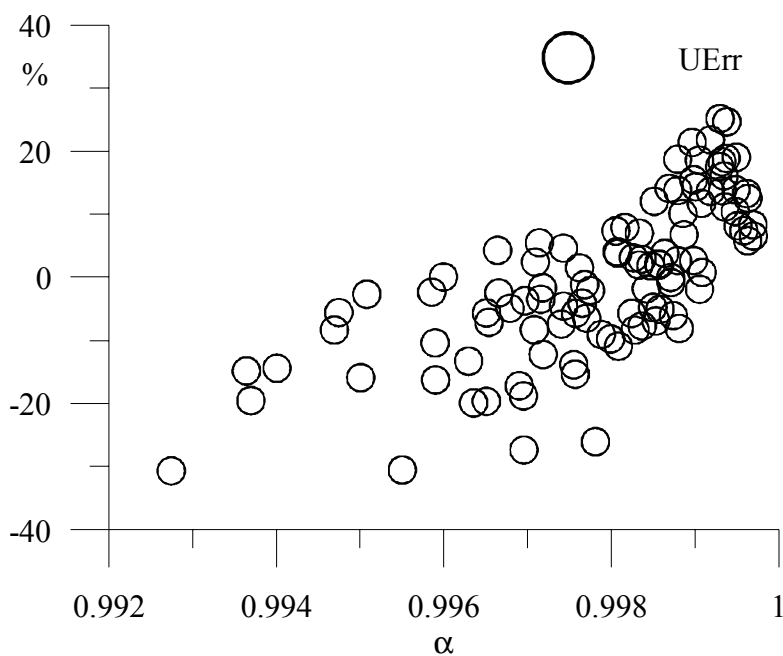Figure 70. Influence of the gas void fraction on the velocity estimation using the β43 slotted plate. Air-oil flow.

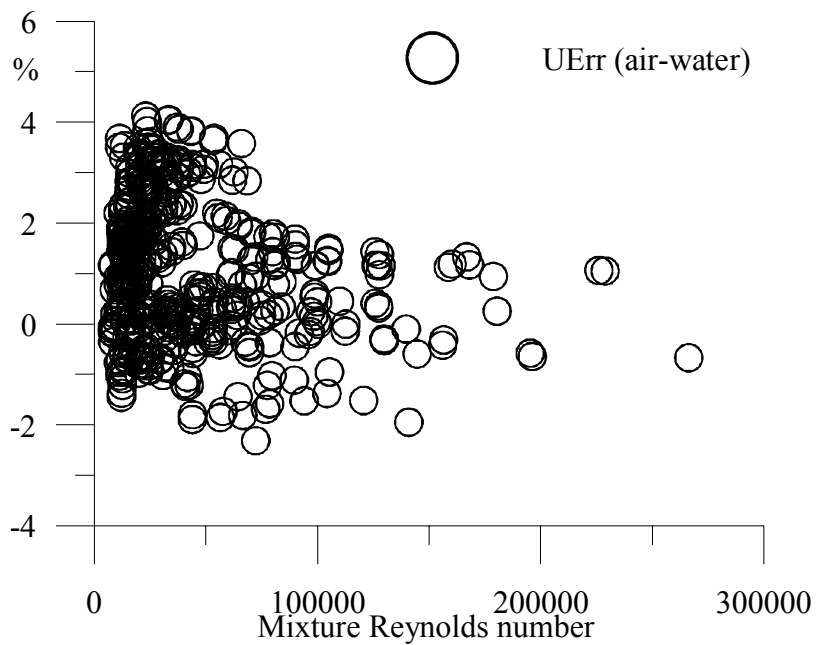Figure 71. Venturi ΔHgoP as a function of Venturi pressure drop and Venturi recovery

pressure. Air-oil flow.
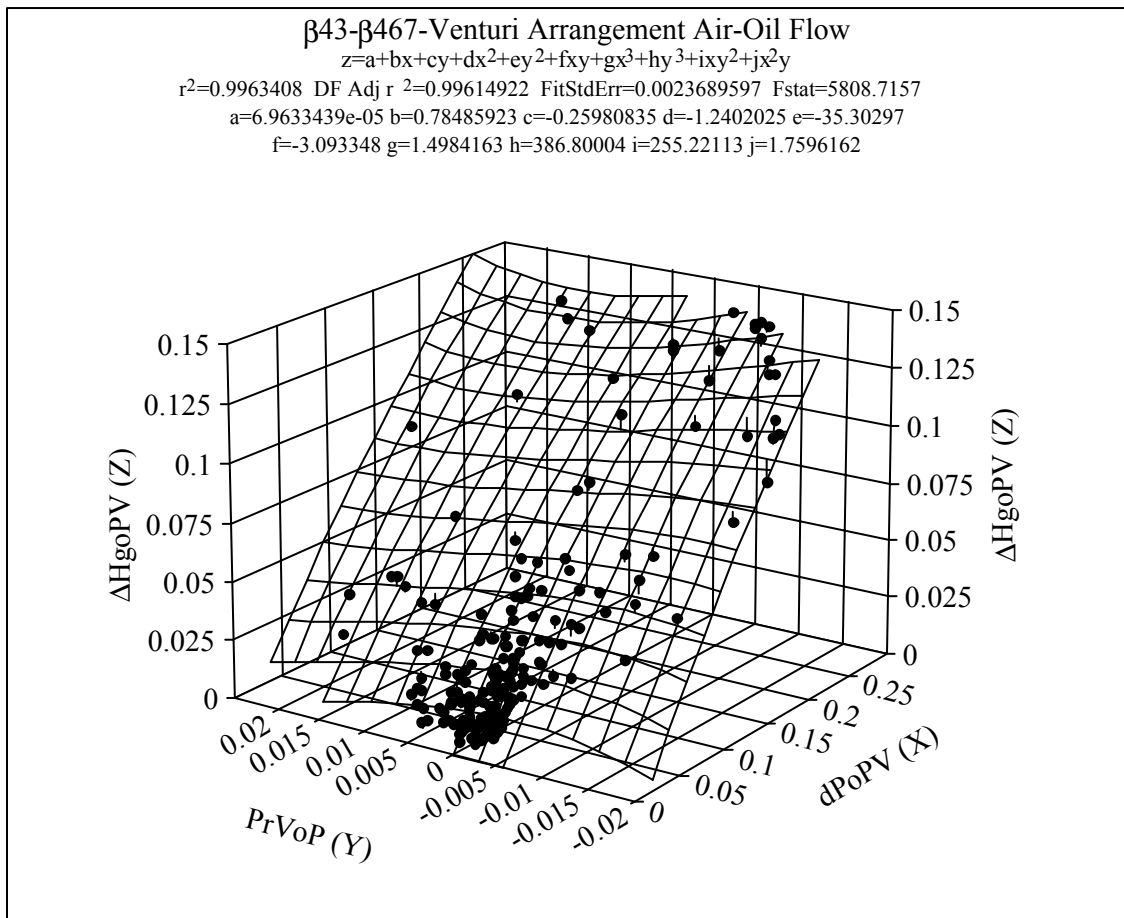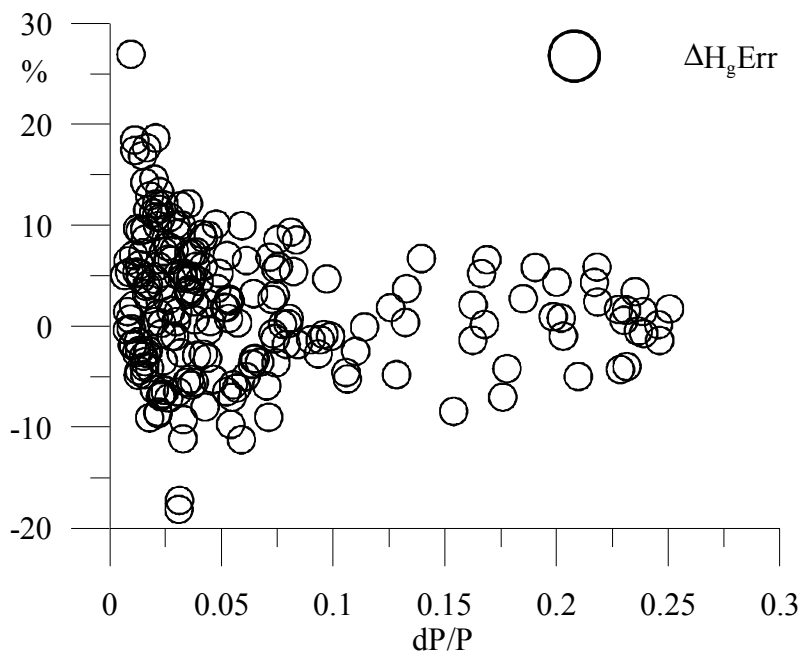
Figure 72. ΔHg computation using the Venturi differential pressure and Venturi recovery pressure. Air-oil flow.
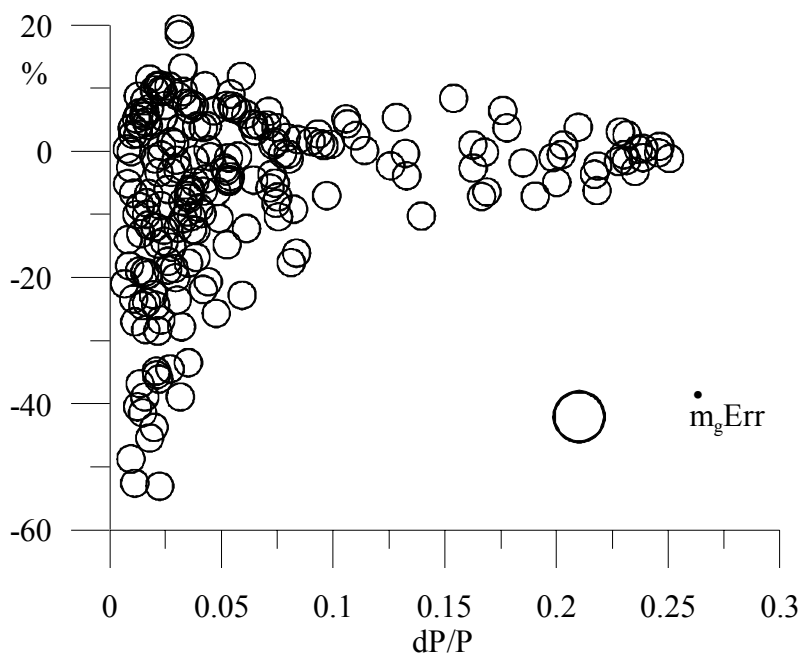
Figure 73. Gas mass flow rate estimation using the Venturi differential pressure and Venturi recovery pressure. Air-oil flow
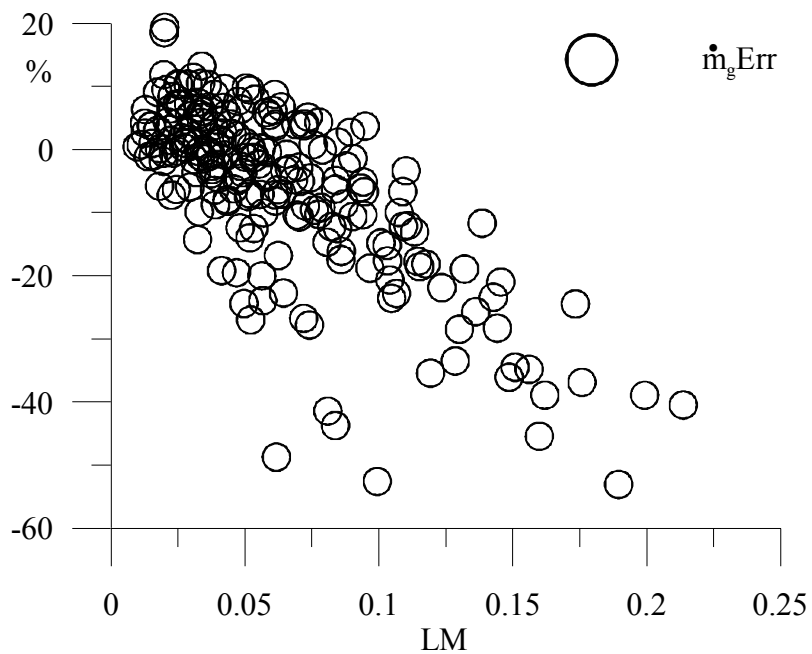
Figure 74. Influence of the Lockhart-Martinelli parameter on the gas mass flow rate estimation using the Venturi meter. Air-oil flow.
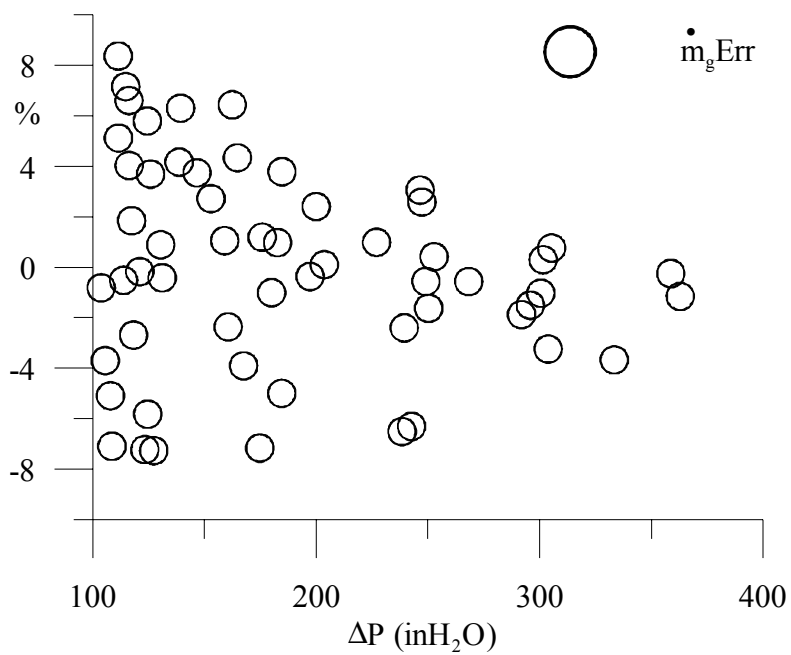
Figure 75. Gas mass flow computation using the Venturi meter for pressure drop greater than 100 in_H_2O.
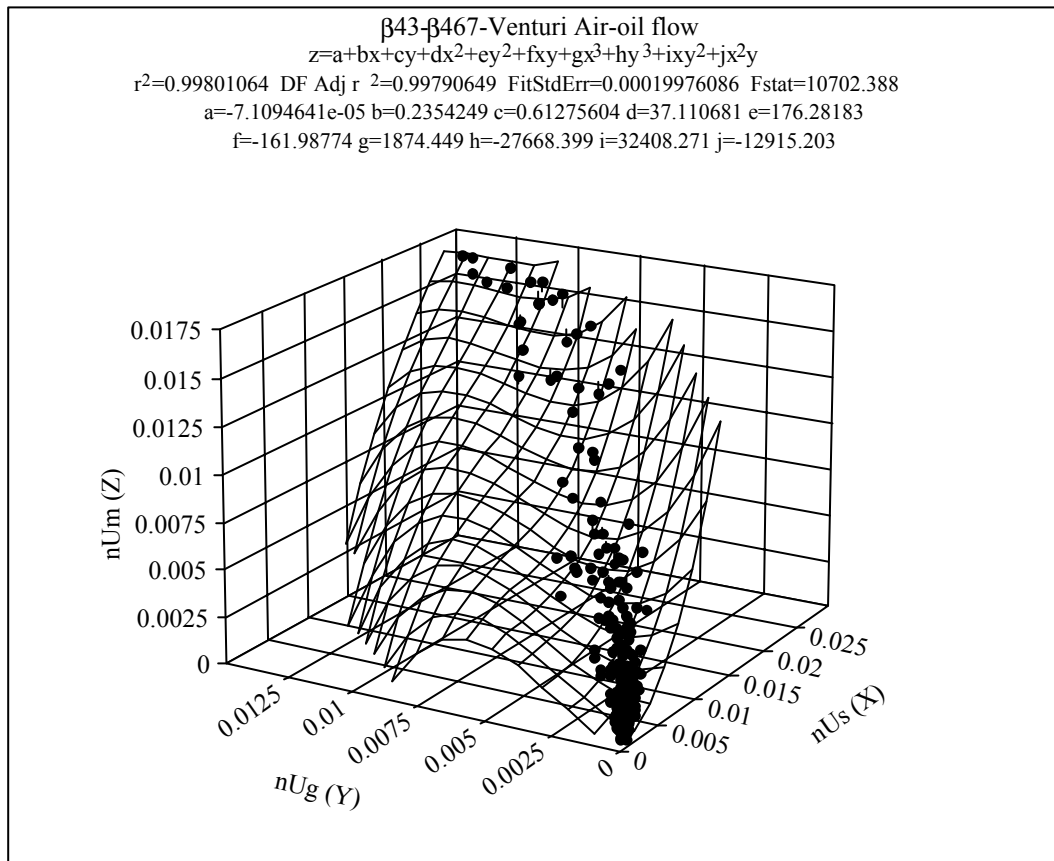
Figure 76. Mixture non-dimensional velocity as a function of the single phase air flow and two-phase air flow non-dimensional velocities. Venturi meter, air-oil flow.
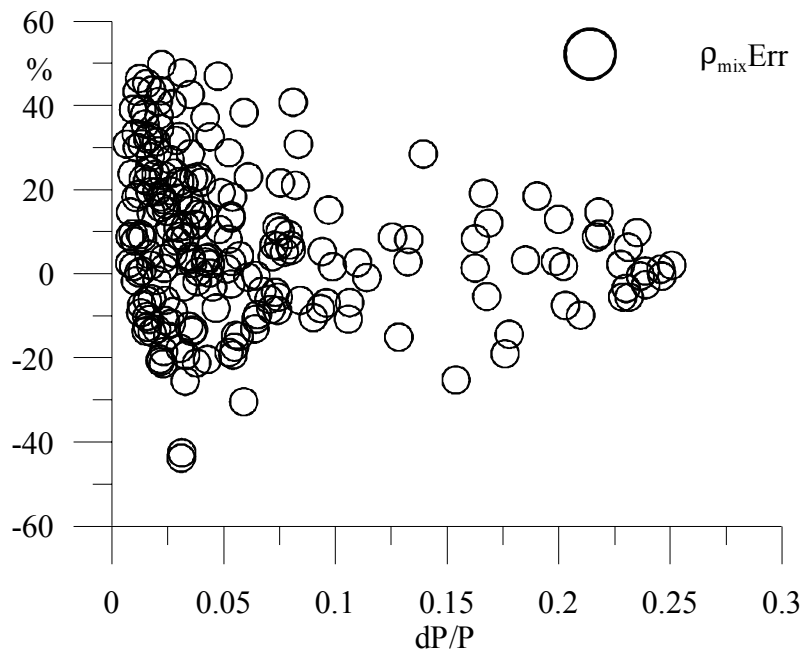
Figure 77. Mixture density estimation using the Venturi meter. Air-oil flow.
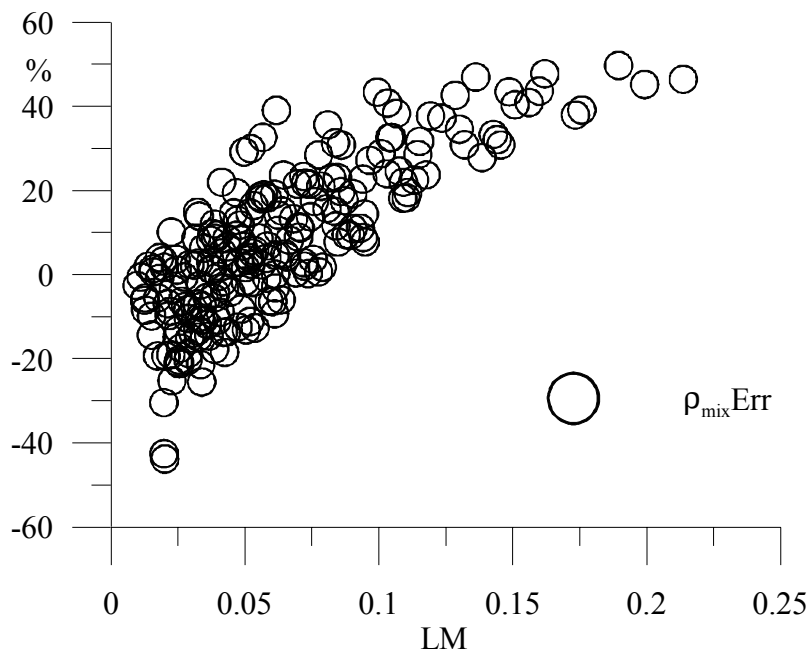
Figure 78. Lockhard-Martinelli parameter influence on the mixture density estimation
using the Venturi meter. Air-oil flow.
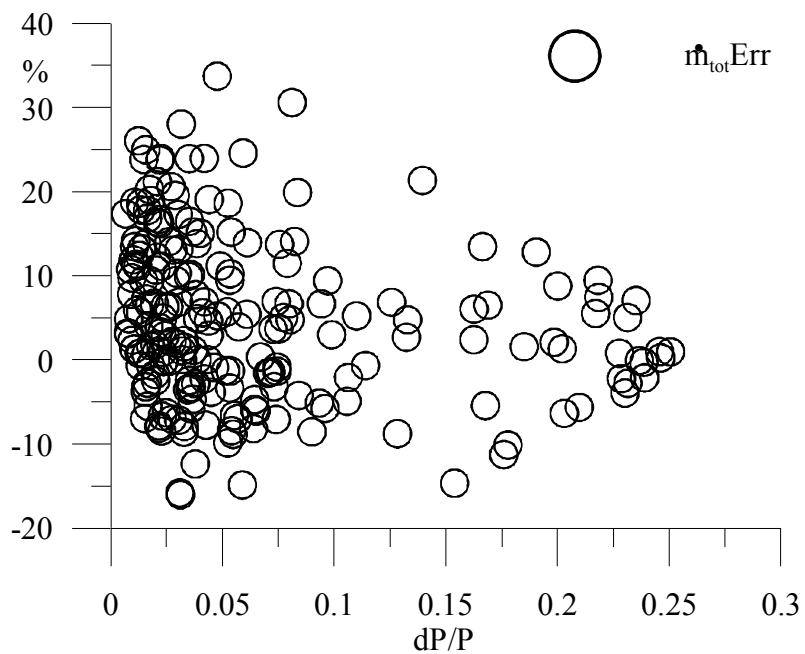
Figure 79. Total mass flow rate computation using the Venturi meter. Air-oil flow.
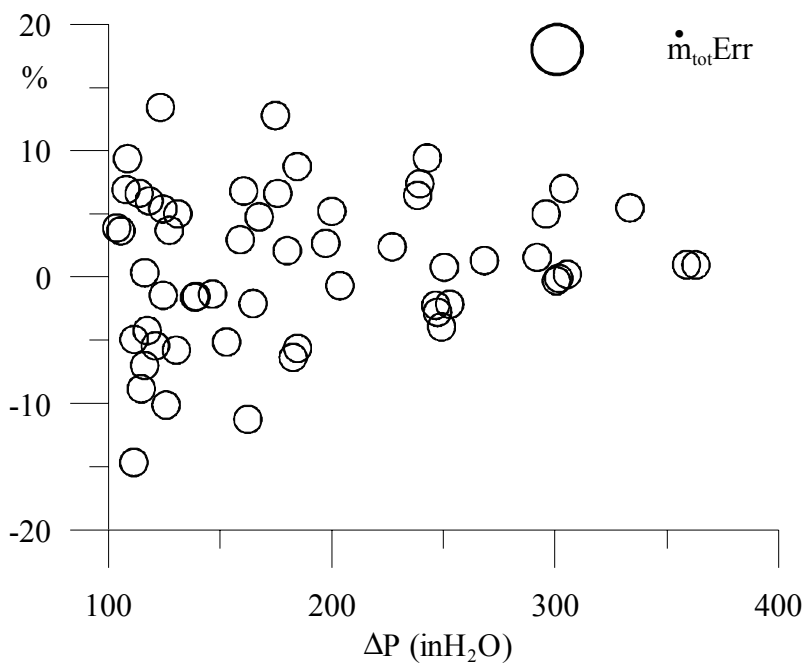
Figure 80. Total mass flow rate computation using the Venturi meter in the 100-363 in_H_2O range. Air-oil flow.
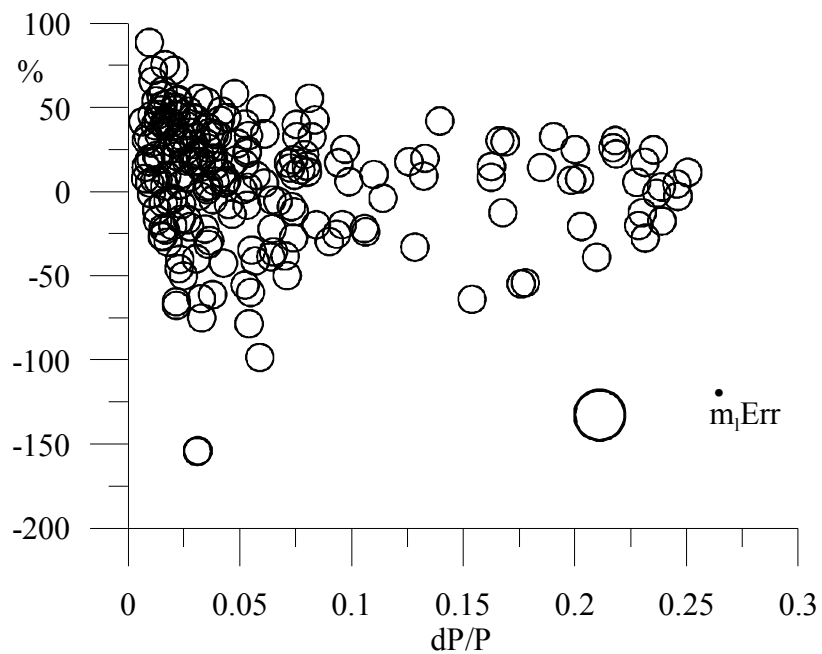
Figure 81. Error in liquid mass flow rate computation using the Venturi meter. Air-oil flow.
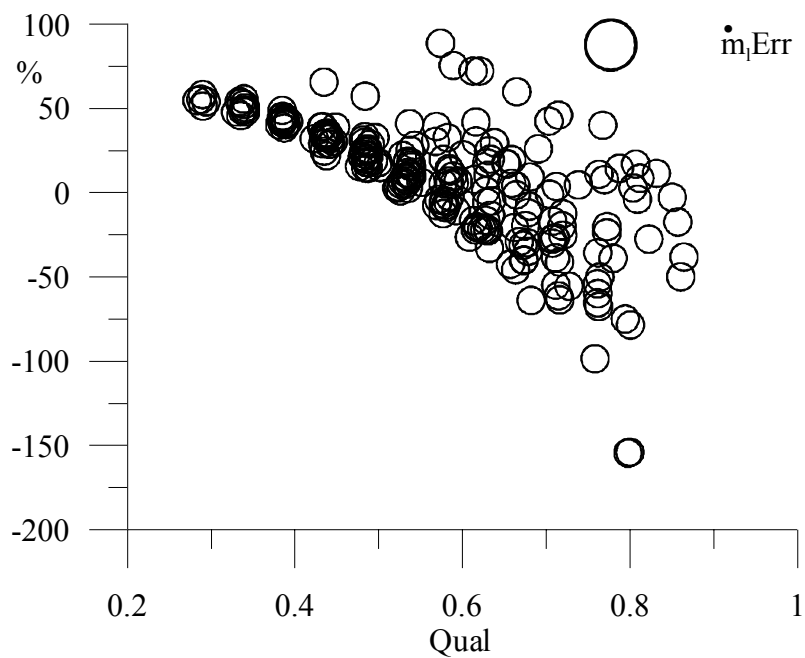
Figure 82. Error in liquid mass computation as function of the quality. Air-oil flow.
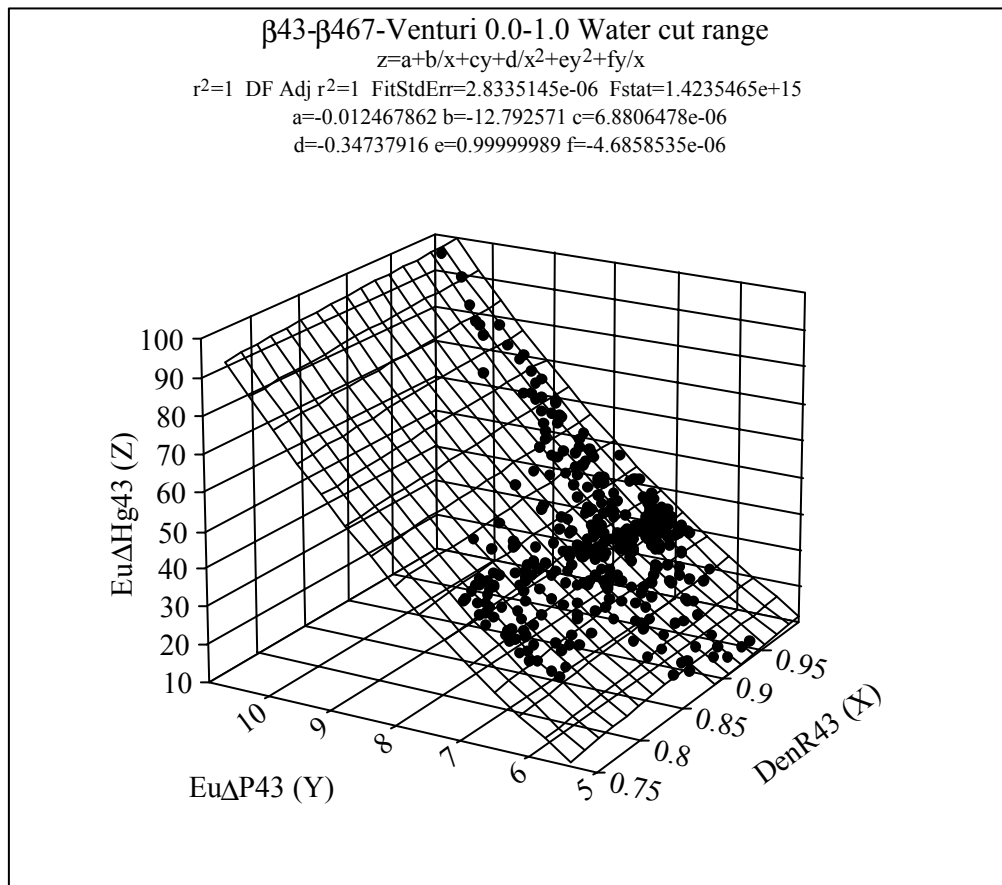
Figure 83. Euler ΔH_g number correlation for the β=0.43 slotted plate. 0.0-1.0 water cut range.
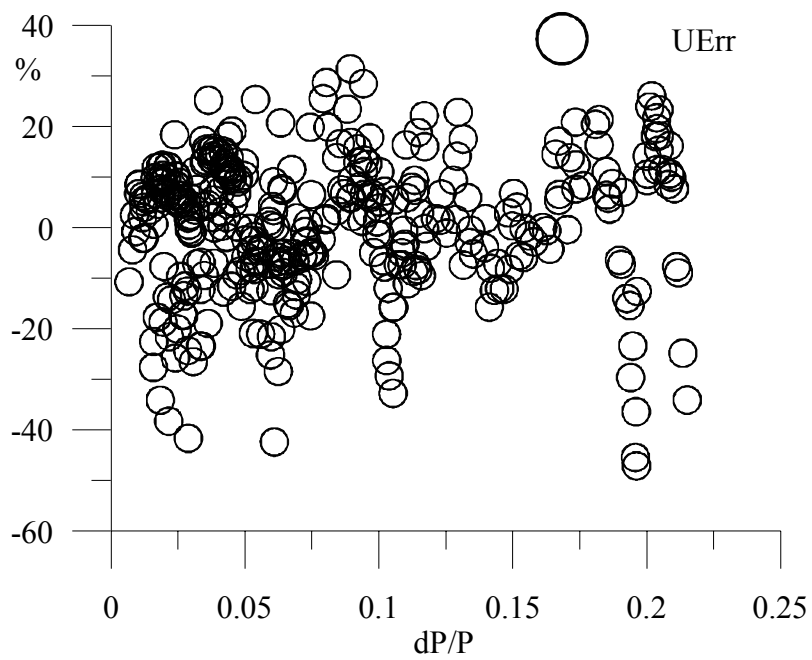
Figure 84. Error in velocity estimation using the β=0.43 slotted plate. 0.0-1.0 water cut range.
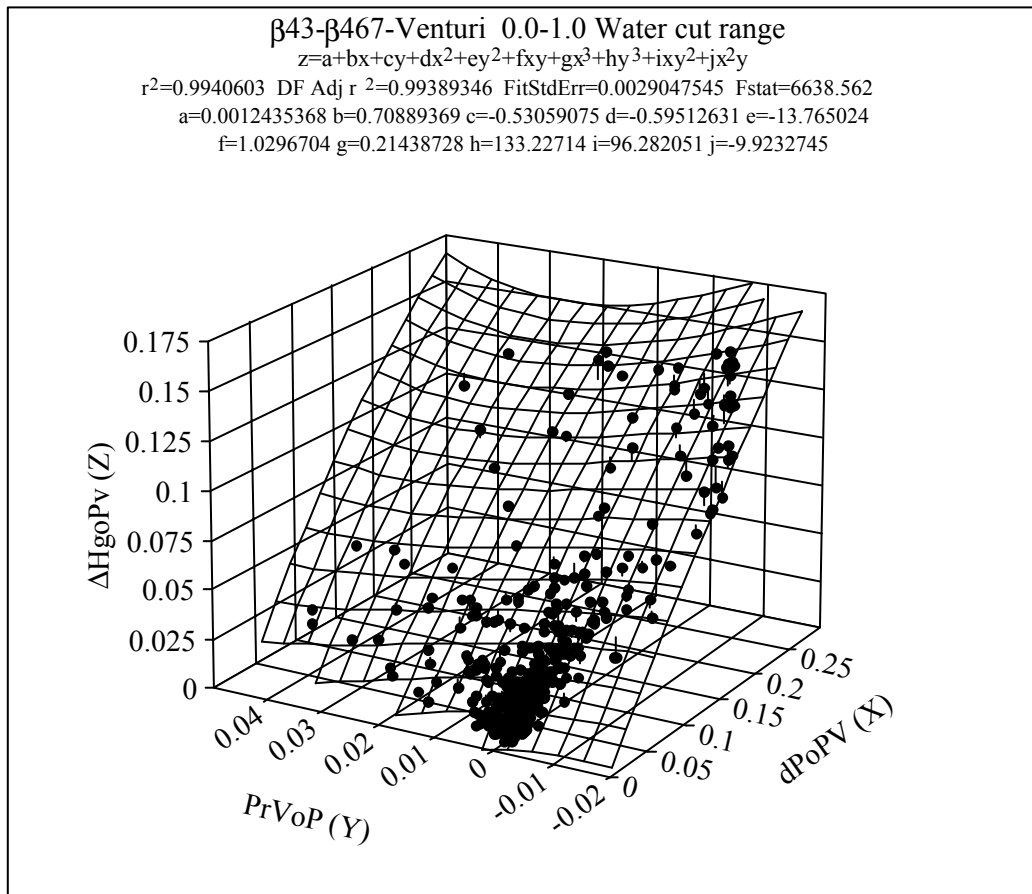
Figure 85. Venturi ΔHgoP as a function of Venturi pressure drop and Venturi recovery pressure. 0.1-1.0 water cut range.
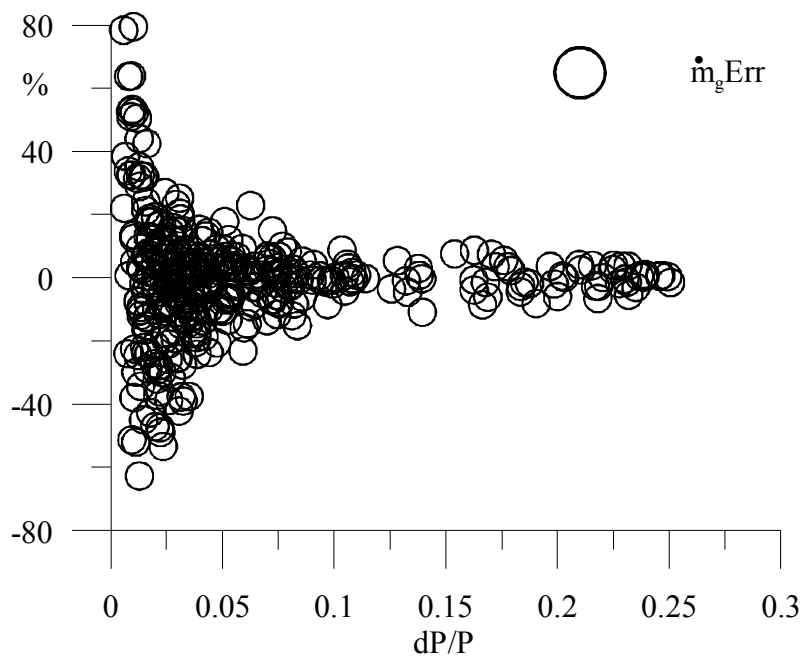
Figure 86. Error in the gas flow rate estimation using the Venturi meter. 0.0-1.0 water cut range.
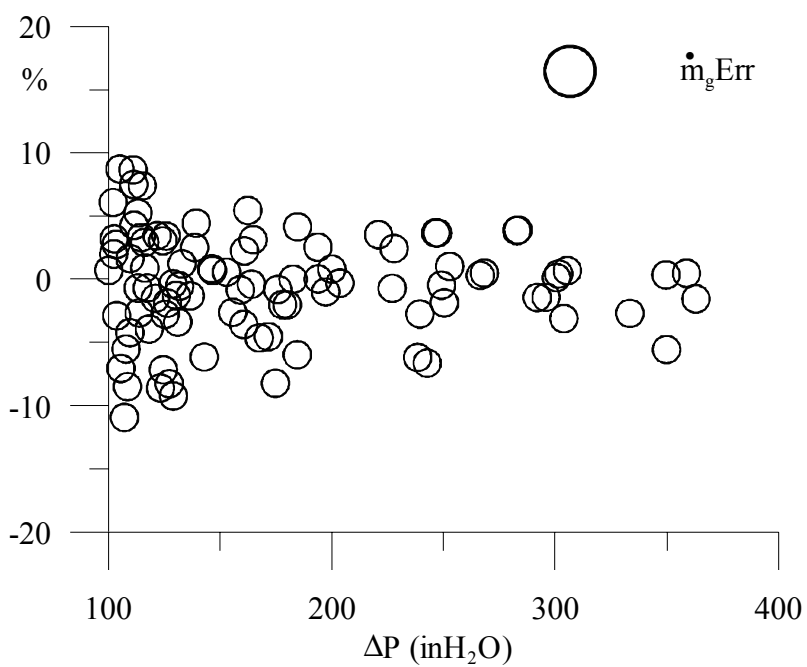
Figure 87. Error in the mass flow rate estimation using the Venturi meter for differential pressures greater than 100 in_H_2O. 0.0-1.0 water cut range.
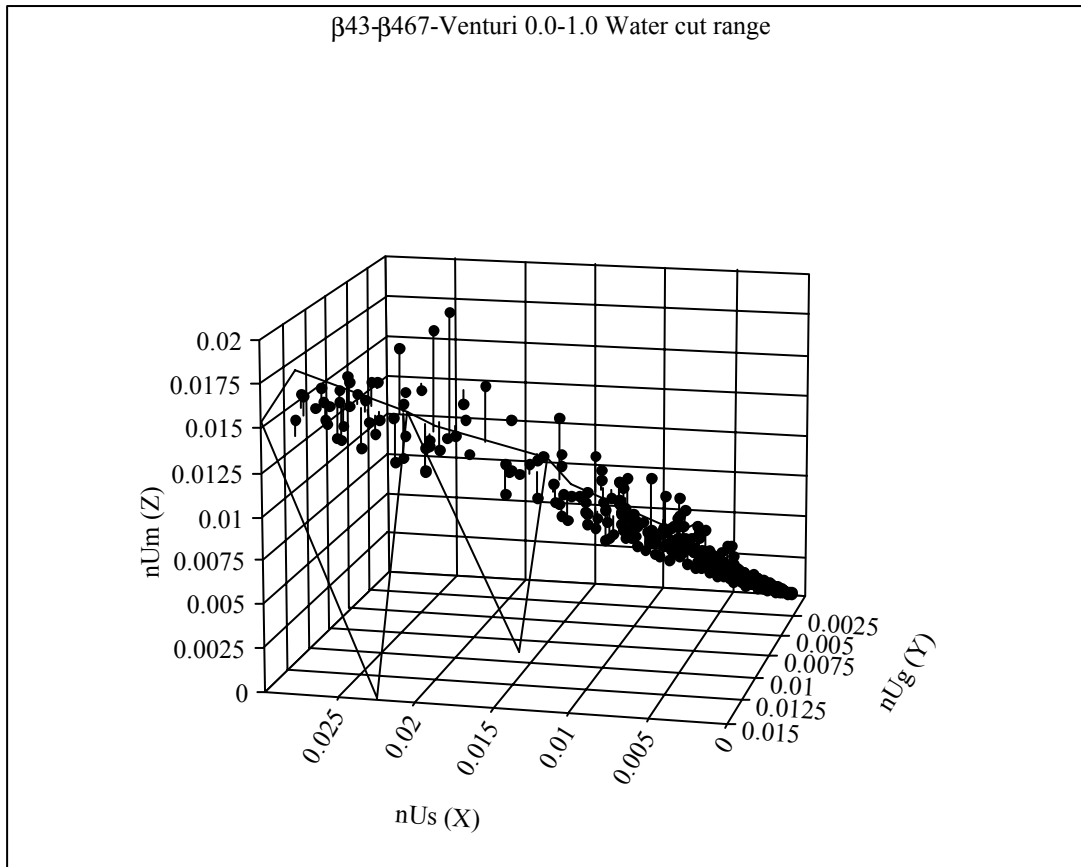
Figure 88. Mixture non-dimensional velocity as a function of the single-phase air flow and three-phase air flow parameters. 0.0-1.0 water cut range.
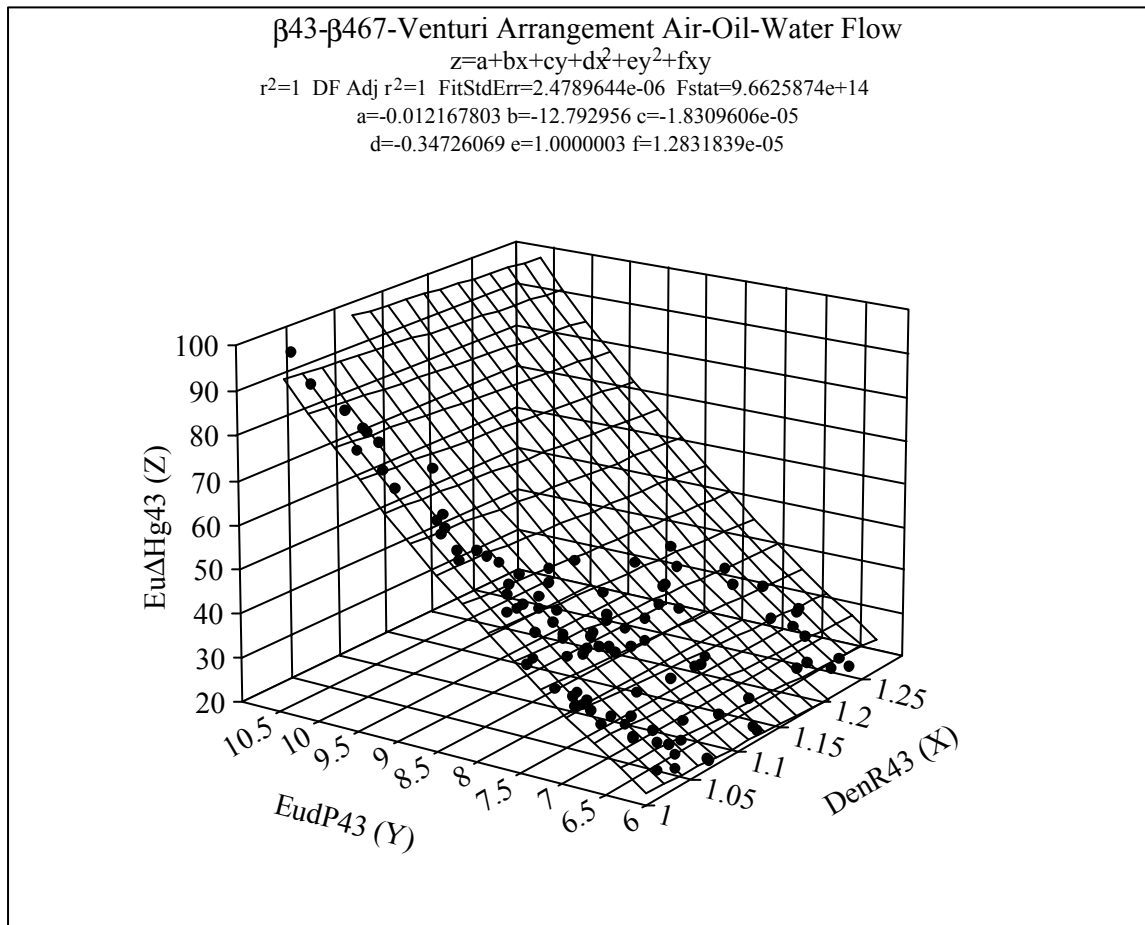
Figure 89. Euler ΔH_g number correlation for the β43 slotted plate. Air-oil-water Flow
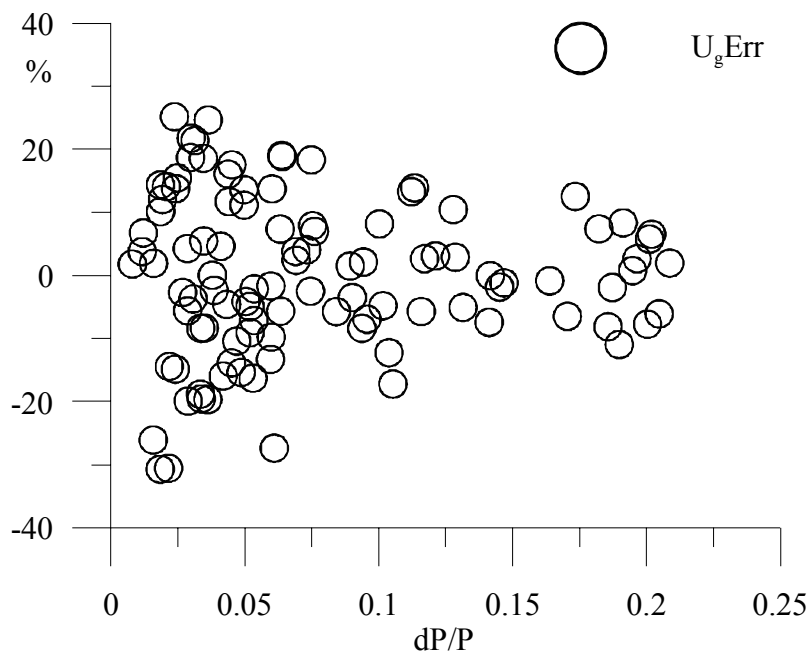
Figure 90. Error in velocity estimation for the β43 slotted plate. Air-oil-water flow.
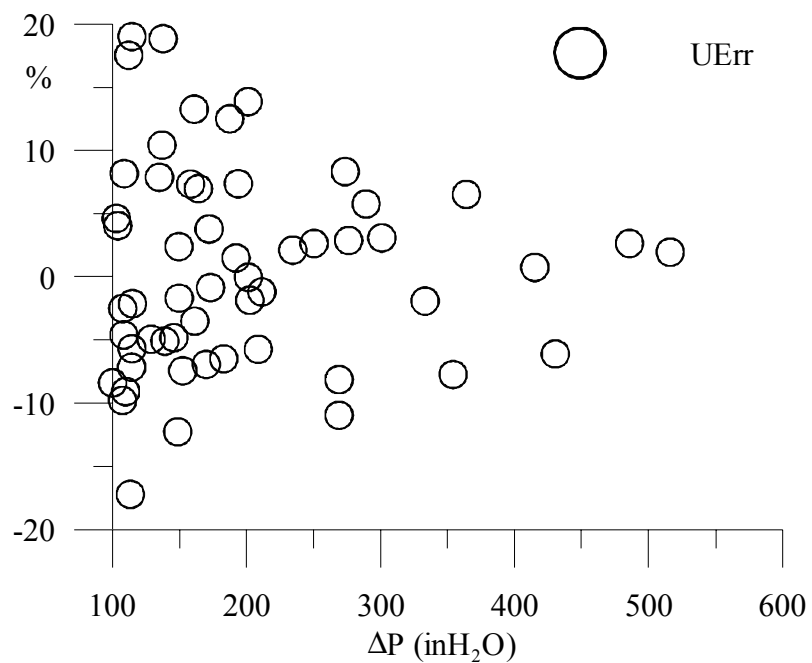
Figure 91. Error in velocity estimation for the β43 slotted plate at differential pressures greater than 100 in_H_2O (37.3 kPa). Air-oil-water flow.

Figure 92. Error dependence on the Lockhart-Martinelli parameter for the velocity estimation using the β43 slotted plate. Air-oil-water flow.

Figure 93. Influence of the gas void fraction on the velocity estimation using the β43 slotted plate. Air-oil-water flow.

Figure 94. Influence of the mixture Reynolds number on the velocity estimation using the β43 slotted plate. Air-water flow.
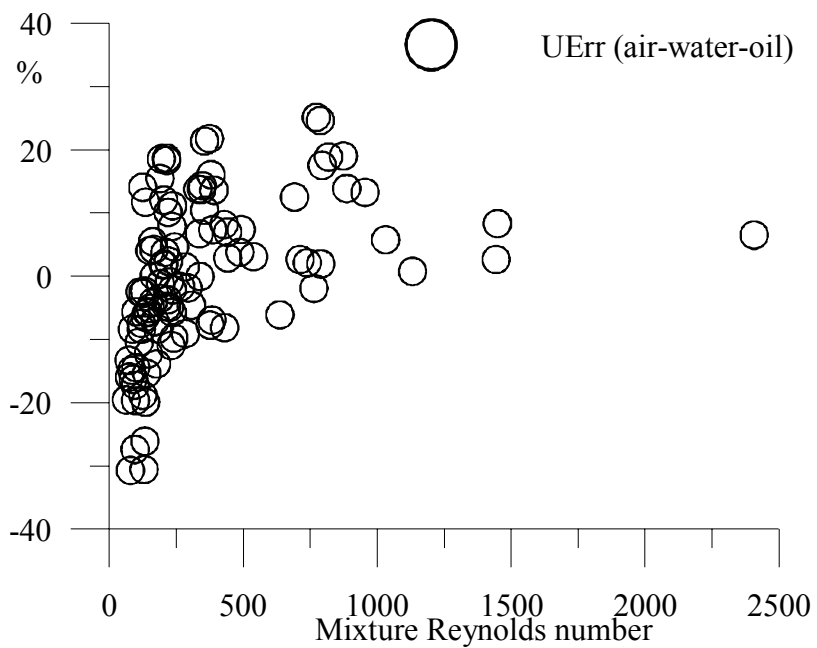
Figure 95. Influence of the mixture Reynolds number on the velocity estimation using the β43 slotted plate. Air-water-oil flow.
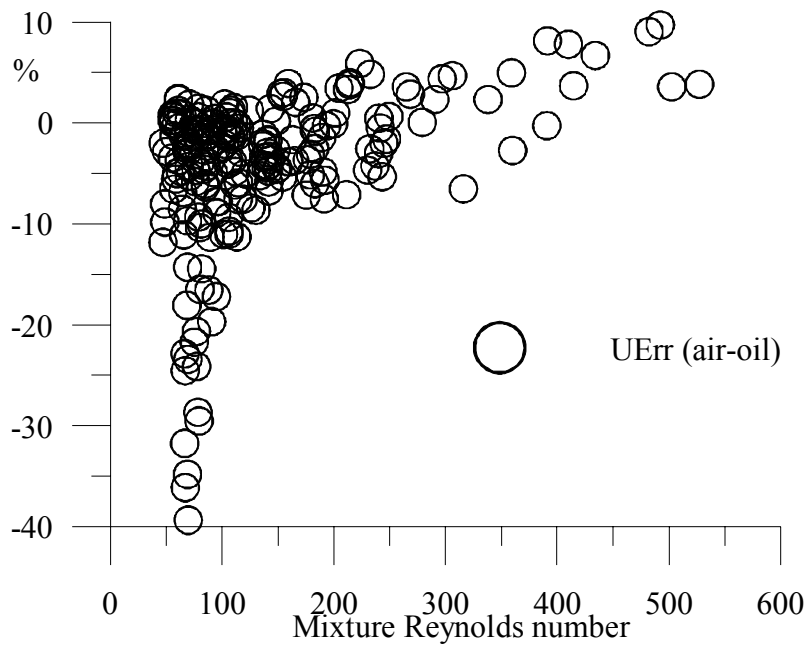
Figure 96. Influence of the mixture Reynolds number on the velocity estimation using the β43 slotted plate. Air-oil flow.
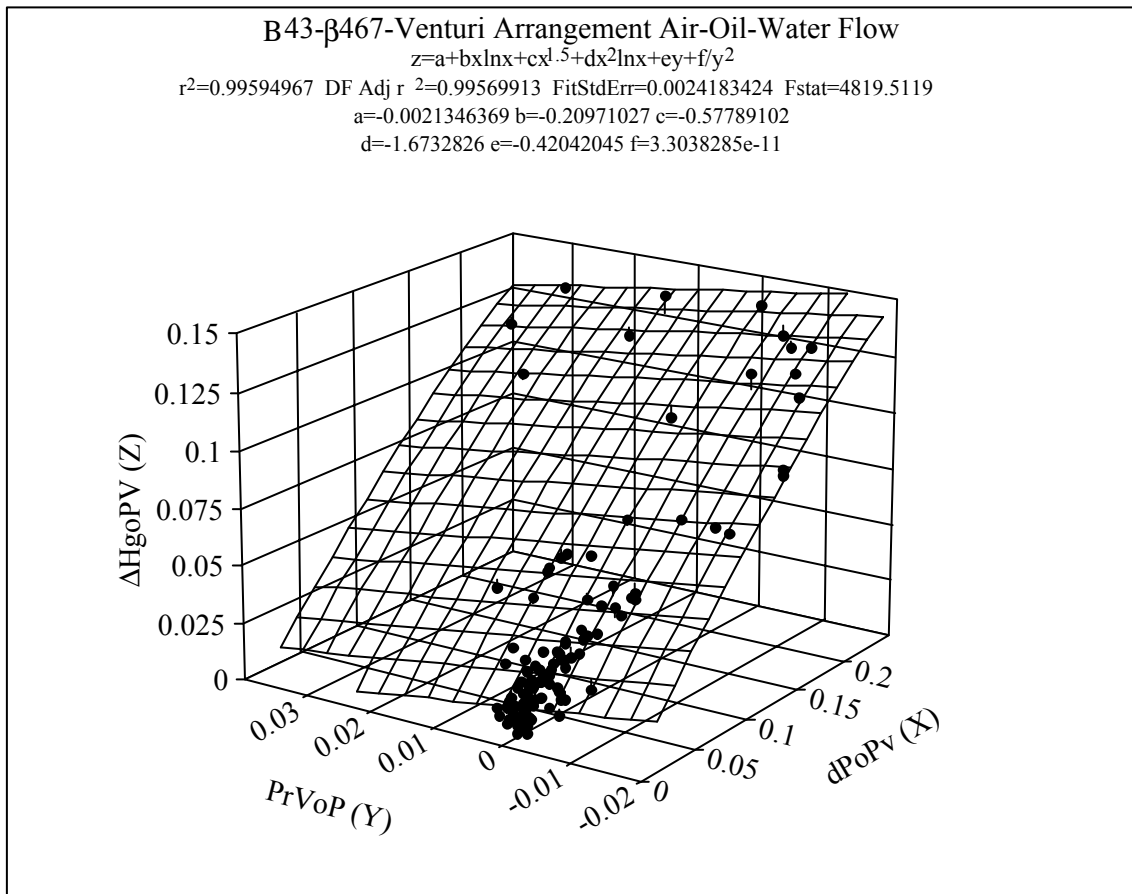
Figure 97. Venturi ΔHgoP as a function of Venturi pressure drop and Venturi recovery
pressure. Air-oil-water flow.
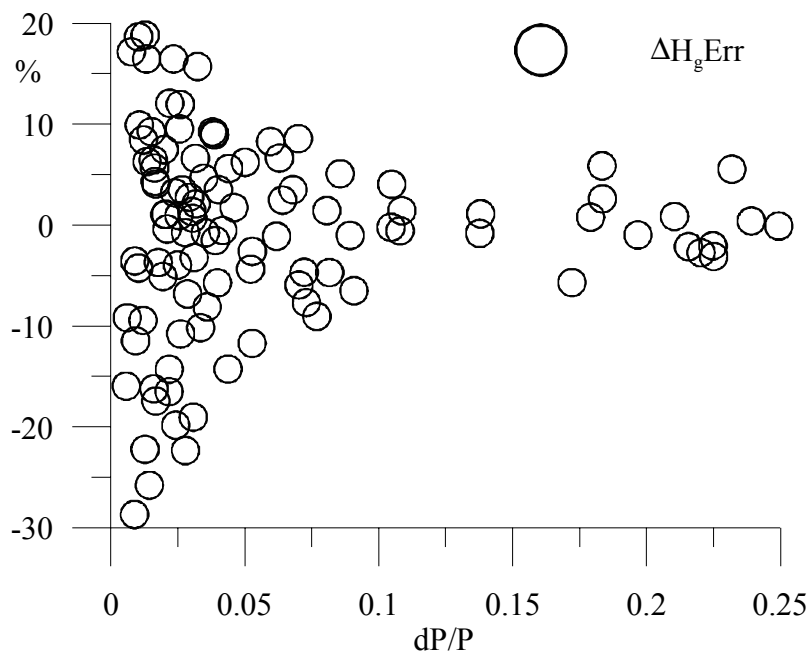
Figure 98. Venturi ΔHg computation using the Venturi pressure drop and Venturi recovery pressure. Air-oil-water flow.
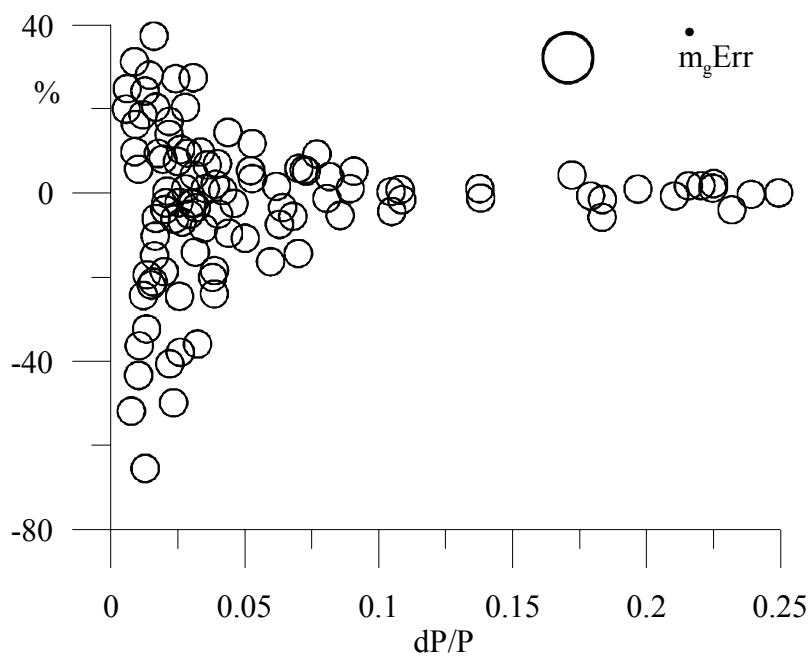
Figure 99. Gas mass flow rate estimation using the Venturi pressure drop and Venturi recovery pressure. Air-oil-water flow.
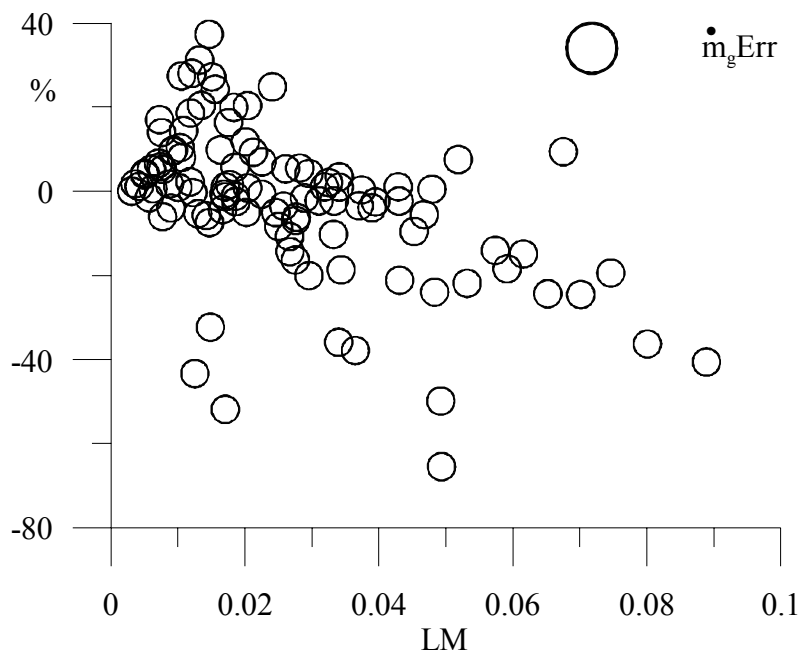
Figure 100. Influence of the Lockhard-Martinelli parameter on the gas mass flow rate estimation using the Venturi meter. Air-oil-water flow.
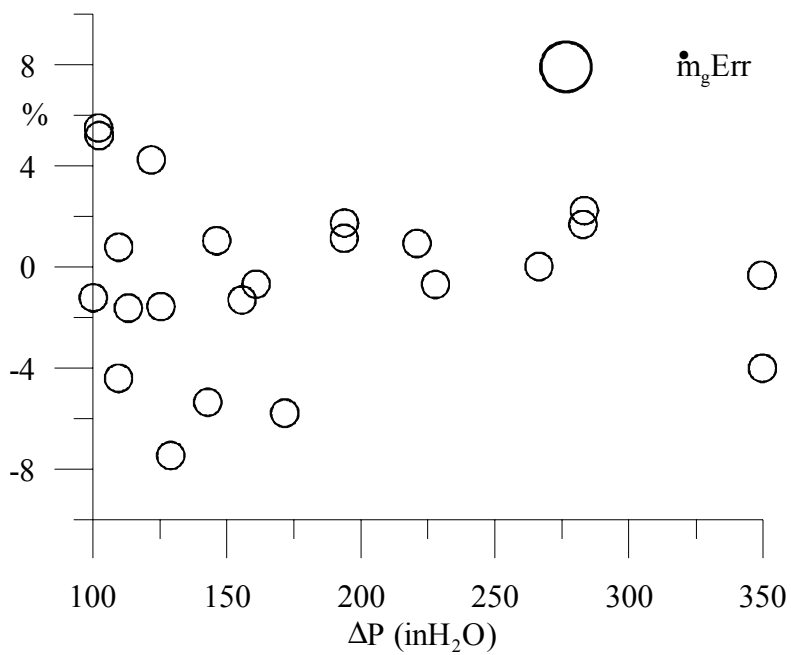
Figure 101. Gas mass flow computation using the Venturi meter for pressure drop greater than 100 in_H$_2$O. Air-oil-water flow.
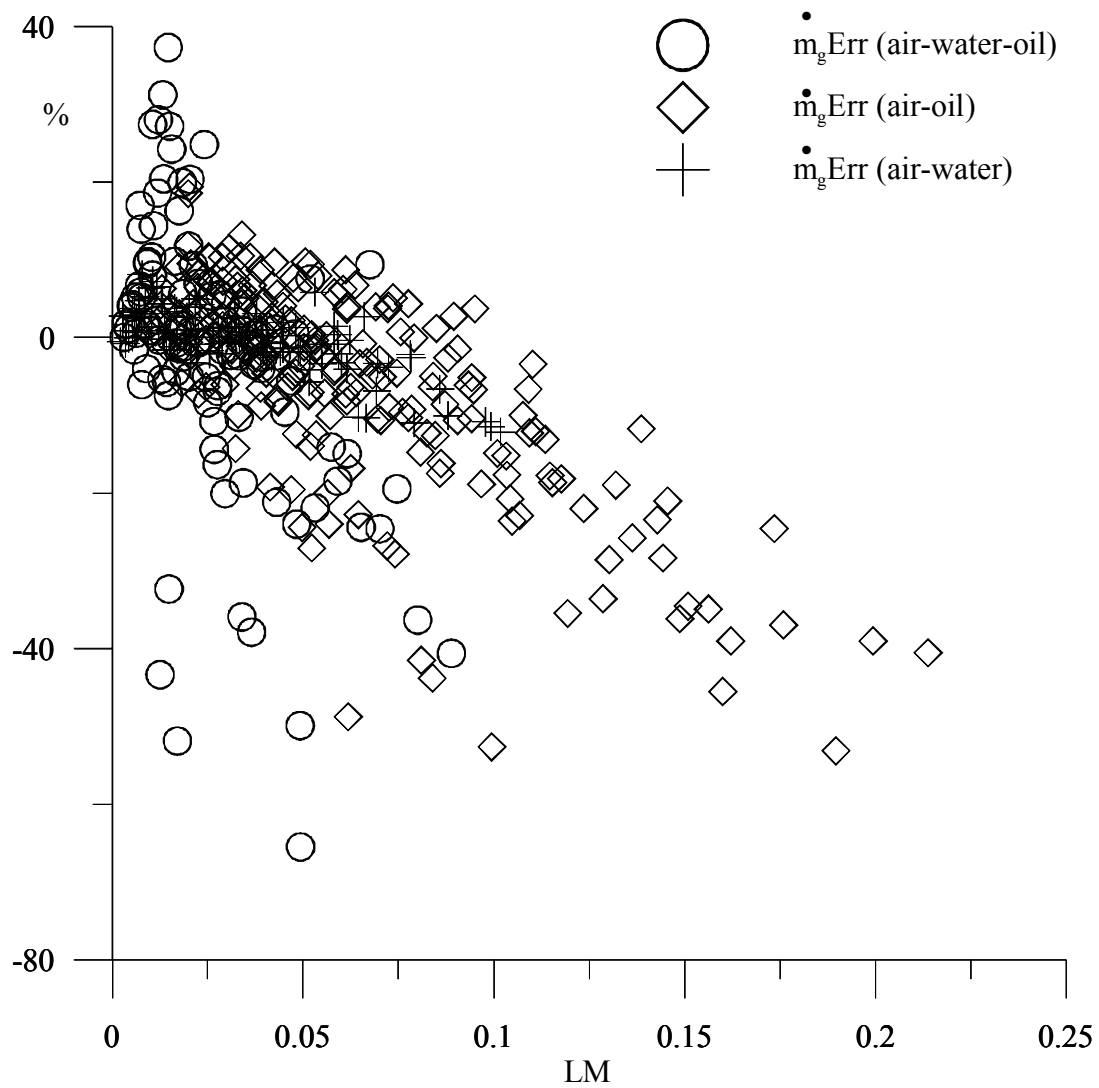
Figure 102. Influence of the LM parameter in the gas mass flow computation at different liquid densities.
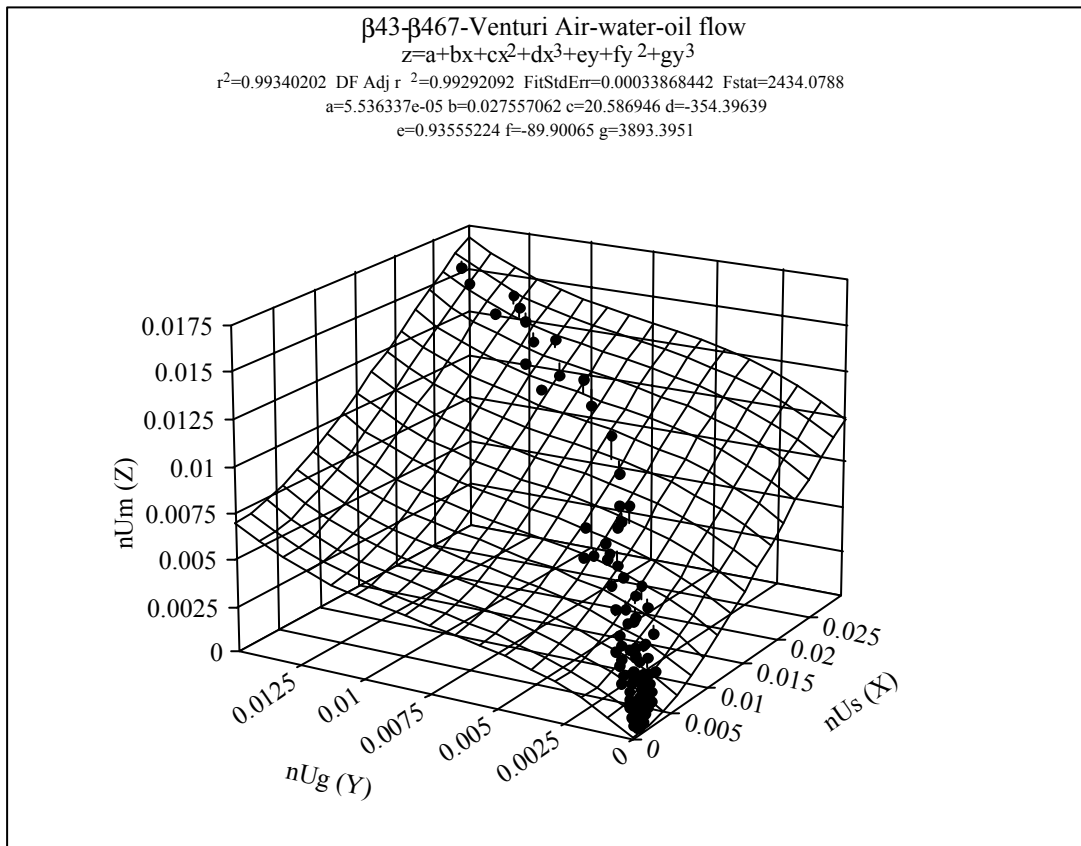
Figure 103. Mixture non-dimensional velocity as a function of the single-phase air flow and two-phase air flow parameters. Venturi meter, air-oil-water flow.
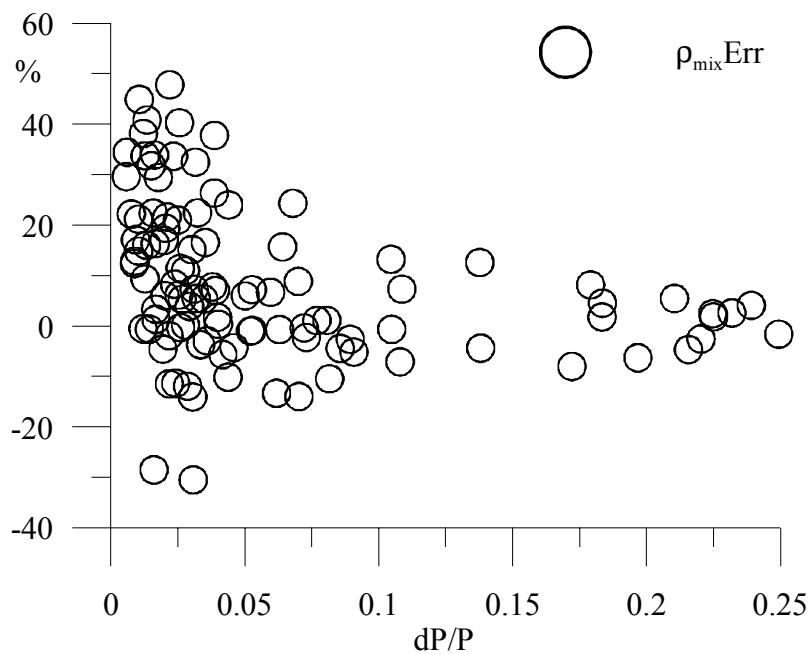
Figure 104. Mixture density estimation using the Venturi meter. Air-oil-water flow.
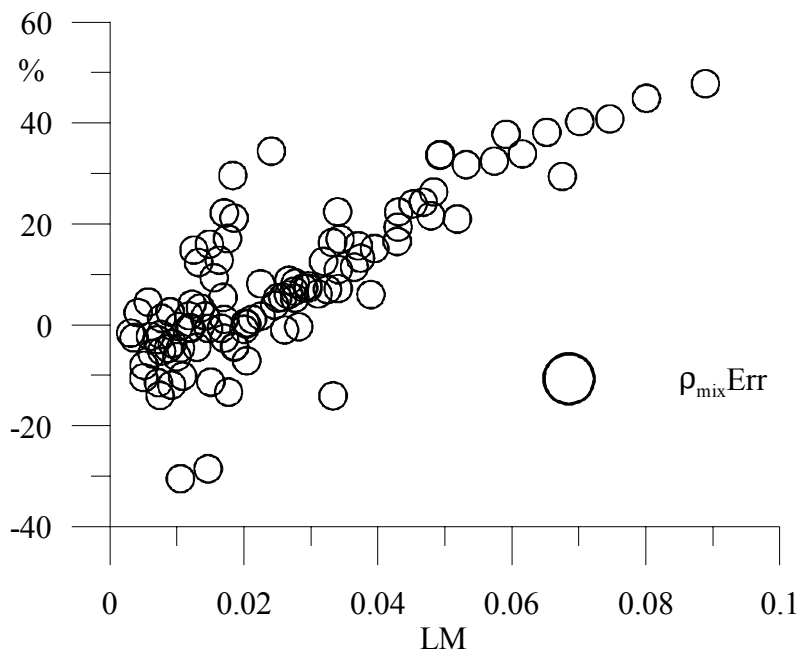
Figure 105. Lockhart-Martinelli parameter influence on the mixture density estimation using the Venturi meter. Air-oil-water flow.
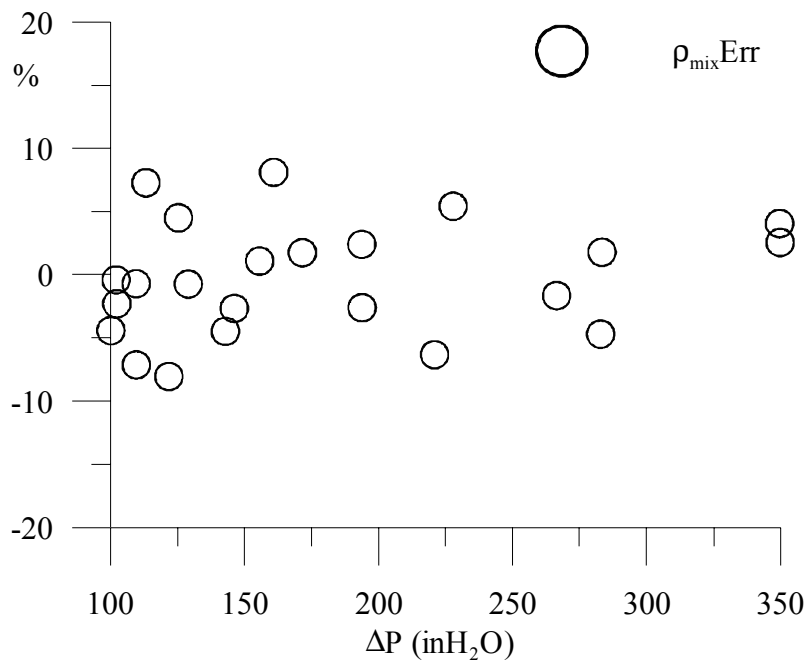
Figure 106. Mixture density estimation using the Venturi meter for pressure drop greater than 100 inH$_2$O.
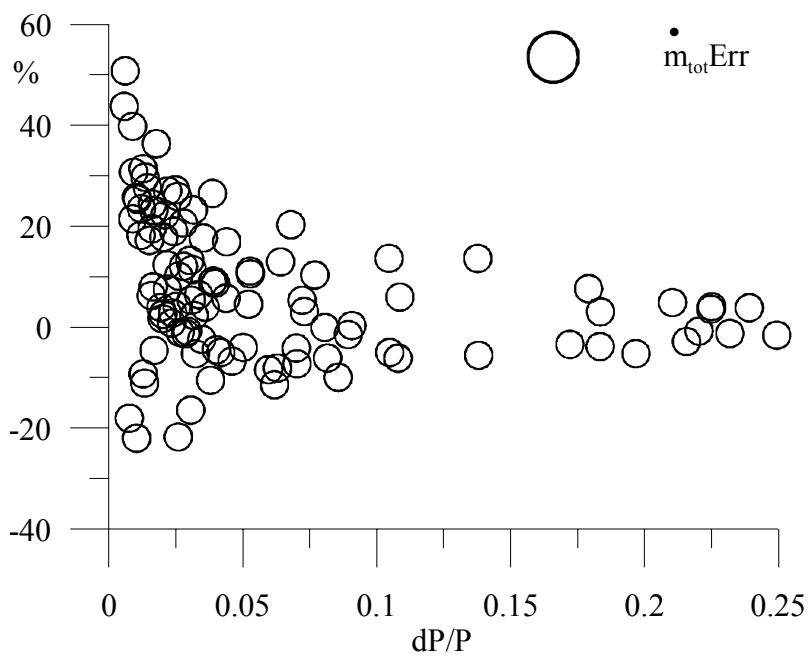
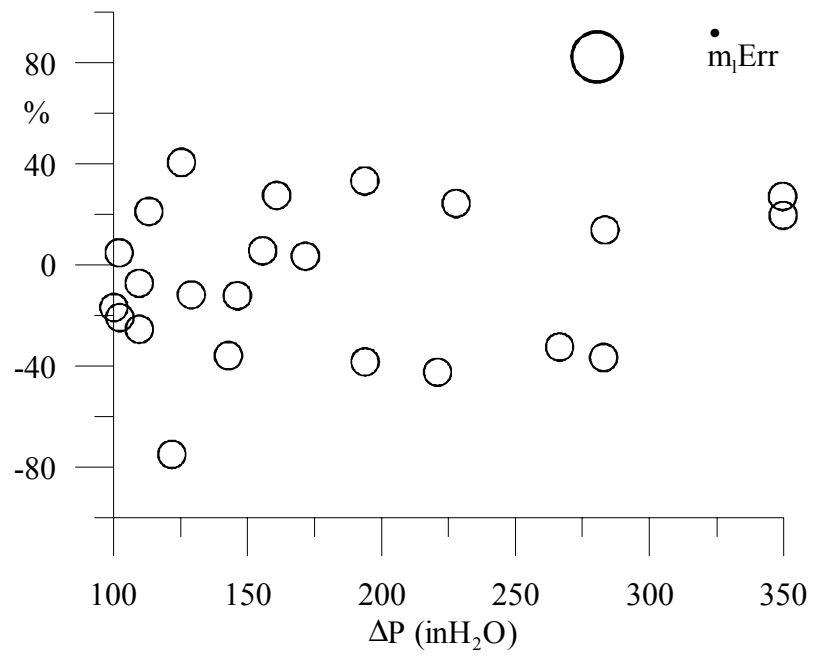Figure 107. Error in the total mass flow estimation using the Venturi meter for the air-oil-water flow.
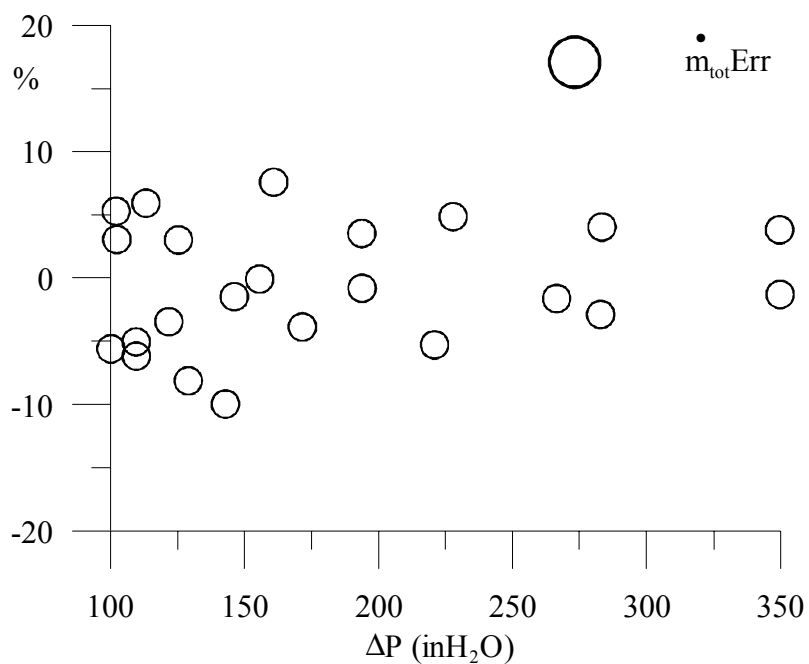
Figure 108. Error in the total flow estimation for the air-oil-water flow using the Venturi meter for pressure drops greater than 100 in_H_2O.
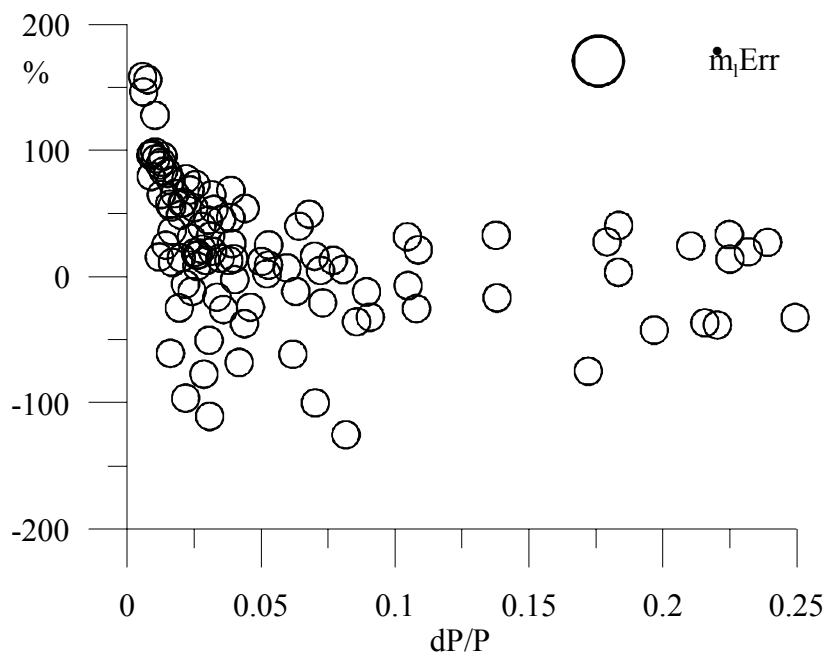
Figure 109. Error in liquid flow estimation using the Venturi meter for the air-oil-water flow.

Figure 110. Error for the liquid flow estimation using the Venturi meter at pressure differential greater than 100 in_H_2O.
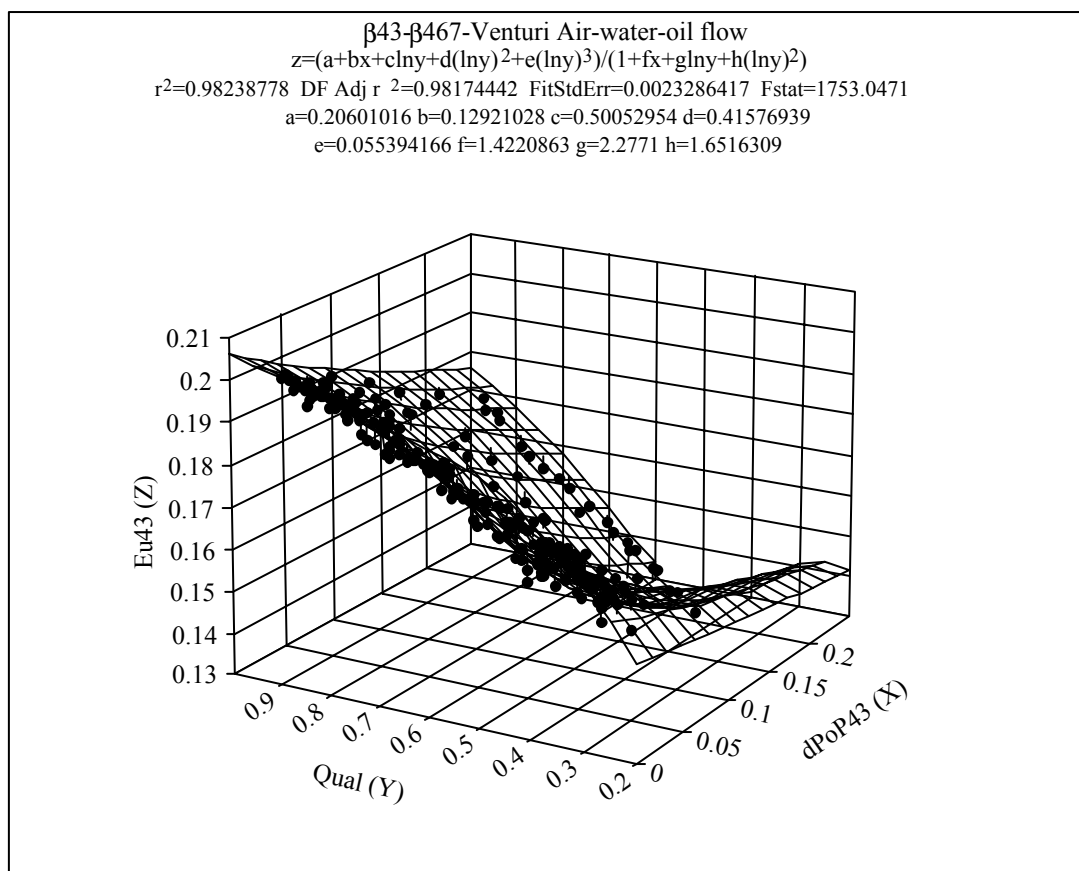
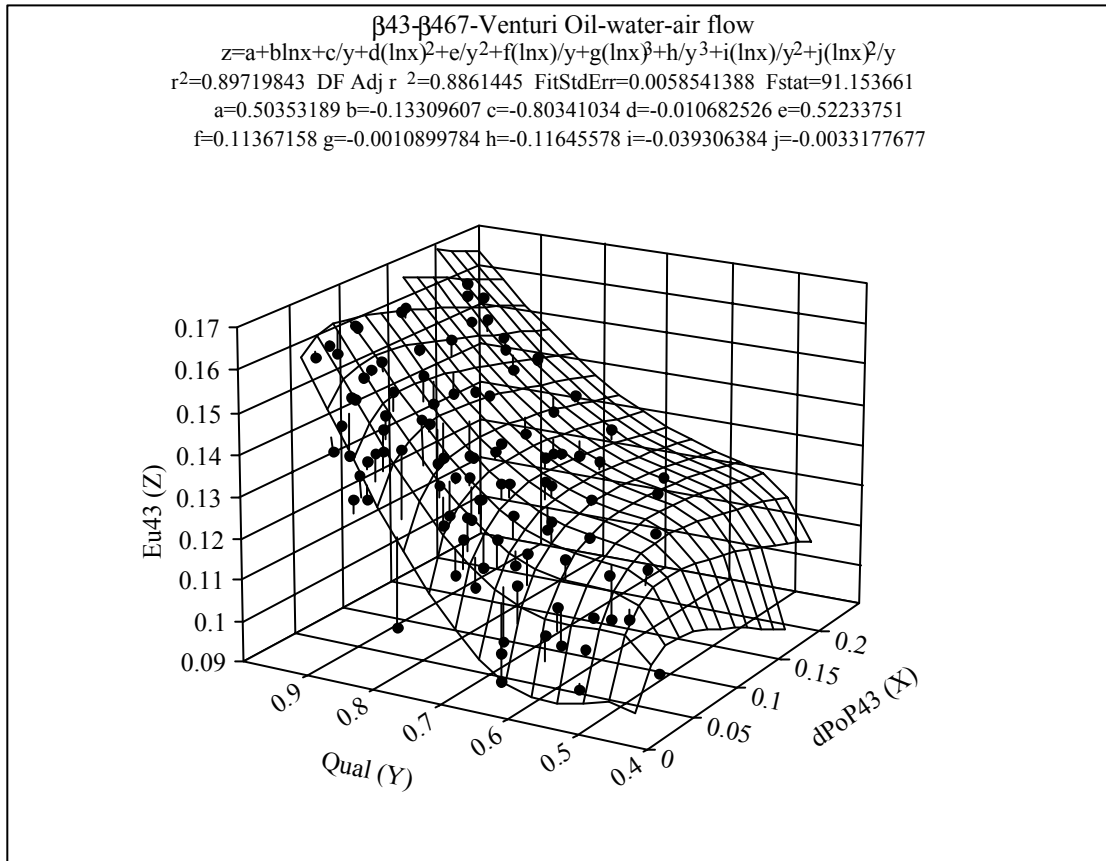Figure 111. Gas Euler number, β43 slotted plate. Air-water flow.

β43-β467-Venturi Oil-water-air flow
$z=a+b\ln x+c/y+d(\ln x)^2+e/y^2+f(\ln x)/y+g(\ln x)^3+h/y^3+i(\ln x)/y^2+j(\ln x)^2/y$
r^2=0.89719843 DF Adj r ^{2}=0.8861445 FitStdErr=0.0058541388 Fstat=91.153661
a=0.50353189 b=-0.13309607 c=-0.80341034 d=-0.010682526 e=0.52233751
f=0.11367158 g=-0.0010899784 h=-0.11645578 i=-0.039306384 j=-0.0033177677

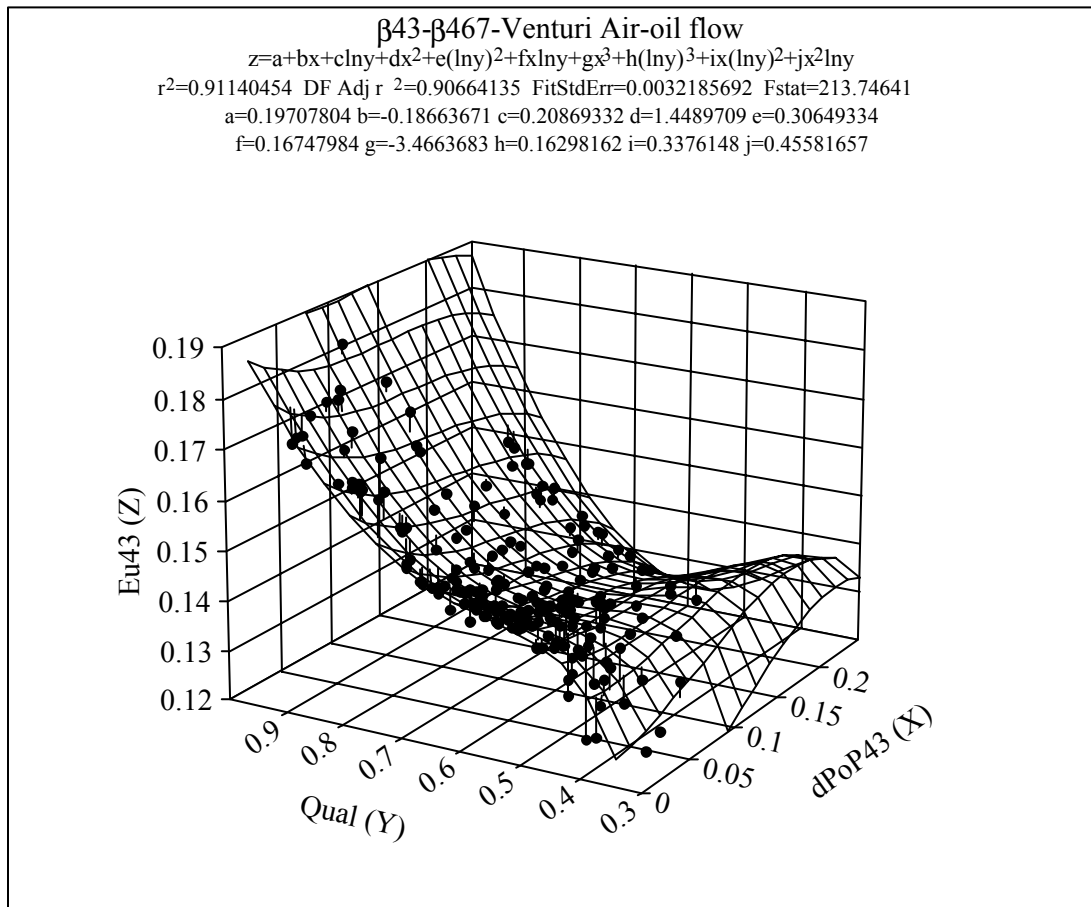Figure 112. Gas Euler number, β43 slotted plate. Air-water-oil flow.

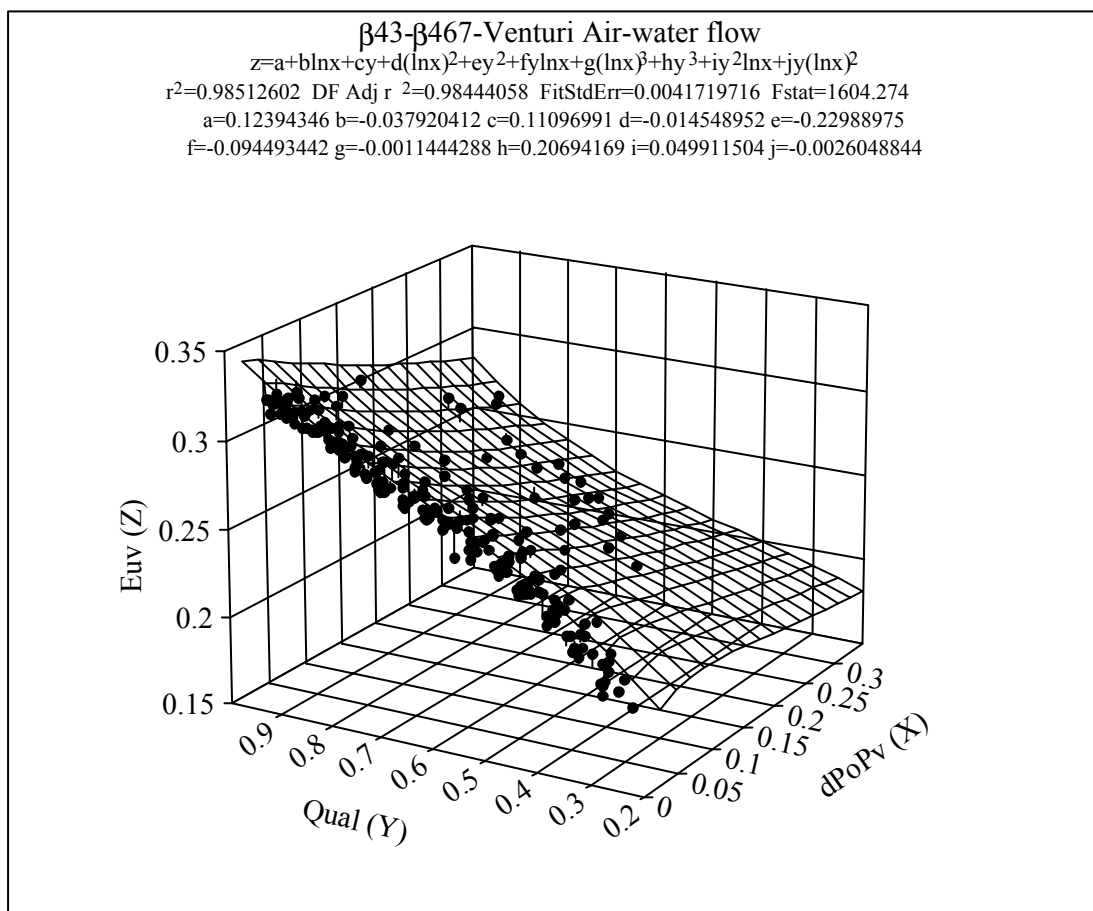Figure 113. Gas Euler number, β43 slotted plate. Air-oil flow.
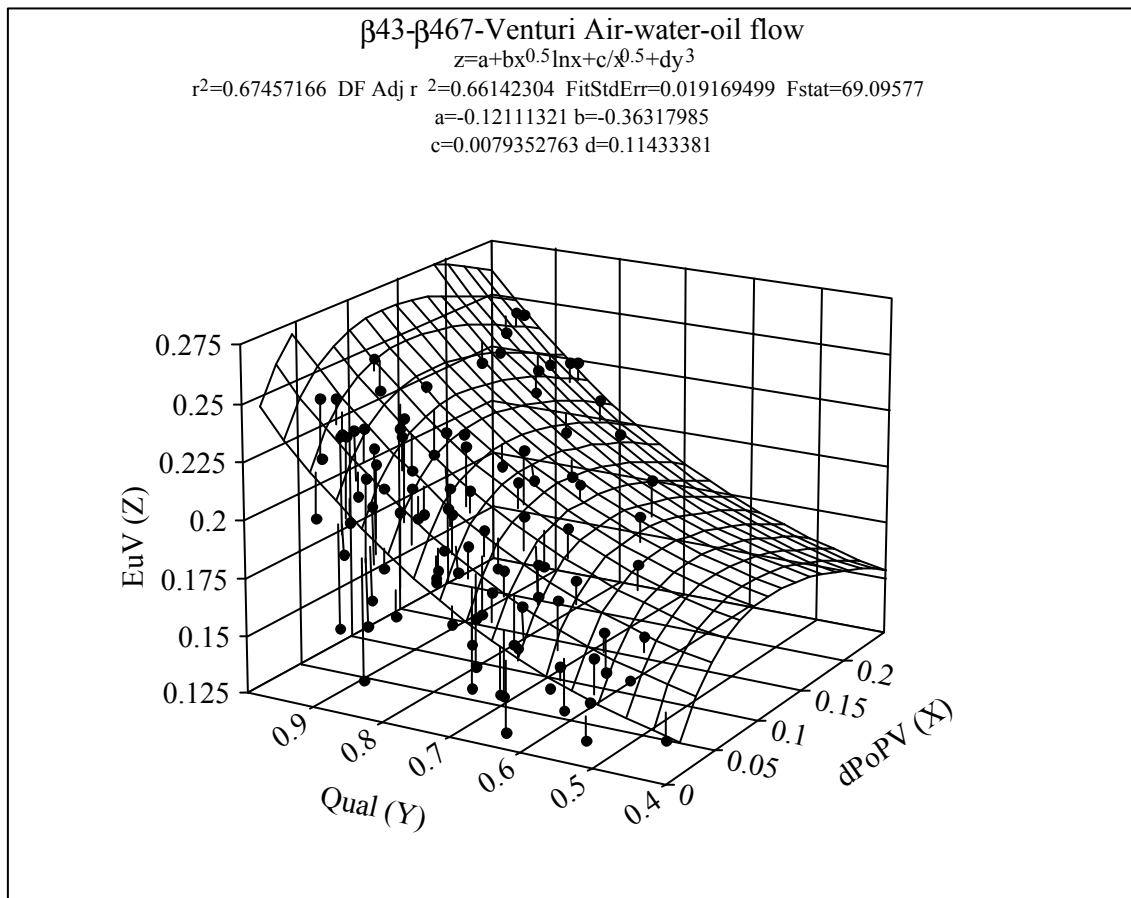
Figure 114. Gas Euler number, Venturi meter. Air-water flow.

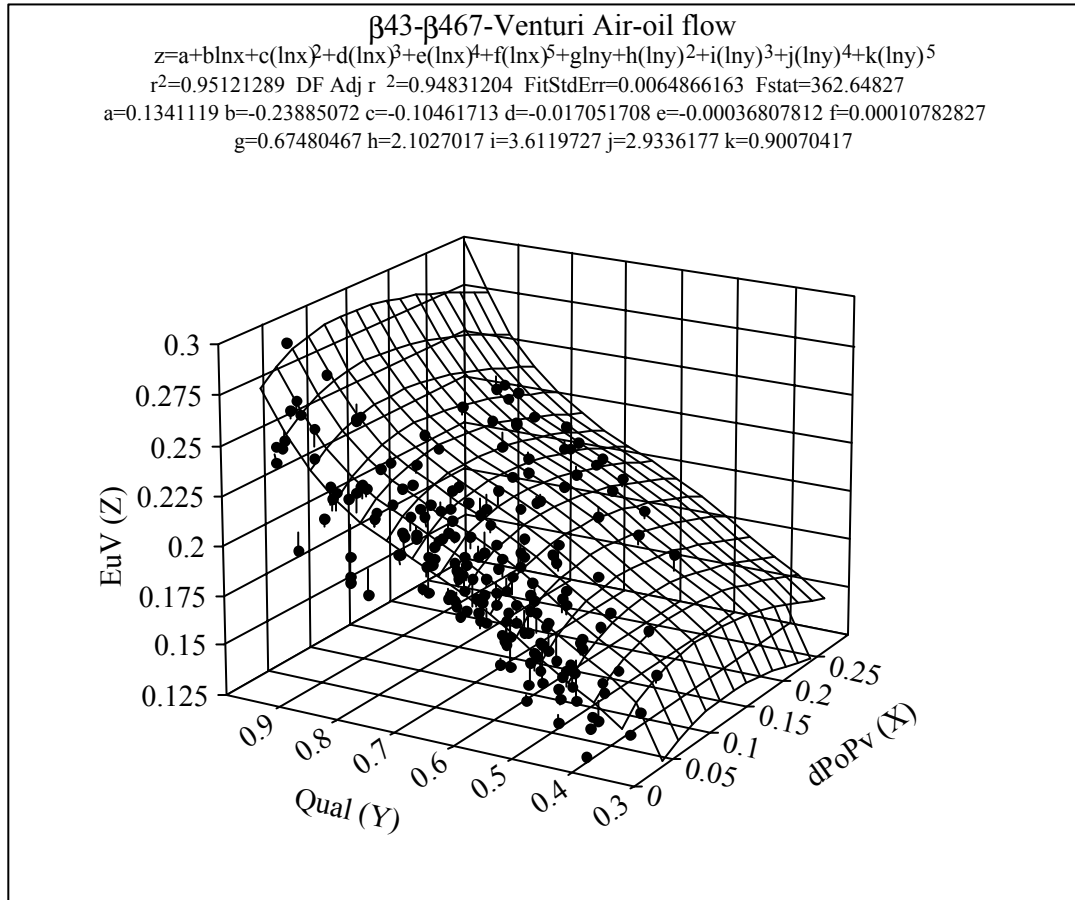Figure 115. Gas Euler number, Venturi meter. Air-water-oil flow.

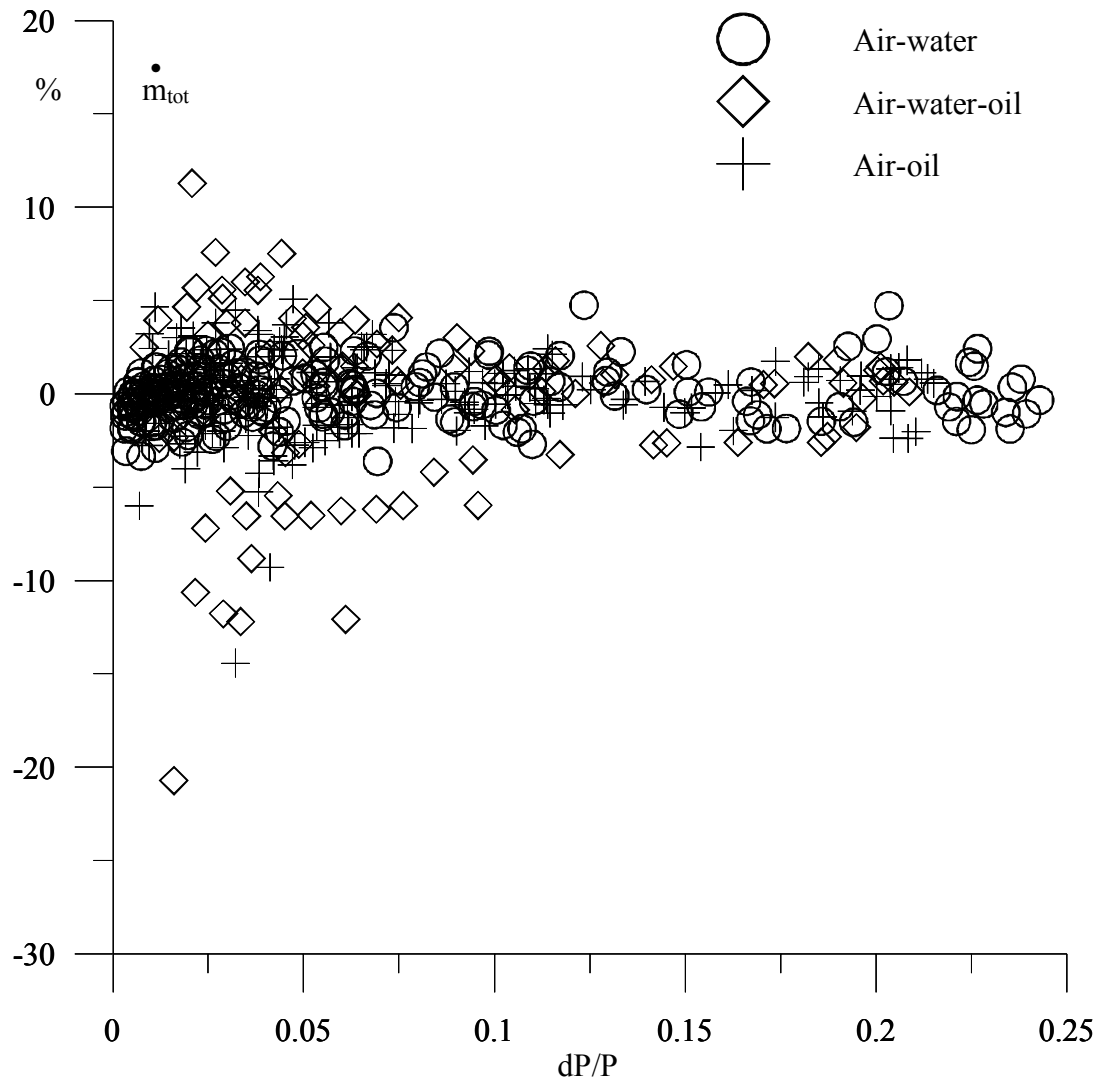Figure 116. Gas Euler number, β43 slotted plate. Air-oil flow.

Figure 117. Total mass flow rate estimation assuming known quality. β=0.43 slotted plate.
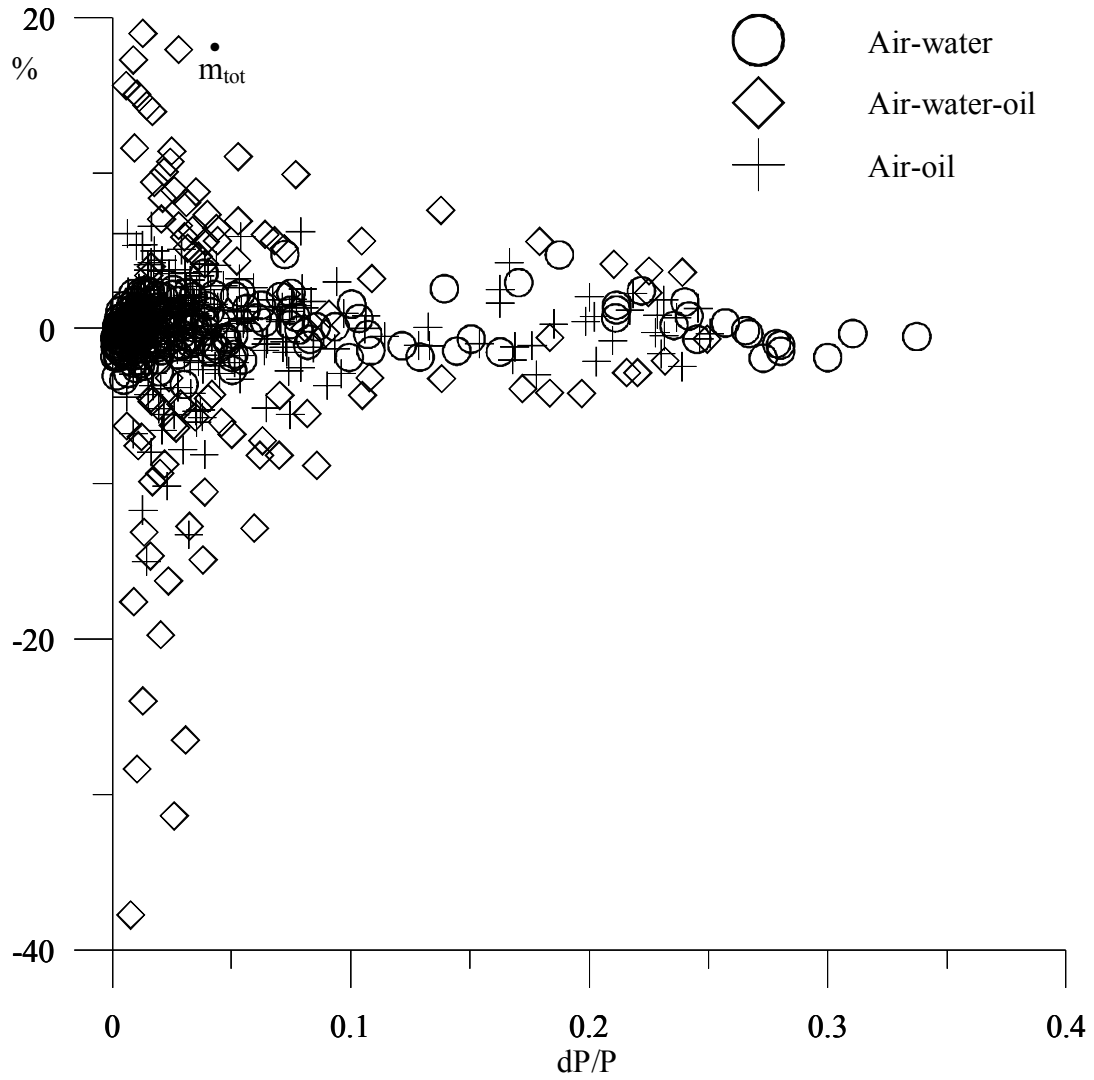
Figure 118. Total mass flow rate estimation assuming known quality. Venturi meter.
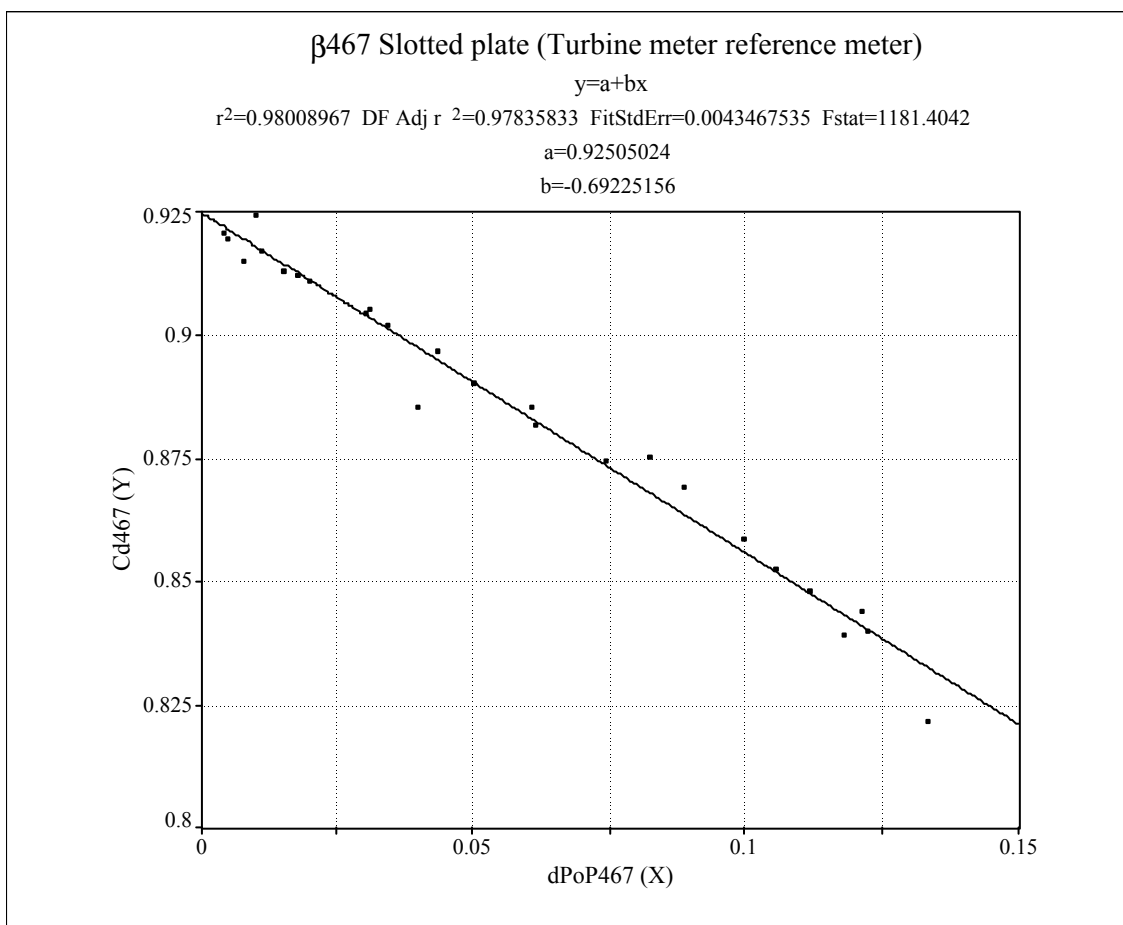
Figure 119. Coefficient C_d correlation as a function of dP/P. Turbine meter reference.
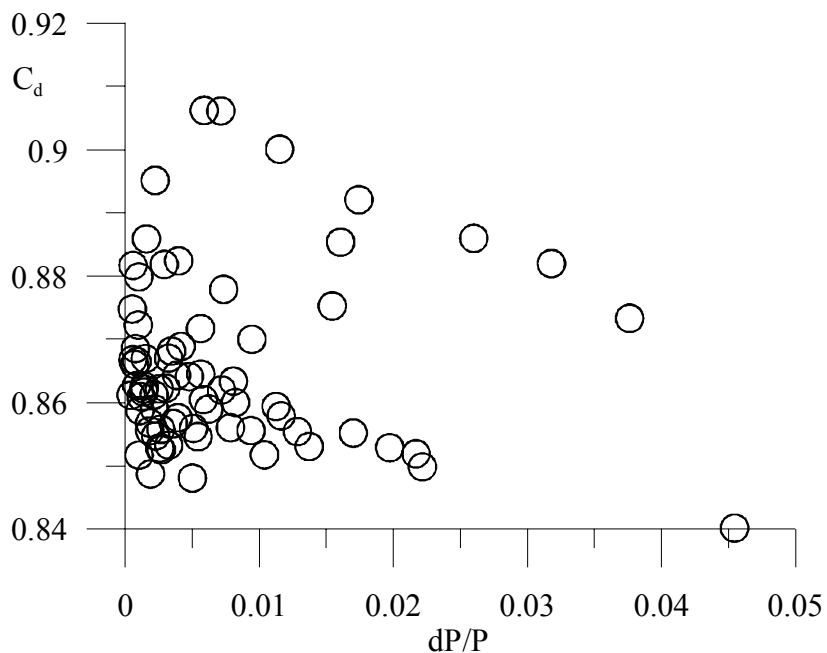
Figure 120. C_d coefficient as a function of dP/P using sonic nozzles bank as reference meter.

Figure 121. Comparison of C_d coefficient at low differential pressure using sonic nozzle bank as reference meter and C_d coefficient for a wider ΔP range using turbine meter as reference.
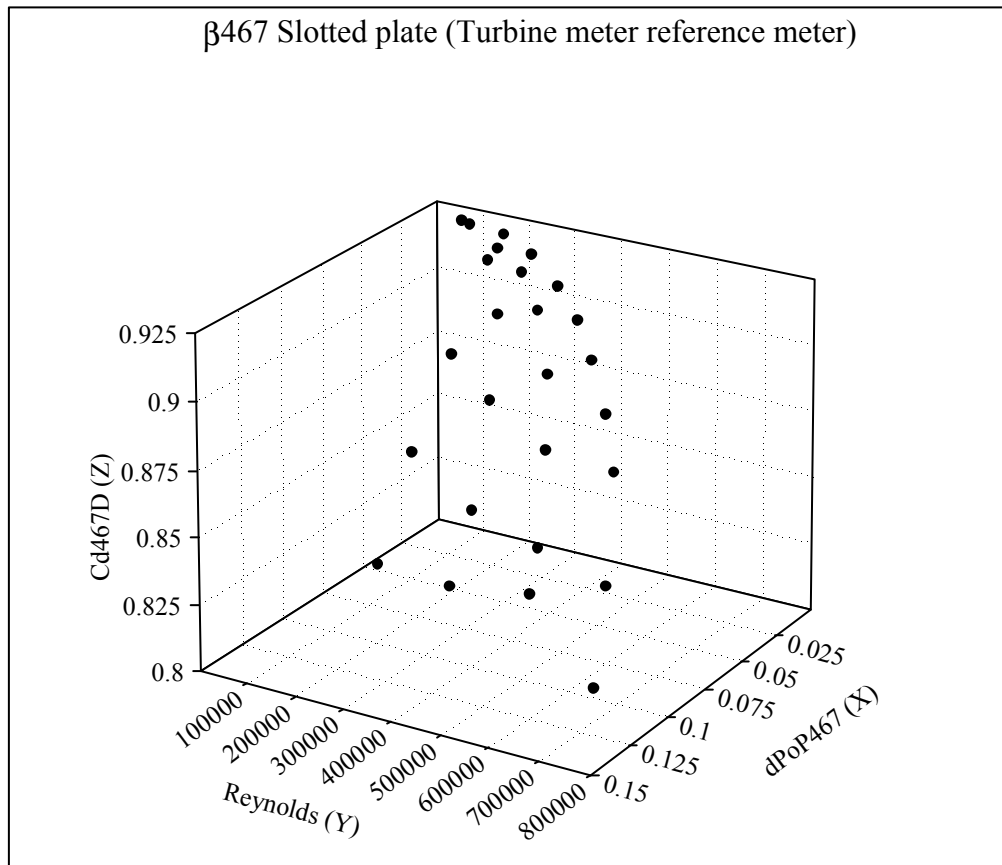
Figure 122. Coefficient C_d as a function of dP/P and Reynolds number. Turbine meter reference.
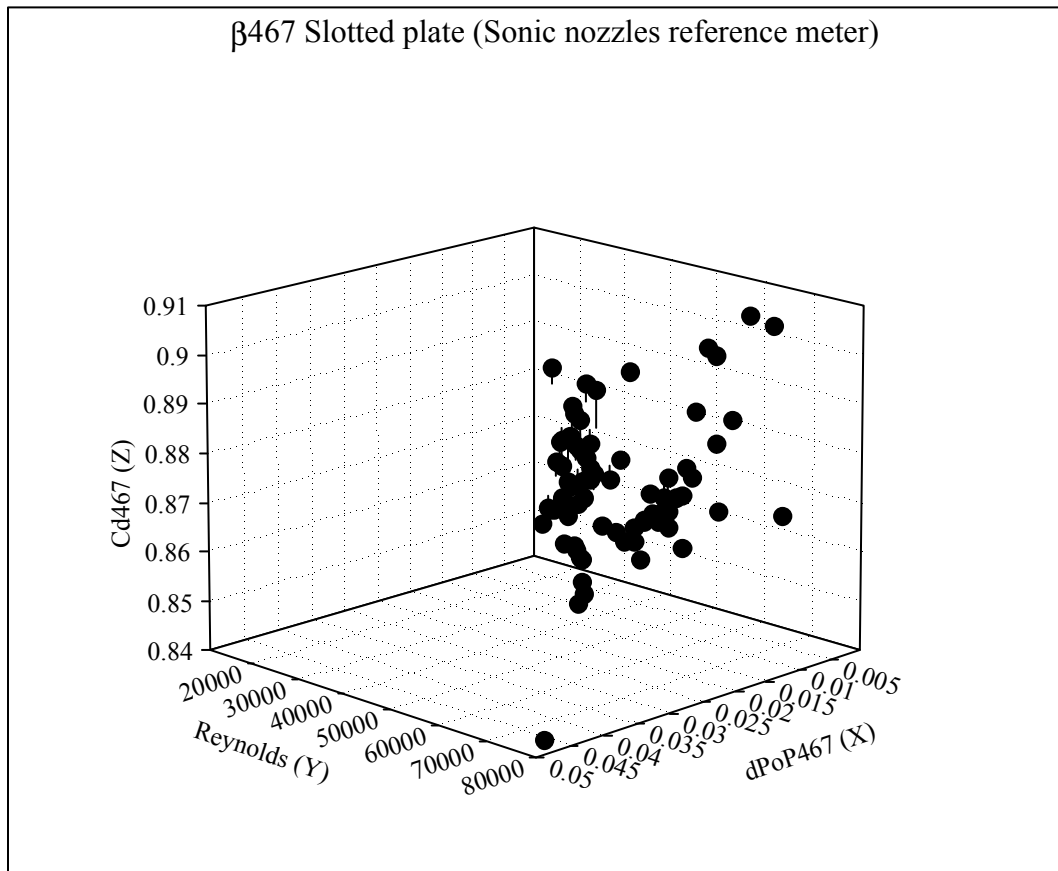
Figure 123. Coefficient C_d as a function of dP/P and Reynolds number. Sonic nozzle bank reference meter.

Figure 124. Coefficient C_d. All data included.
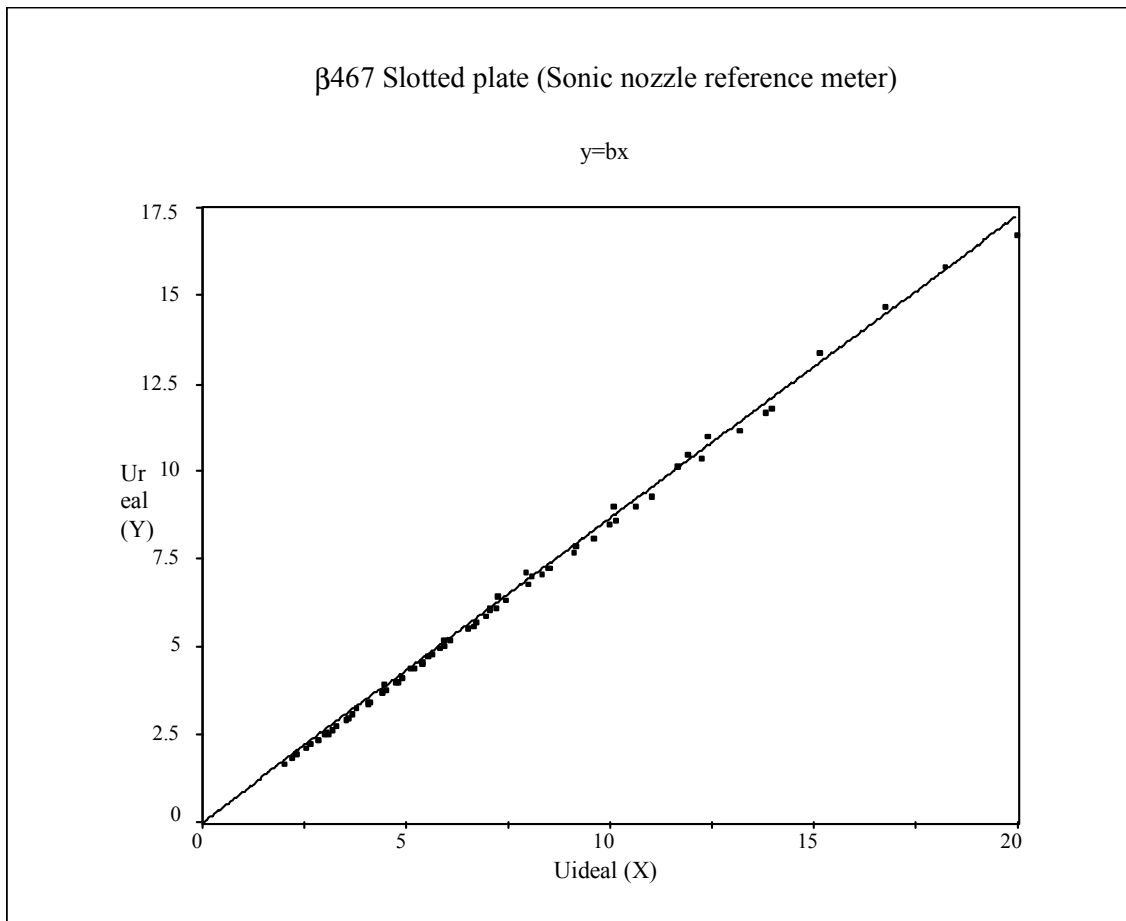
Figure 125. Upstream velocity as function of the ideal value. Sonic nozzle bank reference meter.
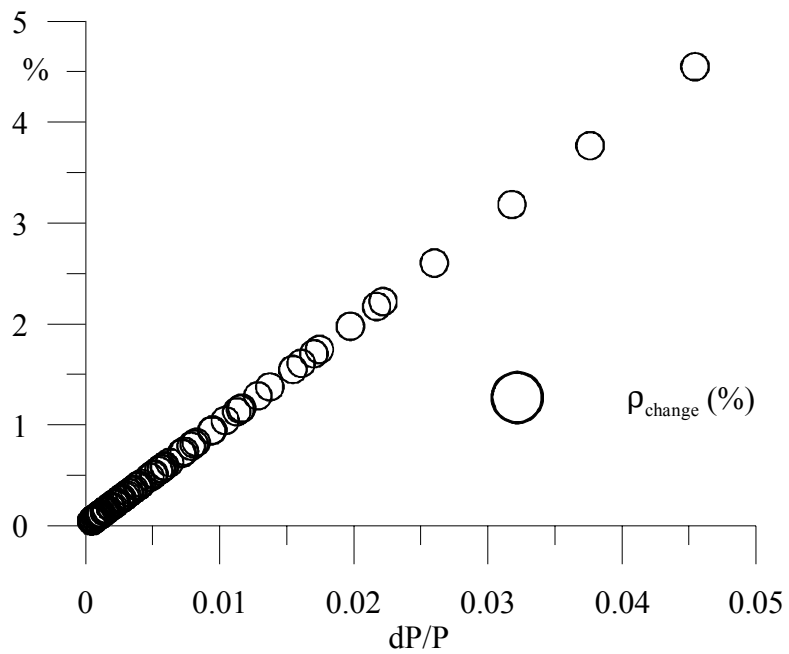
Figure 126. Density variation at low differential pressures.
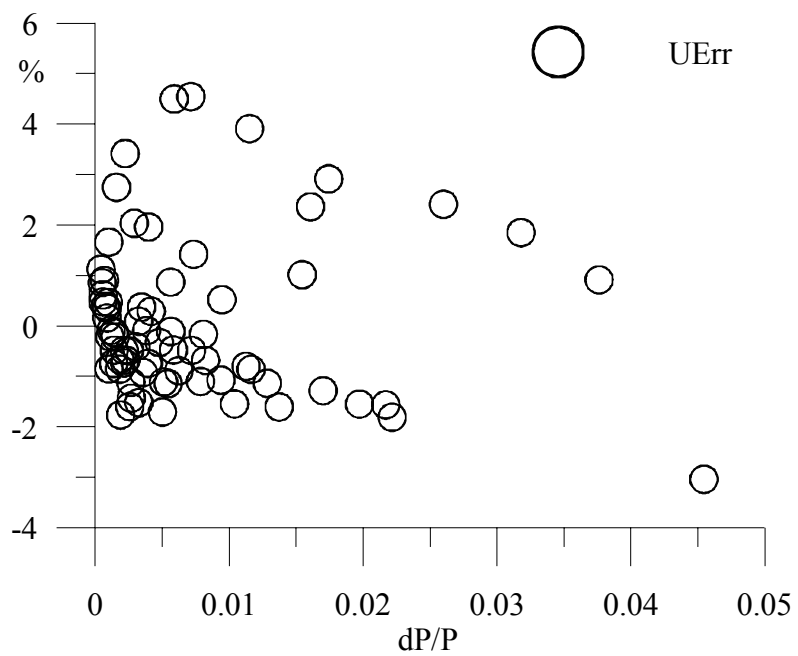
Figure 127. Error in the velocity estimation at low differential pressures.

APPENDIX B

TABLES

Table 1. Differential pressure performance in the air-water flow
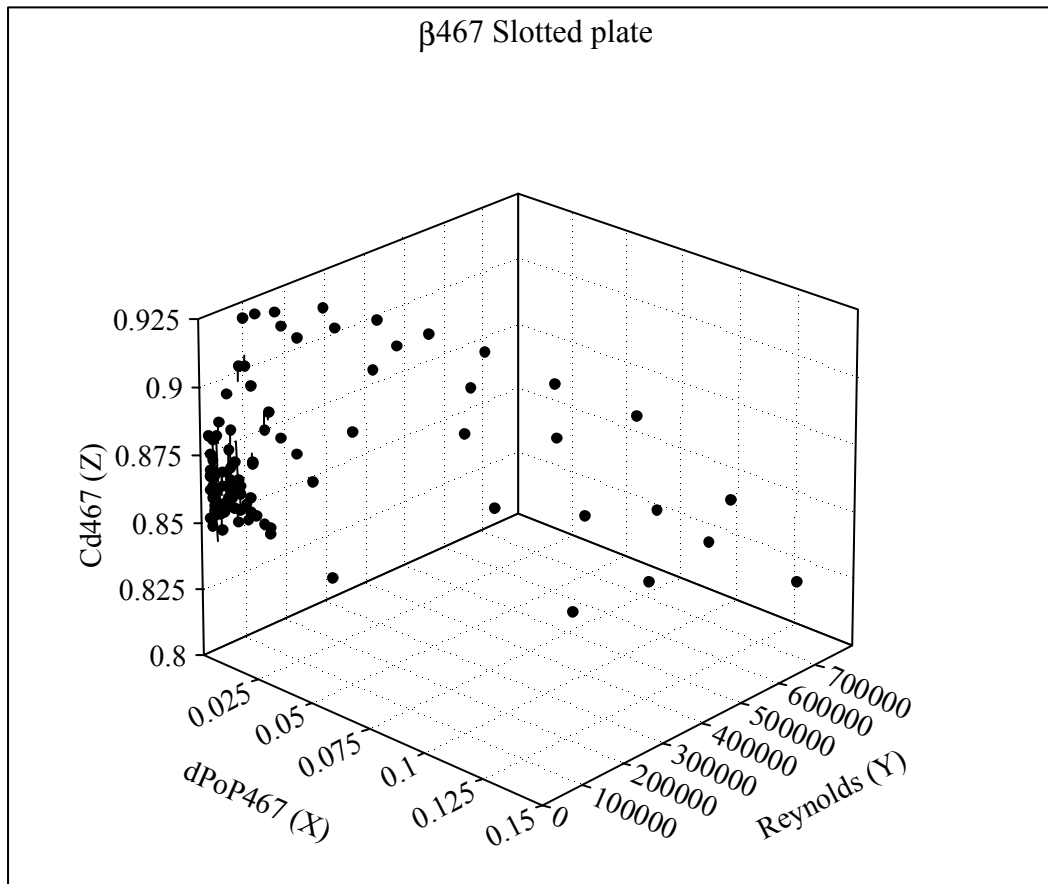
Gas Flow	Empirical equation		Pressure response		Recovery pressure	
	Accuracy %	Dynamic range Kg/min	Accuracy %	Dynamic range Kg/min	Accuracy %	Dynamic range Kg/min
Slotted plate	±4.5	4.85-18.97	--	--	--	--
Venturi meter	±13	4.85-18.97	--	--	±16	2.5-16.5
Standard orifice	±2	5-15.3	±3	5-15.3	--	--

Liquid Flow	Empirical equation		Pressure response		Recovery pressure	
	Accuracy %	Dynamic range Kg/min	Accuracy %	Dynamic range Kg/min	Accuracy %	Dynamic range Kg/min
Slotted plate	±9	0.07-13.1	--	--	--	--
Venturi meter	--	--	--	--	±90	0.41-9.1
Standard orifice	--	--	±29	0.07-9.8	--	--

Table 2. Differential pressure performance in the air-oil flow

Gas Flow	Empirical equation		Pressure response		Recovery pressure	
	Accuracy %	Dynamic range Kg/min	Accuracy %	Dynamic range Kg/min	Accuracy %	Dynamic range Kg/min
Slotted plate	±14	8.4-18	--	--	--	--
Venturi meter	--	--	--	--	±9.5	8.4-18
Standard orifice	--	--	--	5-	--	--

Liquid Flow	Empirical equation		Pressure response		Recovery pressure	
	Accuracy %	Dynamic range Kg/min	Accuracy %	Dynamic range Kg/min	Accuracy %	Dynamic range Kg/min
Slotted plate	--	--	--	--	--	--
Venturi meter	--	--	--	--	±42	2-7.3
Standard orifice	--	--	--	--	--	--

Table 3. Differential pressure performance in the air-water-oil flow

Gas Flow	Empirical equation		Pressure response		Recovery pressure	
	Accuracy %	Dynamic range Kg/min	Accuracy %	Dynamic range Kg/min	Accuracy %	Dynamic range Kg/min
Slotted plate	±9.5	7.2-17.2	--	--	--	--
Venturi meter	--	--	--	--	±8.7	7.2-17.2
Standard orifice	--	--	--	5-	--	--

Liquid Flow	Empirical equation		Pressure response		Recovery pressure	
	Accuracy %	Dynamic range Kg/min	Accuracy %	Dynamic range Kg/min	Accuracy %	Dynamic range Kg/min
Slotted plate	--	--	--	--	--	--
Venturi meter	--	--	--	--	±32	0.71-4
Standard orifice	--	--	--	--	--	--

APPENDIX C
NOMENCLATURE

A	Pipe cross section
Ac	Constant from calibration
ACFM	Actual cubic feet per minute
A_d	Differential pressure device cross section
B_c	Constant from calibration
C	Multiphase discharge coefficient
C_c	Constant from calibration
C_d	Discharge coefficient
d	Differential meter diameter
D	Pipe diameter
DenR	Downstream to upstream gas density ratio
dP/P	Differential pressure to upstream absolute pressure ratio
Eu	Euler number
FitStdErr	Standard deviation from curve fitting software
Fstat	Mean square regression to mean square error ratio
H	Head
k	Air specific heat ratio
LM	Lochkart-Martinelli parameter
M	Murdock number
m	Number of coefficients in the experimental correlation
$\dot{m}$	Mass flow rate
n	Number of sampled points
nU	Non dimensional velocity
P	Manometric pressure
Prv	Venturi recovery pressure
Pρ	Upstream standard plate to upstream slotted density ratio minus standard dP/P
q	Volumetric flow rate

Qual	Quality
R	Universal gas constant
r^2	Coefficient of determination
Re, Reynolds	Reynolds number
RG	Reader-Harris/Gallagher equation
SCFM	Standard cubic feet per minute
T	Absolute temperature
U	Velocity
WC	Water cut
WMF	Water mass fraction
z_I	Sample point
$\bar{z}$	Average sampled points
$\hat{z}_i$	Estimated value
ΔH	Head losses
$\Delta HgoP$	Gas Head loss to absolute pressure ratio
ΔP	Differential pressure
α	Gas void fraction
β	Differential meter to pipe diameter ratio
ε	Inverse of gas void fraction
ρ	Density

Subscripts

abs	Absolute pressure
1,u	Upstream conditions
2,d	Downstream conditions
fit	Parameter obtained by a fitting process
g	Gas
ideal	Computed parameter considering no head losses
l	Liquid

mix	Mixture
o	Stagnation conditions for sonic nozzles
op	Orifice plate
real	Measured value
root	Velocity estimated based on Euler number
s	Single phase gas flow
t	Throat conditions for sonic nozzle
tot	Total
v	Venturi
43	$\beta=0.43$ slotted plate
467	$\beta=0.467$ slotted plate
508	$\beta=0.508$ standard orifice
ΔP	Refers to Euler number computed using the differential pressure

VITA

Justo Hernandez Ruiz was born in Metlaltoyuca Puebla, Mexico on July 29, 1972. His parents are Evodio Hernandez Rojas and Genoveba Ruiz Moran. He has two brothers, Evodio and Jorge and two sisters, Emma and Nohemi. He received his Bachelor in Sciences degree in mechanical engineering from the National Polytechnic Institute in Mexico in 1996. He completed the Master in Sciences program in mechanical engineering also at the National Polytechnic Institute in Mexico in 1998. In August 2004 he complete the Ph.D. program in interdisciplinary engineering in Texas A&M University. His permanent address is Av. Chapultepec 321-7 Colonia Juarez Mexico, D.F. C.P. 06600.